NAVAL POSTGRADUATE SCHOOL

MONTEREY, CALIFORNIA

THESIS

MODELING OF LAMB WAVES AND APPLICATION TO CRACK IDENTIFICATION

by

Epameinondas Palmos

September 2009

Thesis Co-Advisors: Young W. Kwon
Randall D. Pollak

Approved for public release; distribution is unlimited.

THIS PAGE INTENTIONALLY LEFT BLANK

REPORT DOCUMENTATION PAGE		Form Approved OMB No. 0704-0188

Public reporting burden for this collection of information is estimated to average 1 hour per response, including the time for reviewing instruction, searching existing data sources, gathering and maintaining the data needed, and completing and reviewing the collection of information. Send comments regarding this burden estimate or any other aspect of this collection of information, including suggestions for reducing this burden, to Washington headquarters Services, Directorate for Information Operations and Reports, 1215 Jefferson Davis Highway, Suite 1204, Arlington, VA 22202-4302, and to the Office of Management and Budget, Paperwork Reduction Project (0704-0188) Washington DC 20503.

1. AGENCY USE ONLY *(Leave blank)*	2. REPORT DATE September 2009	3. REPORT TYPE AND DATES COVERED Master's Thesis

4. TITLE AND SUBTITLE Modeling of Lamb Waves and Application to Crack Identification	5. FUNDING NUMBERS
6. AUTHOR(S) Epameinondas Palmos	
7. PERFORMING ORGANIZATION NAME(S) AND ADDRESS(ES) Naval Postgraduate School Monterey, CA 93943-5000	8. PERFORMING ORGANIZATION REPORT NUMBER
9. SPONSORING /MONITORING AGENCY NAME(S) AND ADDRESS(ES) N/A	10. SPONSORING/MONITORING AGENCY REPORT NUMBER

11. SUPPLEMENTARY NOTES The views expressed in this thesis are those of the author and do not reflect the official policy or position of the Department of Defense or the U.S. Government.

12a. DISTRIBUTION / AVAILABILITY STATEMENT Approved for public release; distribution is unlimited.	12b. DISTRIBUTION CODE

13. ABSTRACT (maximum 200 words)

The objective of this study is to model Lamb waves generation and sensing for application to crack identification in engineering structures. Three topics were analyzed numerically using multiphysics finite element analysis. Initially, different types of Lamb wave generation techniques were investigated. A comparison between modeling the sinusoidal application of horizontal force (or displacement) as input and modeling the piezoelectric response of an actuator subjected to sinusoidal voltage input was performed. Secondly, the effects of a crack (disbond) between a piezoelectric wafer and the structure were analyzed, both for the piezoelectric actuator that generates the waves and for the sensor that measures the response. Finally, the appropriate fidelity of modeling a structural crack was investigated. In particular, the use of contact elements was evaluated on their role in the accurate prediction of the wave scattering from cracks or defects inside the structure.

14. SUBJECT TERMS Lamb Waves, modeling, finite element, longitudinal, and shear mode, ANSYS, debonding, sensor, piezoelectric.	15. NUMBER OF PAGES 115
	16. PRICE CODE

17. SECURITY CLASSIFICATION OF REPORT	18. SECURITY CLASSIFICATION OF THIS PAGE	19. SECURITY CLASSIFICATION OF ABSTRACT	20. LIMITATION OF ABSTRACT
Unclassified	Unclassified	Unclassified	UU

NSN 7540-01-280-5500 Standard Form 298 (Rev. 8-98)
Prescribed by ANSI Std. Z39.18

THIS PAGE INTENTIONALLY LEFT BLANK

Approved for public release; distribution is unlimited.

MODELING OF LAMB WAVES AND APPLICATION TO CRACK IDENTIFICATION

Epameinondas Palmos
Lieutenant Junior Grade, Hellenic Navy
B.S., Hellenic Naval Academy, 2002

Submitted in partial fulfillment of the
requirements for the degrees of

MECHANICAL ENGINEER
and
MASTER OF SCIENCE IN MECHANICAL ENGINEERING

from the

NAVAL POSTGRADUATE SCHOOL
September 2009

Author: Epameinondas Palmos

Approved by: Young W. Kwon
Thesis Co-Advisor

Randall D. Pollak
Thesis Co-Advisor

Knox T. Millsaps
Chairman, Department of Mechanical and Astronautical Engineering

THIS PAGE INTENTIONALLY LEFT BLANK

ABSTRACT

The objective of this study is to model Lamb waves generation and sensing for application to crack identification in engineering structures. Three topics were analyzed numerically using multiphysics finite element analysis. Initially, different types of Lamb wave generation techniques were investigated. A comparison between modeling the sinusoidal application of horizontal force (or displacement) as input and modeling the piezoelectric response of an actuator subjected to sinusoidal voltage input was performed. Secondly, the effects of a crack (disbond) between a piezoelectric wafer and the structure were analyzed, both for the piezoelectric actuator that generates the waves and for the sensor that measures the response. Finally, the appropriate fidelity of modeling a structural crack was investigated. In particular, the use of contact elements was evaluated on their role in the accurate prediction of the wave scattering from cracks or defects inside the structure.

THIS PAGE INTENTIONALLY LEFT BLANK

TABLE OF CONTENTS

I. INTRODUCTION 1
A. BACKGROUND 1
B. LITERATURE SURVEY 2
C. OBJECTIVES 5

II. ELASTIC WAVES IN TWO DIMENSIONS 7
A. ELASTIC WAVES IN SOLIDS 7
B. THEORY OF ELASTICITY: GOVERNING EQUATIONS 8
C. LAMB WAVES 10
D. PIEZOELECTRICITY 11

III. MODEL DEVELOPMENT 13
A. GENERAL MODEL AND SIMPLIFICATIONS 13
B. IDENTIFICATION OF WAVES 17
C. CONVERGENCE STUDY 21
1. Element Size 21
2. Time Step 23
D. EFFECT OF THE FREQUENCY 24
E. SUMMARY 30

IV. EFFECTS OF INPUT MODELING ON WAVE GENERATION 33
A. STATIC COMPARISON BETWEEN FORCE/DISPLACEMENT INPUT AND PIEZOELECTRIC INPUT 35
B. DYNAMIC COMPARISON BETWEEN FORCE/DISPLACEMENT INPUT AND PIEZOELECTRIC INPUT 37
C. SUMMARY 40

V. EFFECTS OF PIEZOELECTRIC WAFER DEBONDING ON ACTUATOR AND SENSOR 41
A. DEBONDING OF THE ACTUATOR 41
B. DEBONDING OF THE SENSOR 44
C. SUMMARY 59

VI. CRACK MODELING AND IDENTIFICATION 61
A. VERTICAL CRACKS 62
1. Dimensions 1 mm x 50 μm 62
2. Dimensions 0.6 mm x 50 μm 73
3. Dimensions 0.5 mm x 5 μm 77
B. HORIZONTAL CRACK. 80
1. Dimension 1 mm x 0.5 μm 80
2. Summary 82
C. CRACK MODELING FIDELITY - USE OF CONTACT ELEMENTS VERSUS NO CONTACT ELEMENTS 83

VII. CONCLUSIONS AND RECOMMENDATIONS 89
A. CONCLUSIONS 89

B. RECOMMENDATIONS AND FUTURE WORK..... 90
LIST OF REFERENCES..... 93
INITIAL DISTRIBUTION LIST 97

LIST OF FIGURES

Figure 1. A Conceptual Illustration of Structural Health Monitoring [From 2]. 2
Figure 2. Types of Elastic Waves in Solids: (a) Longitudinal Waves (b) Shear Waves (c) Rayleigh waves (d) Love Waves [From 23]. 8
Figure 3. Lamb Waves: S mode (a), A mode (b). 10
Figure 4. Velocities of Lamb Waves: Phase Velocity (a), Group Velocity (b) [From 24]. 11
Figure 5. The Actual Lamb Wave Experiment. 13
Figure 6. The Two-Dimension Simplification of the Three-Dimension Case of Figure 5. 14
Figure 7. The Element Used. 15
Figure 8. TARGE 169 Element Geometry (a), CONTA 172 Element Geometry (b). 15
Figure 9. Modeling of Cracks: Line Cracks (a), Diamond Cracks (b). 16
Figure 10. Identification of Lamb Waves at four different Points (red dots). 18
Figure 11. Voltage Input on the Finite Element Model. 18
Figure 12. Plot of the Sinusoidal Voltage Input used in this Paper. 18
Figure 13. Horizontal Elastic Strain at the four Different Location Shown as Red Dots on Figure 9. The two Lamb Wave Modes are Present. 19
Figure 14. Identification of S0 and A0 Lamb Wave Modes. Comparison of the Horizontal Displacement of the Nodes on Top and on Bottom of the Aluminum Plate. 20
Figure 15 Identification of S0 and A0 Lamb Wave Modes. Vertical Displacement of a Node at the Center Line of the Aluminum Plate. The Response during the Symmetric Wave is almost Zero. 21
Figure 16. The Simplified Model (a) and Displacement Input (b) used for the Element Size Convergent Study. 22
Figure 17. Convergent Study. Horizontal Displacement at the Same Point for Different Element Sizes. 22
Figure 18. Two-nodes' Horizontal Displacement Input. 23
Figure 19. Horizontal Displacement at the Same Point using Three Different Time Steps. 24
Figure 20. Horizontal Displacement at the Same Location using Three Different Input Frequencies 25
Figure 21. Model developed to Investigate the Effect of the Frequency on Lamb Waves and the Voltage Output using Different Piezoelectric Materials. 26
Figure 22. Image of the Diamond-Type Crack used in this Simulation. 26
Figure 23. The Voltage Putput from the pvdf to the Left Side of the Model. Three Wave Forms are Present using Different Frequencies (Input Signal, Reflection from the Crack, Reflection from the end of the Rod). 27

Figure 24. Voltage Output of the Right PVDF Sensor from Figure 19 for Three Different Frequencies: 50, 100, and 200 kHz. 29
Figure 25 The Voltage Output from the PVDF to the Right Side of the Model in Figure 19. S0 and A0 Modes are Present using Different Frequencies. 30
Figure 26. Cross-section of a Typical PZT Sensor [From 8]. 33
Figure 27. Different Methods of Lamb Wave Generation on Finite Element Models. 34
Figure 28. Displaced Structure under the Effect of Horizontal Displacement at the Ends of the aluminum plate (a) and Application of Voltage on top and bottom of the Piezoelectric Material (b). 36
Figure 29. The Model Used for Comparison between the Displacement Input and the Piezoelectric Input. 38
Figure 30. Comparison of the Horizontal Displacement (a) and Horizontal Elastic Strain (b) using two Different Methods of Lamb Wave Generation (Full Multiphysics Simulation and Two-node Simplification) 39
Figure 31. Graphical Representation of the Model with a Crack on the Interface between the Piezoelectric Material and the Aluminum. 41
Figure 32. Small Difference in the Lamb Waves for a Debonding Actuator. The Difference is Obvious in the Amplitude of the Bending Wave. (Ellipse: A Magnification is Available in the next Figure) 42
Figure 33. Nine Percent Difference in the Amplitude of the A0 Mode for the Debonding Actuator. No Difference Between using Singular Elements and not using Them. 43
Figure 34. Theoretical Model of an Actuator With 100% Bebonding. 44
Figure 35. Graphical Representation of the Model with a Crack on the Interface Between the Sensing Material and the Aluminum. Voltage Output from Five Different Points was Compared. 45
Figure 36. The Voltage Output at the Five Locations on top of the PZT Material as shown in Figure 32. Left End of the PZT (a), One-Quarter of the Length from the Left (b), Middle of the Sensor (c), Three-Quarters of the Length from the Left end (d), Right end (e). 46
Figure 37. Voltage Output at Point 1 of Figure 32 for the Debonding and the No-crack Case. 47
Figure 38 Voltage Output at Point 3 of Figure 32 for the Debonding and the No-crack Case 48
Figure 39. Max Voltage Output Throughout the Sensor With and Without Debonding-S0 Mode 49
Figure 40. Max Voltage Output Throughout the Sensor With and Without Debonding-A0 Mode 49
Figure 41. Geometry of the Piezoelectric Sensor with an Adhesive Layer. The Voltage Output was Measured at Seven Different Points. 50
Figure 42. Voltage Output at Point 1 of Figure 36 of the Sensor With and without Debonding. 51

Figure 43. Voltage Output at Point 2 of Figure 36 of the Sensor With and Without Debonding. 52
Figure 44. Voltage Output at Point 3 of Figure 36 of the Sensor With and Without Debonding. 53
Figure 45. Voltage Output at Point 4 of Figure 36 of the Sensor With and Without Debonding 54
Figure 46 Voltage Output at Point 5 of Figure 36 of the Sensor With and Without Debonding. 54
Figure 47. Voltage Output at Point 6 of Figure 36 of the Sensor With and Without Debonding. 55
Figure 48. Voltage Output at Point 7 of Figure 36 of the Sensor With and Without Debonding. 55
Figure 49. Max Voltage Output Throughout the Sensor With and Without Debonding-S0 Mode..... 56
Figure 50. Max Voltage Output Throughout the Sensor With and Without Debonding-A0 mode..... 56
Figure 51 Total Voltage Output from the Sensor for Different Lamb Wave Modes With and Without Adhesive Layer. 58
Figure 52. Different Types of Cracks in Adhesive Layers [From 29]..... 60
Figure 53. Model With a Vertical Crack of 1 mm x 50 μm..... 62
Figure 54. Horizontal Displacement (a) & Elastic Strain (b) at Point A, 0.4 m from the Left. 63
Figure 55. Horizontal Displacement (a) & Elastic Strain (b) at Point B, 0.195 m from the Left. 64
Figure 56. Horizontal Displacement (a) & Elastic Strain (b) at Point C, 0.2 m from the Left. 65
Figure 57. FFT of Horizontal Displacement from Point A at 0.4 m: Uncracked Case (a), Cracked/No Contact Case (b). 67
Figure 58. FFT of Horizontal Displacement at Point B, 0.195 m from the Left End of the Plate. No Crack Case (a), With Crack/No Contact Elements (b). 68
Figure 59. FFT of Horizontal Displacement at Point C, 0.2 m from the Left End of the Plate. No Crack (a), With Crack/No Contact Elements(b). 69
Figure 60. FFT of Horizontal Strain at Point A, 0.4 m from the Left End of the Plate. No Crack(a), With Crack/No Contact Elements(b). 70
Figure 61. FFT of Horizontal Strain at Point B, 0.195 m from the Left End of the Plate. No Crack(a), With Crack/No Contact Elements(b). 71
Figure 62. FFT of Horizontal Strain at Point A, 0.2 m from the Left End of the Plate. No Crack(a), With Crack/No Contact Elements(b). 72
Figure 63. Horizontal Displacement at Point A, 0.4 m from the Left. 73
Figure 64. Horizontal Displacement at Point B, 0.195 m from the Left. 74
Figure 65. Horizontal Displacement of the Plate With and Without Crack, Distance 0.2 m from the Left 74
Figure 66. FFT of Horizontal Displacement at 0.4 m from the Left. Without Crack (a), With Crack (b). 75

Figure 67. FFT of Horizontal Displacement from 0.195 m. No Crack (a), With Crack (b)..... 76
Figure 68. FFT of Horizontal Displacement from 0.2 m. No Crack (a), With Crack (b)..... 77
Figure 69. Horizontal Displacement at 0.4 m..... 78
Figure 70. Horizontal Displacement at 0.2 m..... 78
Figure 71. FFT of the Horizontal Displacement from 0.4 m. No Crack (a), With Crack (b)..... 79
Figure 72. FFT of Horizontal Displacement from 0.2 m. No Crack (a), With Crack (b)..... 80
Figure 73. Horizontal Displacement from 0.4 m..... 81
Figure 74. FFT of Horizontal Displacement from 0.4 m. 82
Figure 75. The Model with the Horizontal Line Crack. 83
Figure 76. Voltage Output from the Actuator of Figure 72. A Reflected Wave from the Crack is Present Inside the Ellipse. 84
Figure 77. Closer Look inside the Ellipse of Figure 73. 85
Figure 78. Voltage Output from the Sensor on the Right Side of the Model in Figure 72. It Demonstrates the Difference when using Contact Elements. 86
Figure 79. Closer Look inside the Ellipse of Figure 75. 87
Figure 80. FFT of the Voltage Output from the Actuator of Figure 72. No Crack: Red; with Crack: Blue..... 88
Figure 81. FFT of the Voltage Output from the Right Sensor of Figure 72. No Crack: Red; with Crack: Blue..... 88

LIST OF TABLES

Table 1. Types and Dimensions of Cracks in this thesis. 17
Table 2. Summary of the Voltage Output of this Model (Figure 19) from the PVDF Sensors on the left of Figure 21, for Different Frequencies..... 28

THIS PAGE INTENTIONALLY LEFT BLANK

ACKNOWLEDGMENTS

I would like to show my gratitude to Professor Young W. Kwon and Major Randall D. Pollak for their encouragement, support and guidance during my research and studies at the Naval Postgraduate School.

Most of all, I offer my regards to my family for their understanding, patience, and support throughout my studies.

THIS PAGE INTENTIONALLY LEFT BLANK

I. INTRODUCTION

A. BACKGROUND

Modern structures, particularly those with military applications, are characterized by complexity and greater performance demands, which together with financial and safety limitations make the completion of present designs challenging. Many times, material selection, design, and safety factors must all be combined so as to create a safe, light structure with low initial and maintenance costs. First stages of failure for critical components should be identified as soon as possible, and preferably with low cost, so as to have adequate time for the appropriate repair within an affordable budget to ensure safety and reliability of the system. Furthermore, damage progression monitoring allows estimates of remaining life and helps establish inspection and maintenance intervals.

A variety of crack identification techniques have been developed over the years to include optical inspection, use of liquid penetrant, use of magnetic particles, ultrasonic inspection, and eddy currents. The majority of these techniques are time-consuming and expensive and require special treatment of the structure, such as disassembly of some parts. Moreover, they generally are not used to identify damage in real time.

The need for real-time, low-cost damage detection, together with the limitations of traditional inspection techniques and the technological improvement in embedded actuators, sensors, reasoning algorithms, and life-prediction methodologies, support the nondestructive evaluation methods under the heading “Structural Health Monitoring” (SHM). SHM can be described as a continuous, autonomous in-service monitoring of a structure by means of embedded or attached sensors [1]. The advantages for safety and economy are

obvious. Furthermore, the picture of a structure can be changed from a mechanical “thing” to a clever organization that can detect localized damage sites similarly to a biological system.

Among SHM techniques, Lamb waves have been investigated for a number of years because these waves of an elastic type can efficiently travel long distances, and their propagation is affected by cracks and other defects in a structure. Thus, the generation and sensing of these waves in a structure can yield information on the state of structural damage. This information can then be used to assess system reliability, residual strength, and/or remaining life.

Figure 1. A Conceptual Illustration of Structural Health Monitoring [From 2].

B. LITERATURE SURVEY

A good starting point for the study of Lamb waves is Viktorov‘s classic 1967 text on Rayleigh and Lamb waves [3]. Viktorov provides both the theoretical foundation for Lamb wave propagation through elastic media and the application of such techniques for ultrasonic flaw detection. In the 1970s, Coppens and Wilson [4] analyzed the governing equations of the Lamb waves in

plates and gave some experimental results from I-bars of different materials. Scandrett studied the propagation of time-harmonic Rayleigh-Lamb waves in a biomaterial plate in the 1980s [5].

After 1990, many papers were published on the subject of Lamb waves, as the technology was well enough developed to consider them for real applications on airplanes and civil structures. Many of these papers also documented modeling of Lamb waves using computer simulations. The recent work of Se Jin Han at the Air Force Institute of Technology [6] was particularly relevant to this thesis. Han determined Lamb wave responses within a thin aluminum plate using finite element models in Abaqus. The results were compared to experimental results under isothermal and thermal gradient conditions. This work was supported by the Air Force Research Laboratory (AFRL). In support of AFRL's efforts to monitor structural integrity of existing and future aerospace vehicles, Olson et al. [7] have focused considerable effort on the analytical modeling of Lamb waves as an SHM technique. In their work, the use of finite element analyses for accurate, yet efficient, simulation of Lamb waves' behavior was demonstrated. They applied force and moment as inputs in their model to generate Lamb waves.

A significant amount of research has also addressed the types of materials and geometries of actuators/sensors to generate and sense Lamb waves in structures. Spedding [8] presented experimental data from sensors of various geometries made of polyvinylidene fluoride (PVDF), a piezoelectric polymer. He mentioned that PVDF offers the opportunity to explore new options in acoustic emission monitoring. He also demonstrated the basic components of sensors made of lead zirconate titanate (PZT), a piezoelectric ceramic that has been widely used in ultrasonics for a variety of applications.

Investigation and application of Lamb wave SHM has been made for both metallic and composite materials. Lee and Staszewski [9], [10] reported an application of the local interaction simulation approach for Lamb wave propagation in metallic structures. In the first part of their publication, they

analyzed the wave propagation, and in the second part they simulated two-dimensional Lamb waves that interacted with slot-type defects. Ihn and Chang [11], [12] developed a piezoelectric-based, built-in diagnostic technique for monitoring fatigue crack growth in metallic structures. Kessler et al. [13] presented part of an experimental and analytical survey of candidate methods for in-situ damage detection of composite materials. A great source of documentation for recent work in this field is Victor Giurgiutiu's book [14]. It provides all the necessary background information for SHM using piezoelectric active sensors.

Kwon and Bang [15] analyzed the finite element method. The knowledge from this book was used in the creation of the finite element models and evaluation of the results. The reference to the singular-type elements was very important for the accurate modeling of the stress field around the crack tips as described in Chapter VI. Delsanto et al. [16]–[18] used a finite difference scheme and parallel computing to investigate ultrasonic wave propagation in a specimen of arbitrary complexity for one-, two-, and three-dimensional cases.

Many other papers applied finite element methods for wave modeling. Marckerle [19] gave a bibliographical review of the finite element modeling of nondestructive material evaluation. Su [20] proposed and evaluated a numerical and experimental elimination scheme for a carbon fiber/epoxy (CF/EP) composite laminate based on Lamb waves. Alleyne and Cawley [21] investigated and checked experimentally the interaction of individual Lamb waves with a variety of defects in a composite plate. Finally, Moulin et al. [22] also showed that Lamb waves may be effectively generated and sensed using a piezoelectric transducer embedded inside a composite plate.

Additional background on the generation and sensing of elastic waves, particularly Lamb waves, is provided in Chapter II. This discussion includes both theoretical and practical considerations.

C. OBJECTIVES

In this thesis, Lamb wave propagation in a thin aluminum plate was modeled using a two-dimensional finite element model. The commercial software ANSYS was used as a multiphysics modeling and analysis environment. Development of the general model is discussed in detail in Chapter III.

The focus of the research was to address the following three modeling issues: First, a comparison of different wave generation inputs to the finite element model was accomplished to analyze the differences between generating the wave using sinusoidal force (or displacement) at specified nodes versus modeling the piezoelectric actuator itself and subjecting it to an applied sinusoidal voltage signal. Chapter IV addresses this first issue. Second, the existence of a crack (i.e., a disbonding of the adhesive layer) between the wave generation device and the structure was analyzed both for the piezoelectric actuator that generates the waves and the sensor that measures the output. This modeling and analysis is discussed in Chapter V. For the final research issue, Chapter VI focuses on the fidelity of structural crack modeling in the finite element model. In particular, the use of contact elements was evaluated to assess their importance for the accurate prediction of the wave scattering from cracks or defects inside the structure.

Finally, Chapter VII presents a summary of conclusions and recommendations from this research. In addition, avenues for future research using the developed model or results are proposed.

THIS PAGE INTENTIONALLY LEFT BLANK

II. ELASTIC WAVES IN TWO DIMENSIONS

A. ELASTIC WAVES IN SOLIDS

Mechanical waves are waves that propagate through a material medium (solid, liquid, or gas) at a wave speed that depends on the elastic and inertial properties of that medium [22]. There are four basic types of wave motion for mechanical waves: longitudinal waves, transverse waves, Rayleigh waves, and Love waves. Figure 2 demonstrates these types of waves and illustrates the difference between the motion of the wave and the motion of the particles in the medium through which the wave is travelling. Of these four types of waves, the first two or a combination of the first three were usually observed.

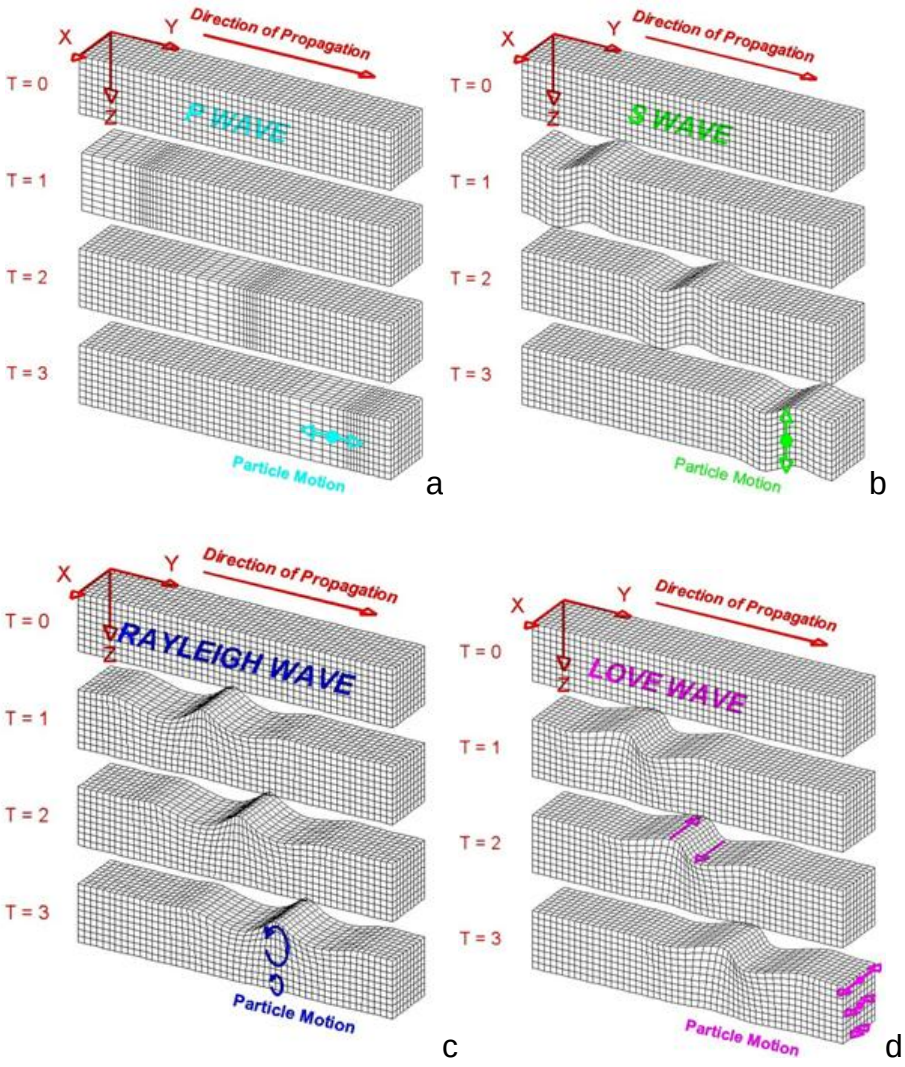

Figure 2. Types of Elastic Waves in Solids: (a) Longitudinal Waves (b) Shear Waves (c) Rayleigh waves (d) Love Waves [From 23].

B. THEORY OF ELASTICITY: GOVERNING EQUATIONS

The equations of motion for the two-dimensional elasticity problem are discussed in detail from Y. W. Kwon [15]. For a two-dimensional case, these equations are

$$\rho \frac{\partial^2 u}{\partial t^2} = \frac{\partial \sigma_x}{\partial x} + \frac{\partial \tau_{xy}}{\partial y} + f_x$$

$$\rho \frac{\partial^2 v}{\partial t^2} = \frac{\partial \tau_{xy}}{\partial x} + \frac{\partial \sigma_y}{\partial y} + f_y$$

where u,v is the displacement in the x and y direction, σ_x and σ_y are the normal stresses, τ_{xy} is the shear stress, and f_x, f_y are the body forces, respectively.

The next set of equations relates the stresses with the strains. For an isotropic material, these constitutive equations have the form

$$\{\sigma\} = [D]\{\varepsilon\}$$

with the matrix [D] having the following form for the plane strain condition:

$$[D] = \frac{E(1-\nu)}{(1+\nu)(1-2\nu)} \begin{pmatrix} 1 & \frac{\nu}{1-\nu} & 0 \\ \frac{\nu}{1-\nu} & 1 & 0 \\ 0 & 0 & \frac{1-2\nu}{2(1-\nu)} \end{pmatrix}$$

where v is the Poisson ratio. On top of these equations, we also have the kinematic equations, which relate strain to displacement.

$$\begin{Bmatrix} \varepsilon_x \\ \varepsilon_y \\ \gamma_{xy} \end{Bmatrix} = \begin{Bmatrix} \frac{\partial u}{\partial x} \\ \frac{\partial v}{\partial y} \\ \frac{\partial u}{\partial y} + \frac{\partial v}{\partial x} \end{Bmatrix}$$

The above equations form a close set of equations that are very difficult to be solved analytically. So, the finite element method is a good tool to obtain a solution.

C. LAMB WAVES

As I. Viktorov describes in his book [3],

> Lamb waves refer to elastic perturbations propagating in a solid plate with free boundaries, for which displacements occur both in the direction of wave propagation and perpendicularly to the plane of the plate.

In general, Lamb waves depend on the elastic properties of the medium (density, modulus of elasticity, shear modulus). Starting from the wave equation, one can find two solutions: a symmetric solution and an antisymmetric solution, which correspond to the two wave forms shown below. References [3] and [14] demonstrate the solution process.

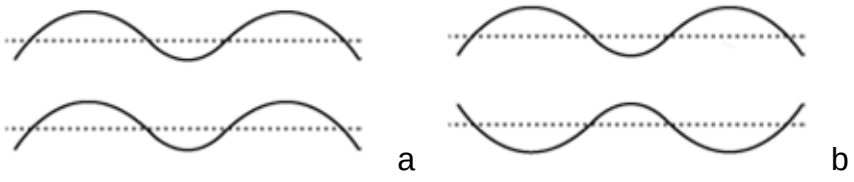

Figure 3. Lamb Waves: S mode (a), A mode (b).

An important parameter of the Lamb waves is their dispersion properties. Their group and phase velocities depend on the properties of the medium, on the frequency, and on the thickness of the structure. Numerical solutions are required for the creation of the dispersion curves. The following figure gives the dispersion curves for aluminum as computed from the Tongji University in Shanghai:

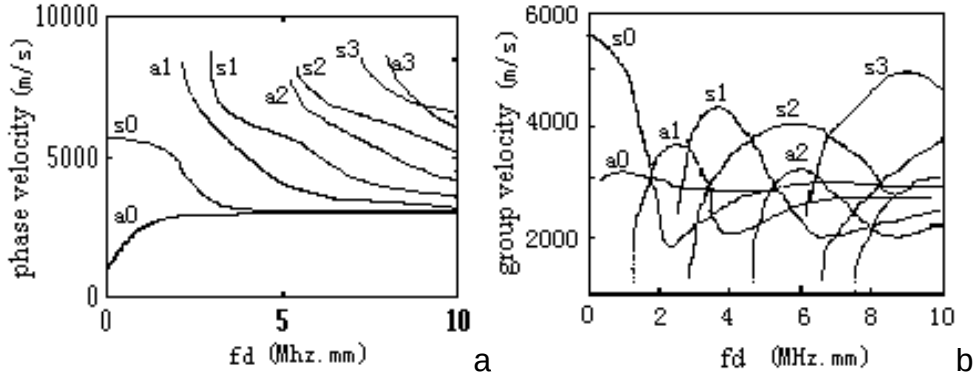

Figure 4. Velocities of Lamb Waves: Phase Velocity (a), Group Velocity (b) [From 24].

D. PIEZOELECTRICITY

Principles of piezoelectricity are described in many books. A good reference for an understanding of the theory is the book from APC International [25] and Giurgiutiu's book [14], which focuses more on SHM applications.

In this section, the constitutive equations of piezoelectricity are presented as they are used in the ANSYS software. In linear piezoelectricity, the equations of elasticity are coupled to the charge equation of electrostatics by means of piezoelectric constants [26]

$$\begin{Bmatrix} \{T\} \\ \{D\} \end{Bmatrix} = \begin{bmatrix} [c^E] & [e] \\ [e]^T & -[\varepsilon^S] \end{bmatrix} * \begin{Bmatrix} \{S\} \\ -\{E\} \end{Bmatrix}$$

where

$\{T\}$ is the stress vector

$\{D\}$ is the electric flux density vector

$\{S\}$ is the strain vector

$\{E\}$ is the electric fluid intensity vector

$\{c^E\}$ is the elasticity matrix whose elements are inserted from the user using the material properties commands

$\{e\}$ is the piezoelectric stress matrix, which relates the electric field vector to the stress vector

$\{\varepsilon^S\}$ is the dielectric matrix that includes the electrical permittivities of the material.

III. MODEL DEVELOPMENT

A. GENERAL MODEL AND SIMPLIFICATIONS

The purpose of this chapter is to model the wave propagation in a relatively large and thin plate like the one shown in Figure 5. The plate has a piezoelectric transmitter, which creates elastic waves, and a strain sensor at a different location. With this formulation, it is possible to monitor stress waves and, of course, to compare the response of a healthy plate with the response of a damaged one.

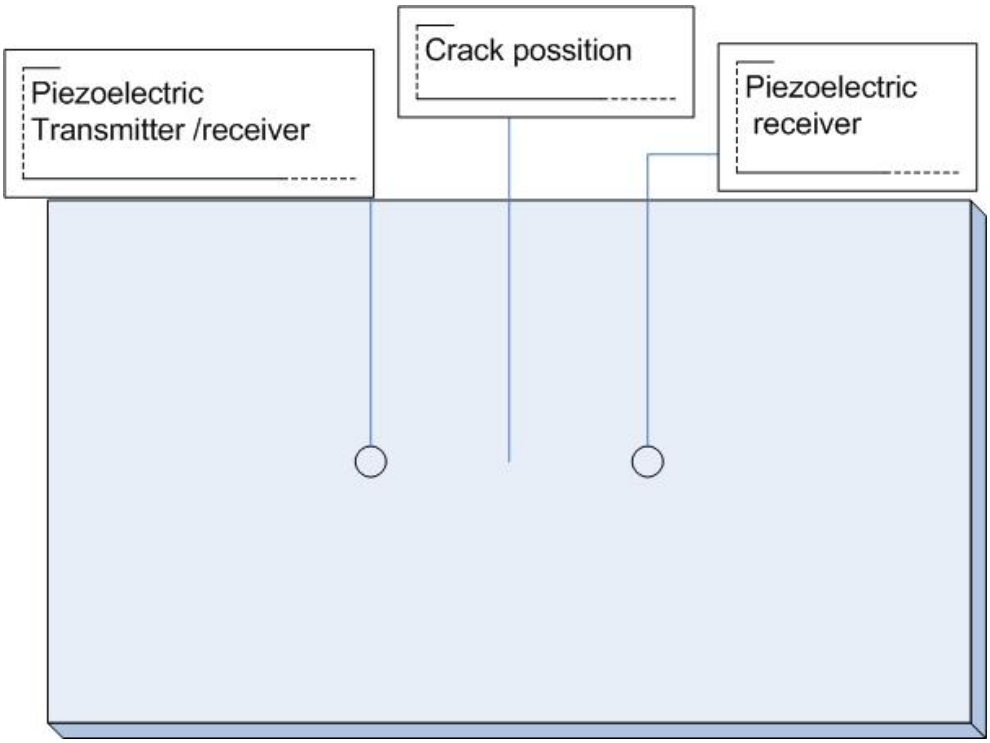

Figure 5. The Actual Lamb Wave Experiment.

To save computational time, a two-dimensional plain strain model was created, as we can see in Figure 6. It is like cutting the above plate along the line that connects the transmitter and the receiver. The rest of the material to the left and to the right of this theoretical cut creates the boundary conditions for the plain strain model.

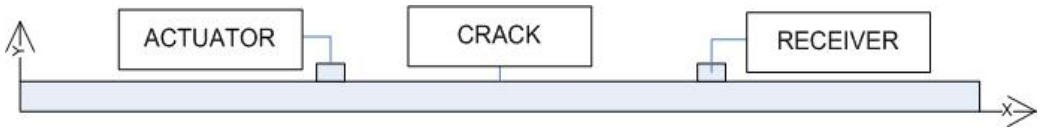

Figure 6. The Two-Dimension Simplification of the Three-Dimension Case of Figure 5.

The box to the left of the above figure is the piezoelectric actuator and to the right is the sensor. The geometry of the plate is simple. A rectangular plate was created in the ANSYS software. The length of the plate was varied from 0.6 m to 3 m according to the needs of every simulation. The model was kept as small as possible to save computational resources. The thickness of the plate was between 1 mm and 3 mm, again depending on the simulation.

The material chosen for the plate was aluminum with the following properties: modulus of elasticity E=68.95 GPa, Poisson ratio v=0.33, density ρ=2767.8 kg/m^3. For some simulations, the piezoelectric actuator and sensor were also modeled. Two different piezoelectric-elastoelectric materials were used: polyvinylidene fluoride (PVDF) and lead zirconate titanate (PZT-4) with material properties from the ANSYS documentation.

The elements that were used are the PLANE 82 type for the aluminum and the PLANE 223 for the piezoelectric-elastoelectric materials. They are both two-dimensional elements with eight nodes and two or three degrees of freedom per node: translation in the x direction, translation in the y direction, and electric potential. They are relatively accurate elements and can be used in difficult geometries without loss of accuracy. Moreover, for precise modeling of the cracks, singular elements were used around the crack tip. These elements were the triangular version of the above two, as shown in Figure 7. As it is mentioned in Kwon's book [15], the proper selection of the position of the nodes creates a rapid increase of the stress field inside the element, a characteristic of the crack's tips. Finally, contact elements were also used throughout this thesis for cases where overlapping of different materials should be prevented. These are the TARGE 169 and CONTA 172 from the ANSYS library. Figure 8 presents these

types of elements. ANSYS 11.0-release documentation gives a lot of information about the use and the different options available for these types of elements. It is important to be mentioned that the use of contact elements makes the analysis nonlinear, and the computational time increases dramatically, especially when the elements are active. For this case, many iterations were performed from the FE software to achieve the required convergence.

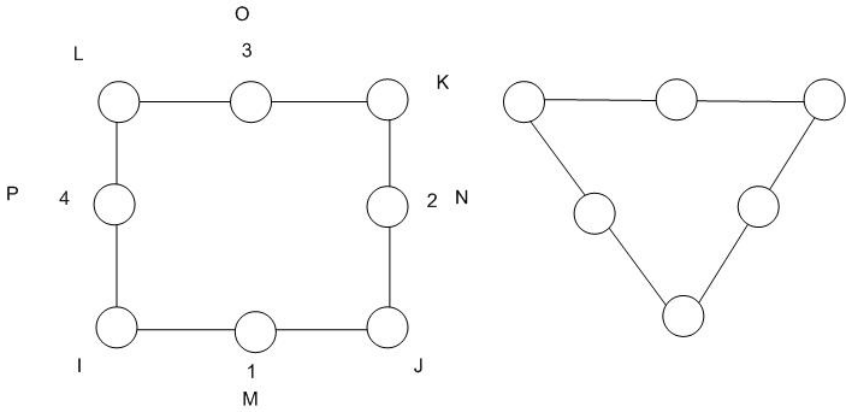

Figure 7. The Element Used.

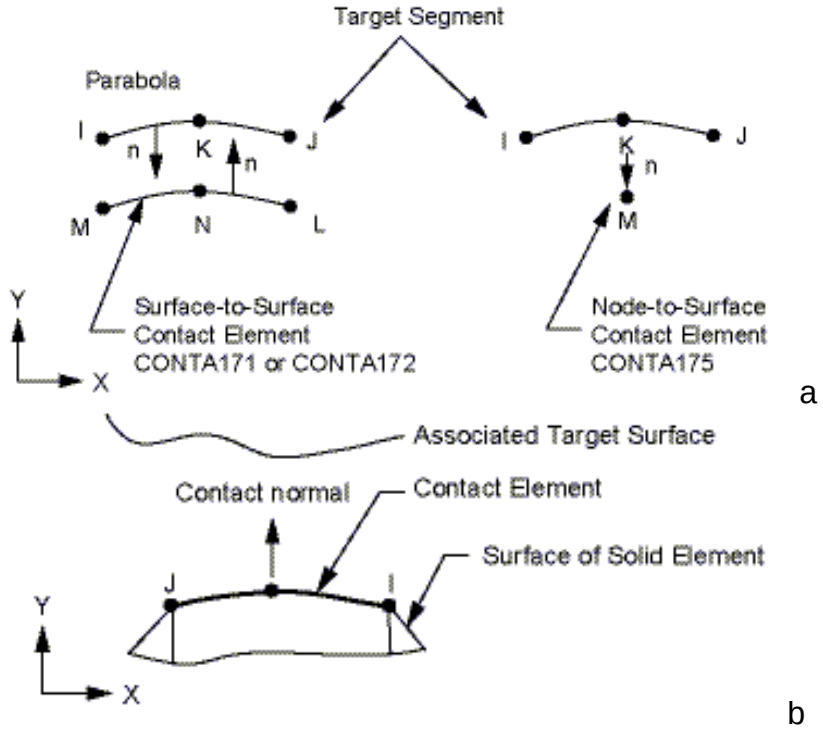

Figure 8. TARGE 169 Element Geometry (a), CONTA 172 Element Geometry (b).

The element size chosen was small enough so as to have an accurate solution. A convergence study as a function of the element size is available in the third chapter.

Cracks inside the plate were modeled in two different ways. Initially, a simplified approach of a small gap inside the aluminum was used. From the initial homogeneous plate, a small area was removed. The thickness of this area was kept low compared to the length of the crack. The second approach was more realistic. A line crack was created with an initial zero opening. Singular elements were placed around the crack tips, and contact elements were used to avoid overlapping of the two sides of the crack. Figure 9 shows these two types of cracks:

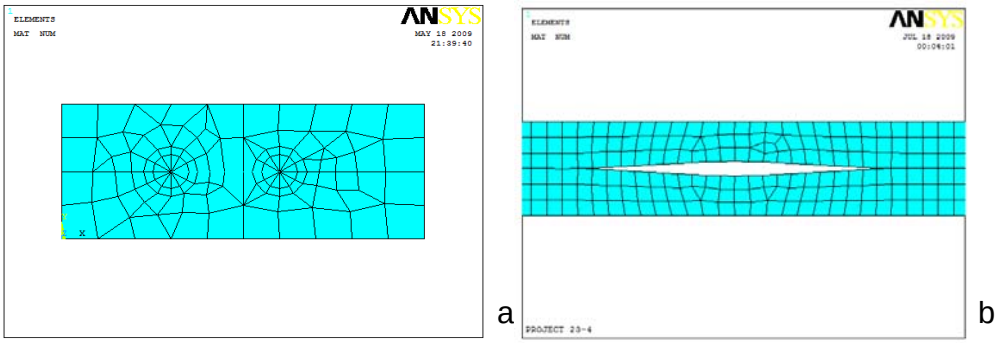

Figure 9. Modeling of Cracks: Line Cracks (a), Diamond Cracks (b).

Different sizes of horizontal and vertical cracks were modeled. All the cracks were positioned in the middle of the plate's thickness. The following table summarizes the dimensions and types of all the cracks that were used in this study. In the majority of the simulations, the finite element mesh was refined around the crack so as to have an accurate solution.

Types and Dimensions of Cracks			
Line Cracks		Diamond-type Cracks	
Horizontal	10 cm x 0 mm	Horizontal	1 mm x 5 μm
		Vertical	1 mm x 50 μm
		Vertical	0.6 mm x 50 μm
		Vertical	0.5 mm x 5 μm

Table 1. Types and Dimensions of Cracks in this thesis.

The type of analysis was full Transient. The time step was chosen so as to have an accurate solution but also a reasonable computational time. Geometric boundary conditions were not applied to the model. The plate was kept as free as possible so as to give an accurate response. ANSYS allows a choice between Newmark and HHT algorithms for time integration. The first was chosen with the default settings.

B. IDENTIFICATION OF WAVES

Before using the finite element model to attack the research questions, it was important to verify the existence of the two types of waves and to compare the theoretical values of velocities with those from the model of Figure 6. A full multiphysics analysis was performed, and the actuator and sensor were modeled as piezoelectric materials made of PZT-4. Voltage was applied top and bottom to the actuator. The voltage was a function of time, and it consisted of five periods of a sine wave with a central frequency 100 kHz. The sinusoidal form of the input was selected because it reduces the energy at frequencies other than the excitation, as is mentioned by Han [6] and, of course, it is a realistic input, available in every laboratory. In Han's work, this input produced great agreement between the numerical and experimental results. The exact equation of the voltage input was:

$$V(t) = 100\sin(40000\pi t)\sin(200000\pi t)$$

The following figures present the already-described model. Of course, for the identification of the Lamb waves, no crack was modeled in the middle of the bar.

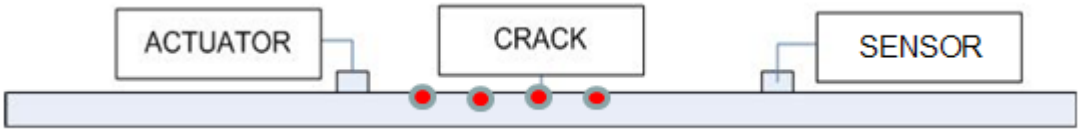

Figure 10. Identification of Lamb Waves at four different Points (red dots).

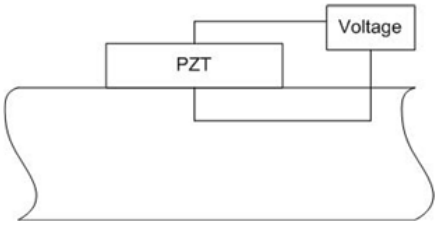

Figure 11. Voltage Input on the Finite Element Model.

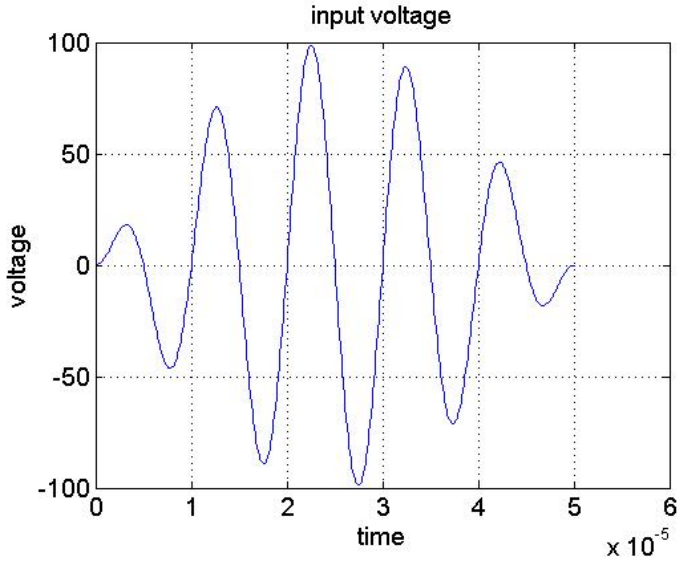

Figure 12. Plot of the Sinusoidal Voltage Input used in this Paper.

The horizontal elastic strain at four different points on the upper surface of the aluminum plate of Figure 10 was compared. The following figure gives these four different plots.

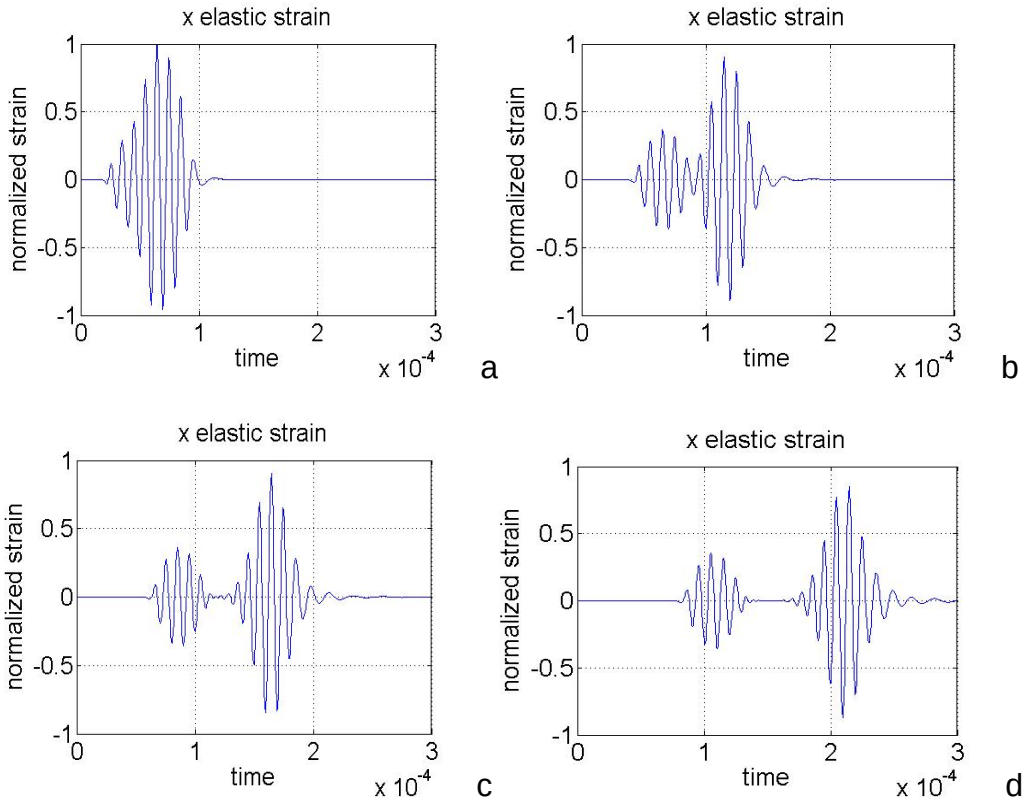

Figure 13. Horizontal Elastic Strain at the four Different Location Shown as Red Dots on Figure 9. The two Lamb Wave Modes are Present.

The subplot “a” represents the first check point, which is very close to the excitation. There are two wave forms but they overlap. The next subplot, “b,” gives the strain at the second point away from the actuator. The two wave forms are clearer here. On the third and forth, the longitudinal and shear waves are separated, and the theoretical speed of these two waves can be estimated easily and compared with the experimental values for the frequency and thickness of the aluminum plate as they are presented in Chapter II.

The clear recognition of these two wave forms, S0 and A0, is very important for this paper, so a second test was performed to verify that these two

waves that are present in Figure 12 are indeed the longitudinal and the shear waves respectively. At a specific distance away from the excitation (PZT-4 input), the horizontal displacement of two different nodes was compared. The first node was on the upper surface of the aluminum plate and the second on the bottom of it. Figure 14 gives the results.

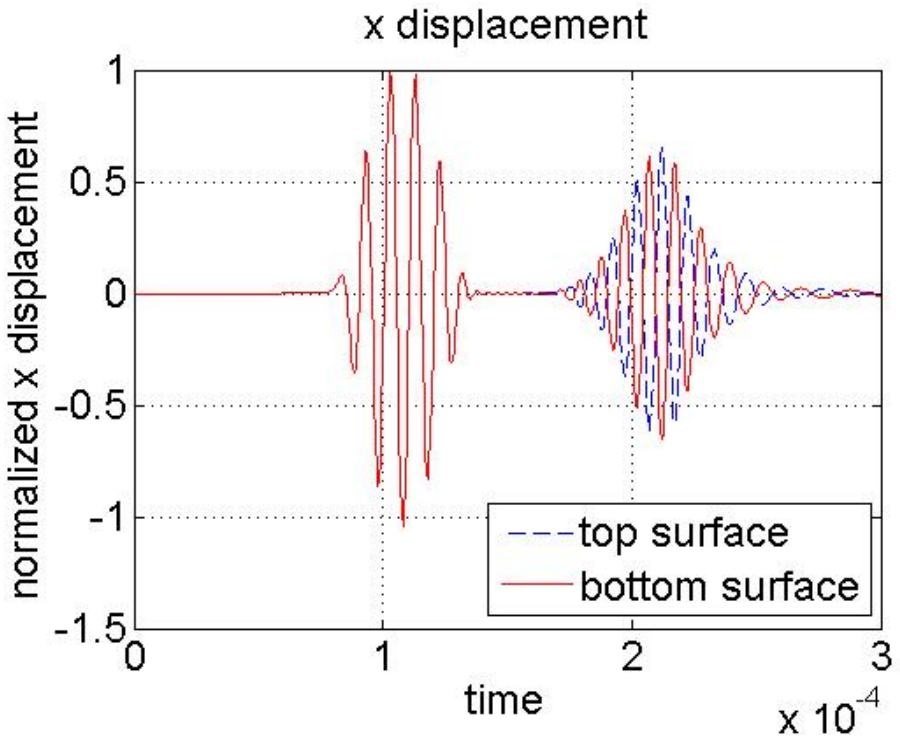

Figure 14. Identification of S0 and A0 Lamb Wave Modes. Comparison of the Horizontal Displacement of the Nodes on Top and on Bottom of the Aluminum Plate.

It is obvious that during the first wave form (longitudinal wave), the top and bottom nodes are moving in the same direction, while during the second wave, the nodes are moving in exactly opposite directions. This phenomenon validates the assumption that the first is the longitudinal wave and the second is the transverse wave. Finally, a third test was performed. The vertical displacement of a node exactly on the center line of the aluminum plate was plotted in Figure 10.

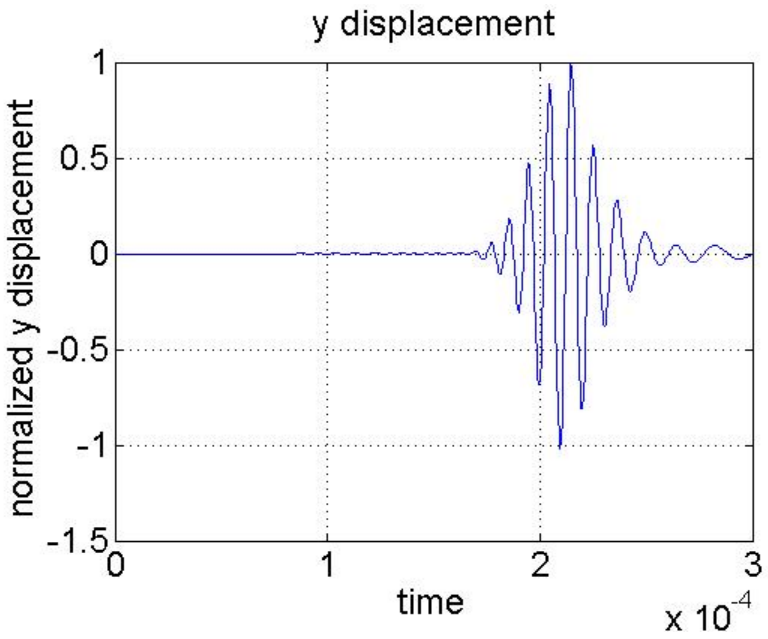

Figure 15. Identification of S0 and A0 Lamb Wave Modes. Vertical Displacement of a Node at the Center Line of the Aluminum Plate. The Response during the Symmetric Wave is almost Zero.

In Figure 15, only one wave form is present. This makes sense because during the longitudinal wave, the middle nodes do not move because it is a symmetric wave form. The transverse wave is the same as in Figure 14.

C. CONVERGENCE STUDY

1. Element Size

The first step in our research was to verify the results from the numerical calculations. The commercial package ANSYS was used in the project, so we started with a convergence study by comparing the results using different sizes of elements and time steps. The input was as simple as possible. Horizontal displacement was applied at one node on top of the aluminum plate, which had a 3-mm thickness, as shown in Figure 16.

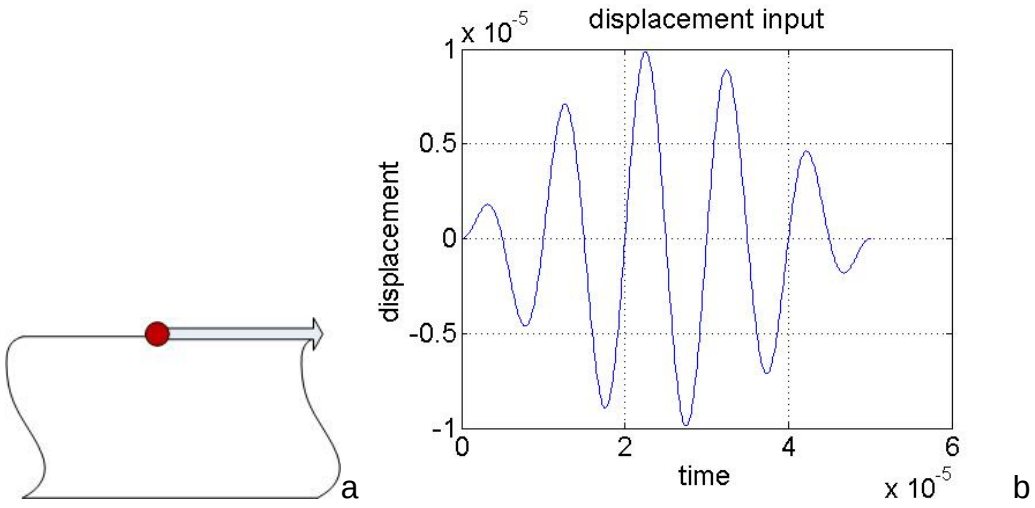

Figure 16. The Simplified Model (a) and Displacement Input (b) used for the Element Size Convergent Study.

This horizontal displacement generated Lamb waves. Exactly the same problem was run using four different element lengths, 1 mm (1 element per thickness), 0.5 mm (2 elements per thickness), 0.2 (5 elements per thickness), 0.1mm (10 elements per thickness). The normalized horizontal displacement at the same point was compared and presented on the following graph.

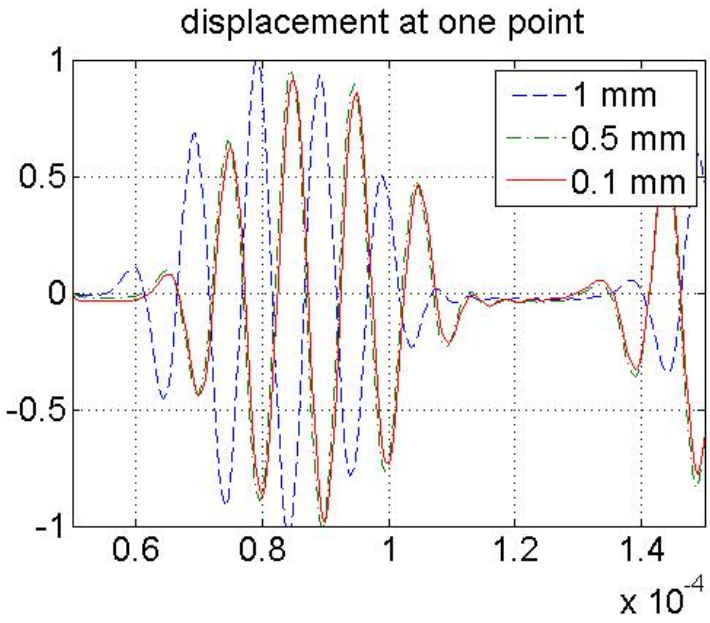

Figure 17. Convergent Study. Horizontal Displacement at the Same Point for Different Element Sizes.

By comparison, an element with length 0.5 mm is good enough. Usually, in our calculations elements with lengths of less than 0.5 mm were used, but again, keeping in mind the increase in computational time.

2. Time Step

The next important issue was the effect of time step. For this convergent study, Lamb waves were generated by application of horizontal displacement at two nodes on top of the aluminum plate. These two nodes would be the theoretical end points of the piezoelectric material that could be used in a real experiment, as we can see in the next figure. The displacements were the same as this in Figure 16 but with opposite signs for the left and right node.

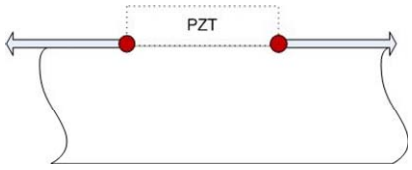

Figure 18. Two-nodes' Horizontal Displacement Input.

The results are shown in Figure 19. Of course, the time step must be chosen according to the frequency of the excitation and the element size. In our study, for the majority of simulations, the frequency used was 100 kHz and the element size was smaller than 0.5 mm. Time steps smaller than 500 nsec worked very well. In fact, for the greater part of our simulations, we used 50 nsec.

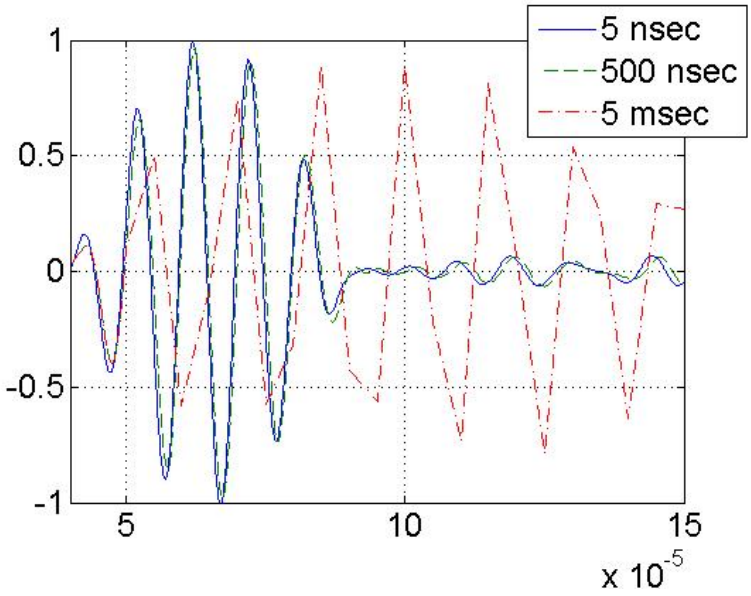

Figure 19. Horizontal Displacement at the Same Point using Three Different Time Steps.

D. EFFECT OF THE FREQUENCY

In this part of the paper, the effect of the input's frequency on the wave propagation and interaction with cracks was investigated using two different simulations. The first was performed in the first stages of the research; the second, at the end. Both of them are mentioned here to demonstrate an important parameter of the ANSYS software. For the first simulation the time-dependant load was applied using the "ramp load" option from the ANSYS menu, whereas the last uses the "step load" choice. Although both simulations answered the question of this heading, the results are better using the second option of ANSYS. This is an important point to remember for future simulations.

For the first simulation an aluminum plate was chosen with dimensions 3 m x 3 mm. To generate Lamb waves, the same two-node approach described in the previous heading was used (Figure 18). The frequencies of the inputs were 20 kHz, 80 kHz, and 160 kHz. For this set of simulations, only one period of a

sine wave was applied. The horizontal displacement at the same point away from the excitation can be shown in the next figure for all three of the different input frequencies.

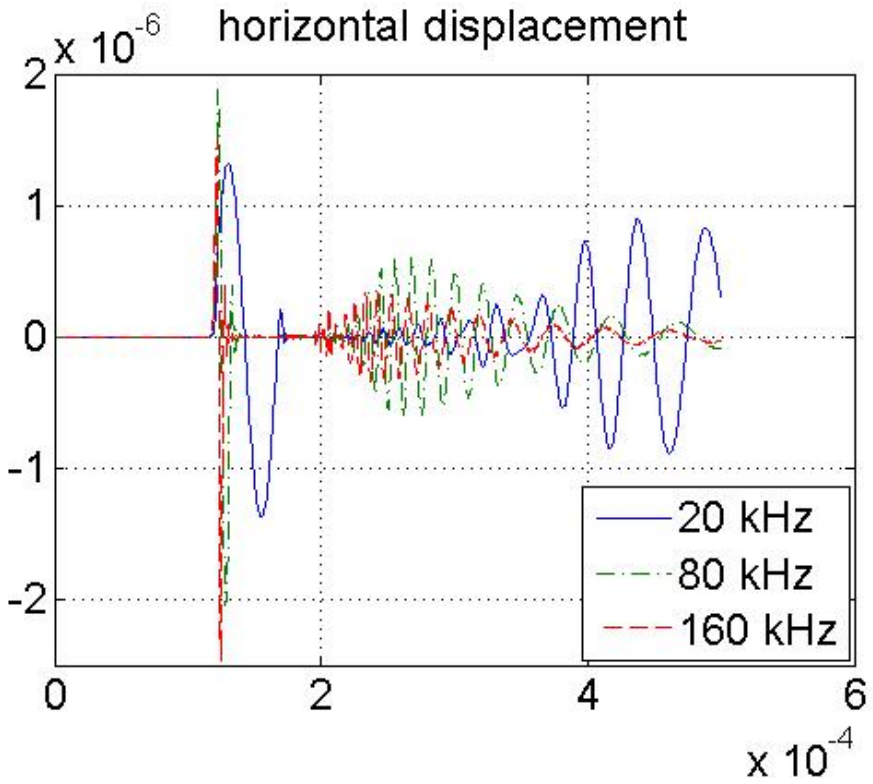

Figure 20. Horizontal Displacement at the Same Location using Three Different Input Frequencies

Comparing the responses, it can be argued that the velocity of the longitudinal wave is the same, independent of the frequency of the excitation. Likewise, the antisymmetric wave (second wave in the figures) is affected by the input frequency. Differences are detected in the maximum values of the bending waves and in the time that these values occur. The maximum value of the bending wave for the 20 kHz excitation happens at 0.438 msec, while the maximum for 80 kHz and 160 kHz is at about 0.269 msec and 0.242 msec respectively. A final comment on the above responses is that the wave forms are not smooth. The longitudinal wave is not symmetric around the horizontal axis. This is more obvious in the third case (160 kHz) excitation. Furthermore, at the

end of the longitudinal wave there are small oscillations. These can be caused by the quick change in the magnitude of the one-cycle sine wave used as an input here.

To investigate further the effect of the frequency on our model, the following complete simulation was developed:

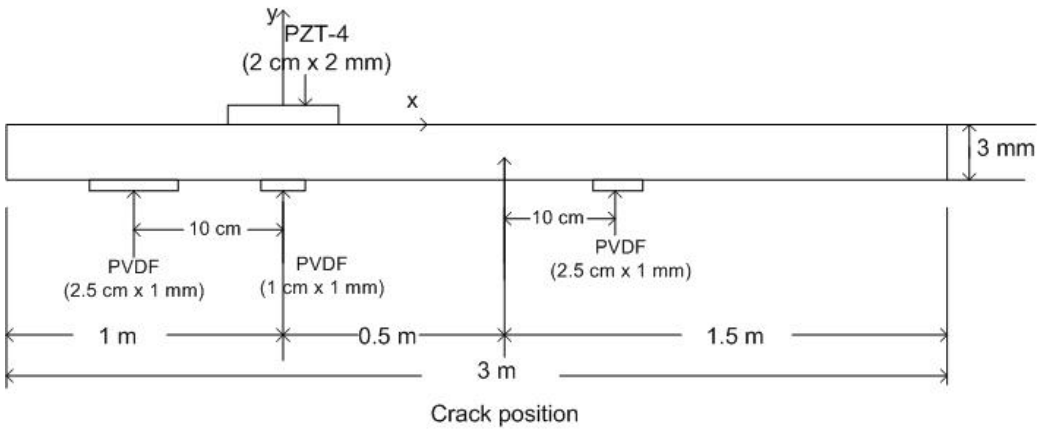

Figure 21. Model developed to Investigate the Effect of the Frequency on Lamb Waves and the Voltage Output using Different Piezoelectric Materials.

It consists of an aluminum plate (2.5 m x 3 mm), and it has three piezoelectric patches on the upper surface. Two of these are from PVDF, and one is made of PZT-4. In the middle of the plate, a horizontal crack was created with dimensions 1 cm x 0.5 mm as in the next figure.

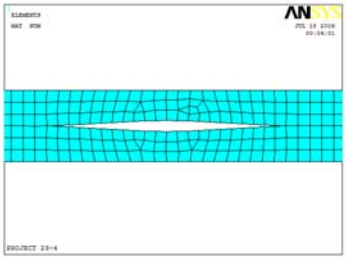

Figure 22. Image of the Diamond-Type Crack used in this Simulation.

Voltage was applied on the top and bottom of the PZT-4 material with maximum amplitude of 100 volts. The same simulation was run using 50, 100,

and 200 kHz for the excitation. The main purpose of the above three simulations was to compare the voltage output of the sensors for the same geometry but using different frequencies. At the same time, as a secondary objective, this model uses different piezoelectric materials to investigate the possible differences on the output caused by the different piezoelectric properties. Direct comparison between the voltage output caused by the reflected S0 wave from the position of the crack and measured on the PZT-4 and PVDF sensors validates the statement published by Spedding [8] that PVDF can be used as an alternative for PZTs.

Moreover, a first step on the interference between cracks and different frequency Lamb waves was done. The voltage output of the PVDF sensor to the left follows:

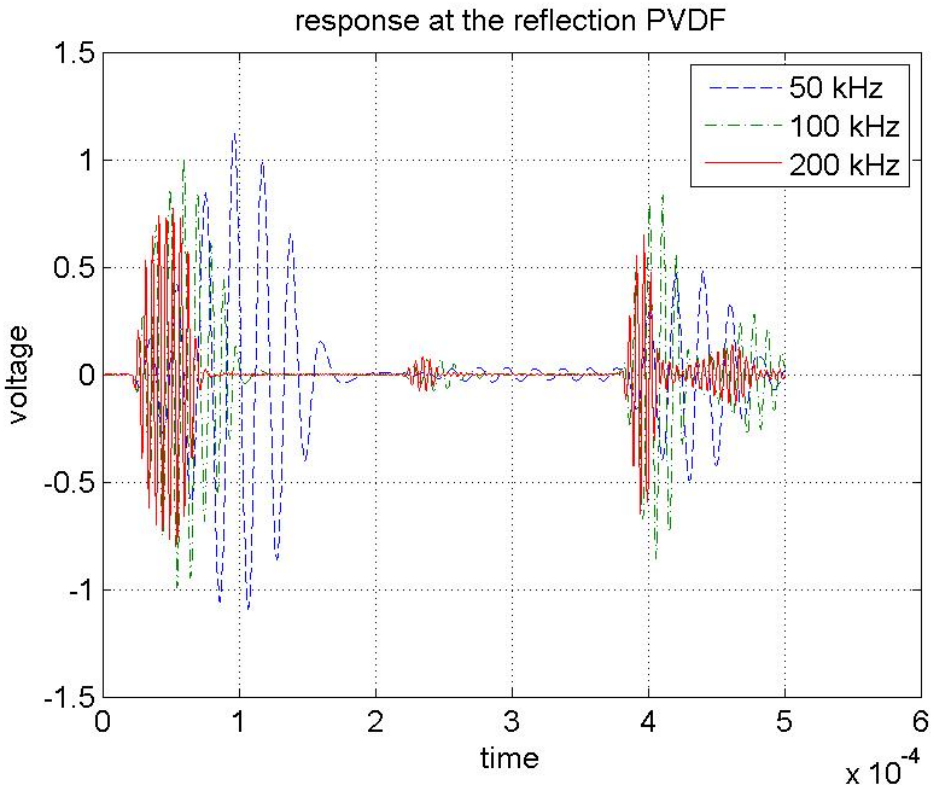

Figure 23. The Voltage Putput from the pvdf to the Left Side of the Model. Three Wave Forms are Present using Different Frequencies (Input Signal, Reflection from the Crack, Reflection from the end of the Rod).

In Figure 23, three wave packages are present. From 0 to 0.2 msec is the voltage output because of the initial Lamb waves that travel from the excitation (PZT-4) to the left. At around 0.23 msec the reflected wave from the crack's position starts, according to the pulse-echo technique. Finally, at time 0.38 msec the reflection of the longitudinal wave from the left end of the bar starts.

The amplitude of the voltage output for the first wave package decreases for higher frequencies. This means that the PVDF sensor has a larger output for 50 kHz than for 200 kHz. This voltage output is caused from both the longitudinal and the shear waves as they are still overlapped at this location on the aluminum plate, which is close to the excitation. Probably this overlapping of the two modes of Lamb waves develops different maximum average strain at the sensor and it decreases the voltage output. Another reason could be the relative size of the sensor compared to the wave length of the longitudinal wave, as this could also develop different average strains in the PVDF.

Comparatively, a close observation of the reflection from the crack (at 0.23 msec) shows that higher frequencies give better results. The maximum voltage output for 50 kHz is less than that of 100 and 200 kHz. This is consistent with the common idea that higher frequencies reflect better from small defects. The next table and figure summarize the top voltage outputs for these three different frequencies.

	Type of wave	
	First wave S0 + A0 modes	Reflection from the crack S0 mode
50 kHz	1.122 V	0.03336 V
100 kHz	1 V	0.07434 V
200 kHz	0.7752 V	0.07925 V

Table 2. Summary of the Voltage Output of this Model (Figure 19) from the PVDF Sensors on the left of Figure 21, for Different Frequencies.

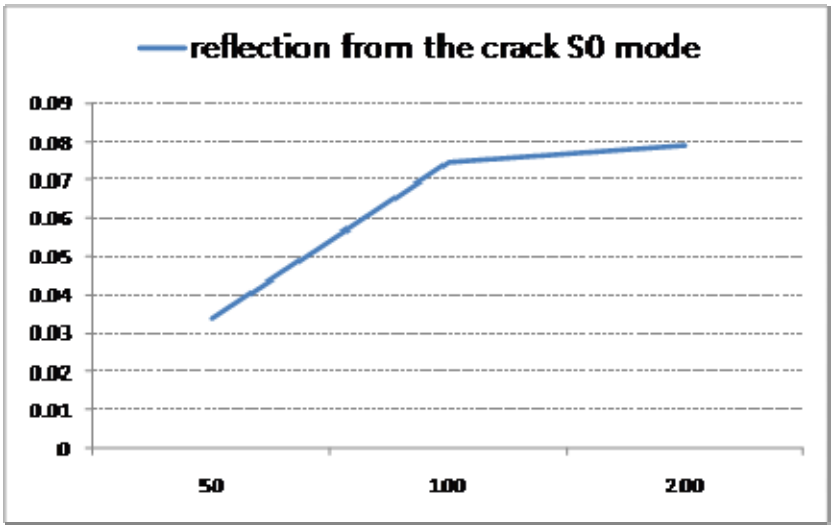

Figure 24. Voltage Output of the Right PVDF Sensor from Figure 19 for Three Different Frequencies: 50, 100, and 200 kHz.

The above three-point plot shows that higher frequencies work better for crack identification techniques. The voltage output starts to flatten out above 100 kHz. Although frequencies above 200 kHz were not used in this paper, it looks as though this plot is consistent with the experimental observations from various papers that an optimum frequency for SHM applications is at around 300 kHz.

Similarly, the following figure gives the voltage output from the sensor to the right of the crack. At every frequency the two wave forms (S0 and A0) are present. As has already been presented in Figure 18, the S0 mode is not affected very much from different frequencies but the A0 mode changes a lot.

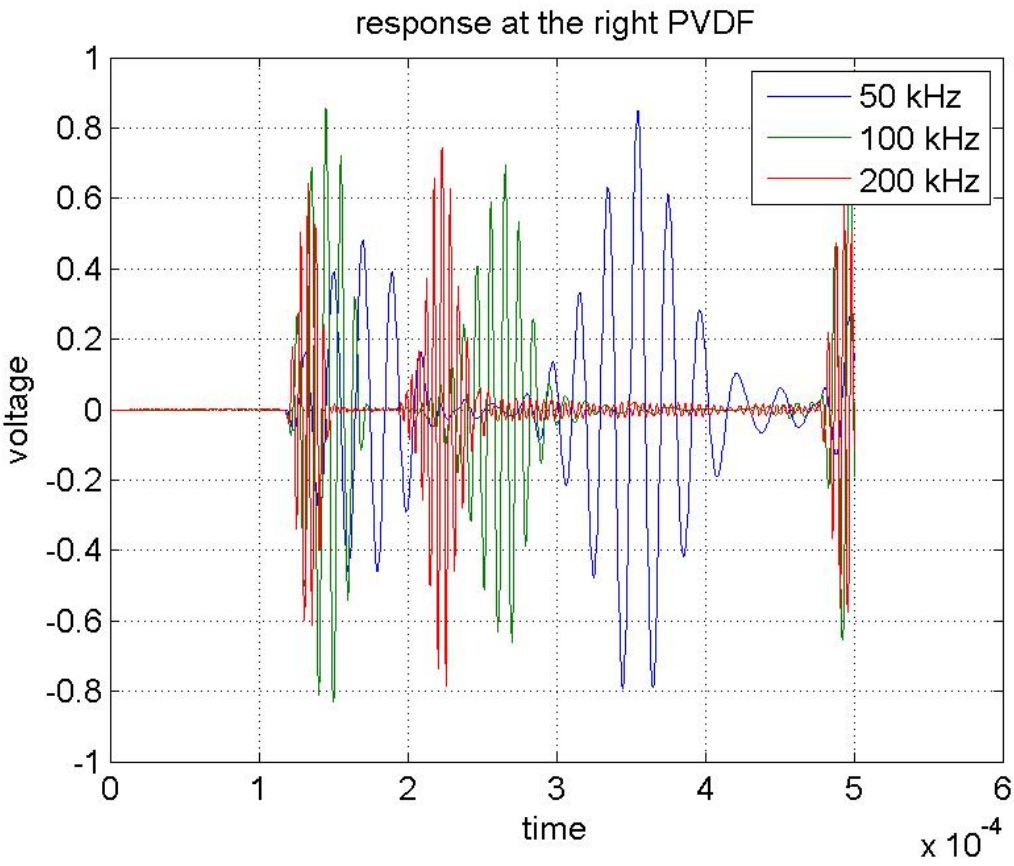

Figure 25 The Voltage Output from the PVDF to the Right Side of the Model in Figure 19. S0 and A0 Modes are Present using Different Frequencies.

E. SUMMARY

Comparing all the figures in this chapter, some interesting conclusions can be made. The primary (S0) wave is almost the same as the input signal, and it is not affected as much as the antisymmetric one. On the contrary, the shear wave is different. Many previous studies mentioned in the literature survey verify that the bending waves are affected more from external parameters such as thickness and frequency. Indeed, a closer look at the secondary wave in Figure 14 shows that the period of the shear wave's oscillations is smaller at the beginning of the A0 mode and larger at the end. This indicates roughly that the S waves contain different frequencies. As a result, we believe that a structural health monitoring technique based on Lamb waves could take advantage of both

of these two different features. For instance, crack identification using the pulse-echo technique is better utilizing the advantage of the S0's constant shape and higher velocity. Likewise, using the pitch-catch technique, the SHM system can easily identify damage initially from a reduction on the amplitude of the longitudinal wave and secondly from the change on the easily affected shear wave because of the crack's existence, which changes the local properties of the rod. More numerical simulations in Chapter VI support the above statements.

The results presented in this chapter are used to attack the research questions of this paper. In particular, the element size and time step were kept below the critical values for accurate results. Although different frequencies are used in this section and some of them give better reflection waves from the crack, the rest of the thesis uses the 100-kHz excitation frequency.

THIS PAGE INTENTIONALLY LEFT BLANK

IV. EFFECTS OF INPUT MODELING ON WAVE GENERATION

Going back to our first research question, one of the most critical issues for a finite element model that deals with Lamb waves is the generation of these elastic waves. In reality, piezoelectric materials are glued onto the structure and voltage is applied on the top and bottom of them. Spedding [7] gives a lot of information on the geometry and pictures of how a commercial piezoelectric actuator/sensor is manufactured. In the following figure, it is obvious that the voltage is applied almost homogeneously on top and on bottom of the piezoelectric material.

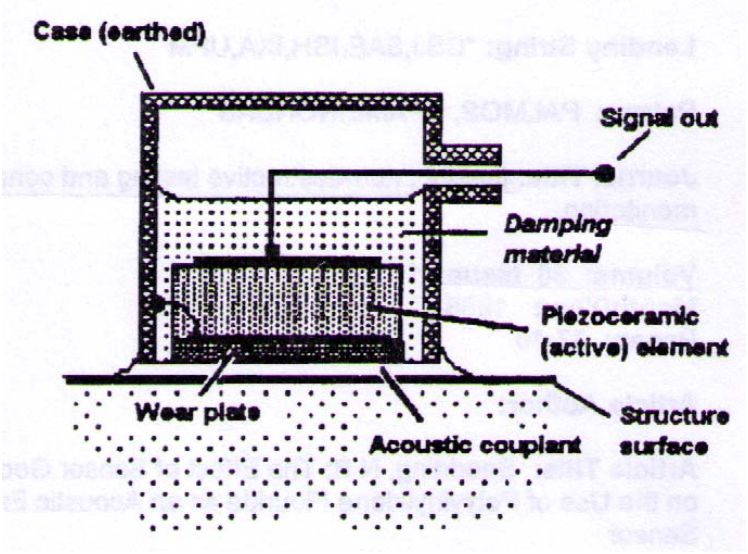

Figure 26. Cross-section of a Typical PZT Sensor [From 8].

In general, there are different ways to generate Lamb waves on a finite element model. Some of them that are commonly used are shown in the next figure.

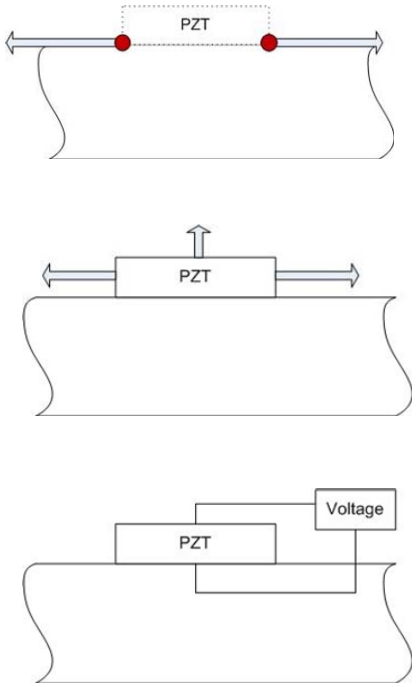

Figure 27. Different Methods of Lamb Wave Generation on Finite Element Models.

As a simple approximation, the piezoelectric actuator is not modeled at all. The elastic waves are generated by the application of horizontal force or displacement on two nodes on the free surface of the structure. These nodes would be the ends of the theoretical piezoelectric material. Our study has shown that there is no important difference between the application of horizontal displacement and force, a fact that is generally valid for linear elastic materials. A successful example of applying force for wave generation is Han's thesis [6]. Besides that, applying displacement has the following advantage: From the difference of the displacement, one can get an idea of the average elastic strain that is generated from the theoretical piezoelectric material using the fundamental equation:

$$\varepsilon = \frac{\Delta l}{l_0}$$

In other words, it is easier to make a rough estimation of the value of the displacement required for the generation of a reasonable strain. In contrast, the application of force needs a trial-and-error procedure. The researcher has to run multiple simulations or use some analytic equations to be sure that the elastic strain that is generated on the finite element model is close to the one from real actuators.

The next step in elastic wave generation (middle part of Figure 25) is to model the piezoelectric material; but instead of voltage, a combination of forces and moments is applied. This case can be used when a multiphysics finite element package is not available or when the reduction of the computational time is important. It has the advantage that the effect of the piezoelectric actuators and sensors on the Lamb waves can be investigated, but again it requires some simulations and analytical calculations so as to find a combination of forces that works well.

The last step is the careful modeling of the piezoelectric actuator and the application of voltage on the material as in the real experiment. It is the most realistic case, but it requires a multiphysics finite element package and it is more computationally expensive. In this paper, a direct comparison between the first and most generally used case and the last one is performed.

A. STATIC COMPARISON BETWEEN FORCE/DISPLACEMENT INPUT AND PIEZOELECTRIC INPUT

Before the comparison of the results from the full transient analysis, a static model was developed. It was a two-dimensional, aluminum, plane strain, simply-supported plate. Initially, horizontal force and displacement were applied on the top two corners. The simulation showed no difference between these two cases, so results from the application of horizontal displacement are presented here. Secondly, a piezoelectric material (PZT-4) was glued on the top surface, and a voltage difference of 100 V was applied as shown in Figure 24. The next two pictures give the displaced structure for every case.

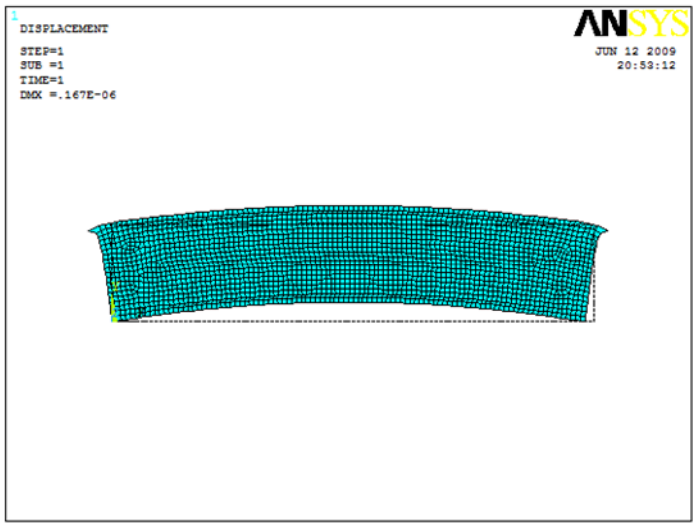

a

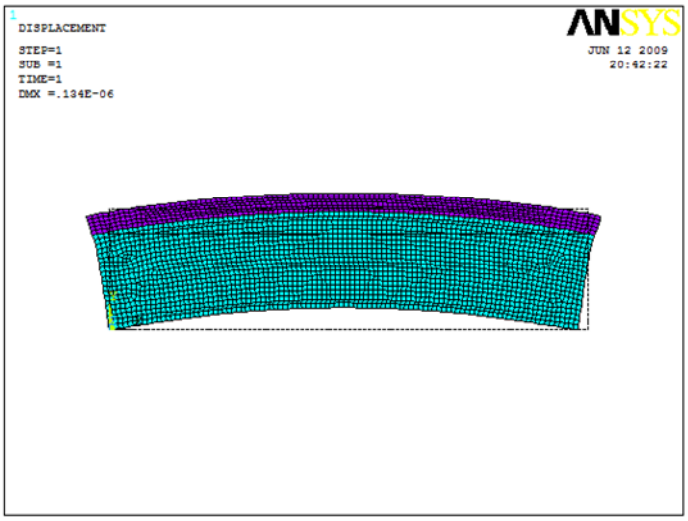

b

Figure 28. Displaced Structure under the Effect of Horizontal Displacement at the Ends of the aluminum plate (a) and Application of Voltage on top and bottom of the Piezoelectric Material (b).

For the first type of load, the displaced structure does not look naturally deformed, especially close to the applied displacement nodes (top right and left corners). The ratio of the change in length in the vertical direction over the change in length in the horizontal direction for the upper surface of the aluminum was about 0.487:

$$\frac{\Delta lvertical}{\Delta lhorizontal} = 0.487 .$$

This means that a point at the middle of the top surface of the aluminum moved up half the change in length of the aluminum in the horizontal direction.

For comparison purposes, it is mentioned that, on the same model, the application of force instead of displacement produced the same displaced structure with a 0.489 ratio of the vertical over the horizontal change in displacement:

$$\frac{\Delta lvertical}{\Delta lhorizontal} = 0.489 .$$

Finally, the displaced structure using the piezoelectric material looks much more natural. The same ratio for this case was 2.083.

$$\frac{\Delta lvertical}{\Delta lhorizontal} = 2.083 .$$

This large difference demonstrates that the structure bends more in the case of the piezoelectric excitation. The implications of this phenomenon on the dynamic simulation are to be evaluated next.

B. DYNAMIC COMPARISON BETWEEN FORCE/DISPLACEMENT INPUT AND PIEZOELECTRIC INPUT

For the dynamic simulation only, a comparison between the horizontal displacement and the piezoelectric case is presented in this paper. The following model was used with a 2 mm thick piece of aluminum and a PZT-4 actuator having a 1-cm length and 0.5-mm thickness. The voltage was applied as usual on the top and bottom of the piezoelectric material.

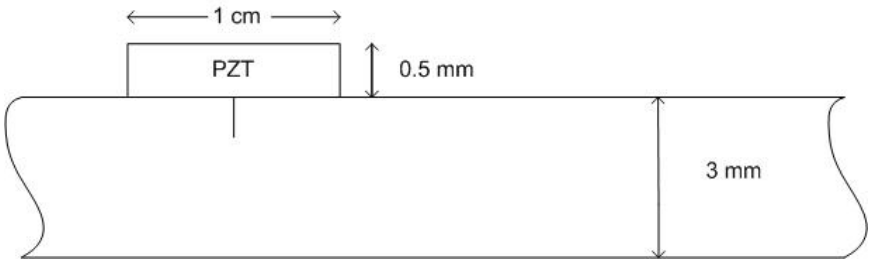

Figure 29. The Model Used for Comparison between the Displacement Input and the Piezoelectric Input.

Special attention was given for a fair comparison between the two input models. So, the maximum applied displacement was triggered to give the same amplitude of the longitudinal wave as in the multiphysics model. The following figure gives the x displacement and the x elastic strain of a node on top of the aluminum plate and to the right of the Lamb wave actuator.

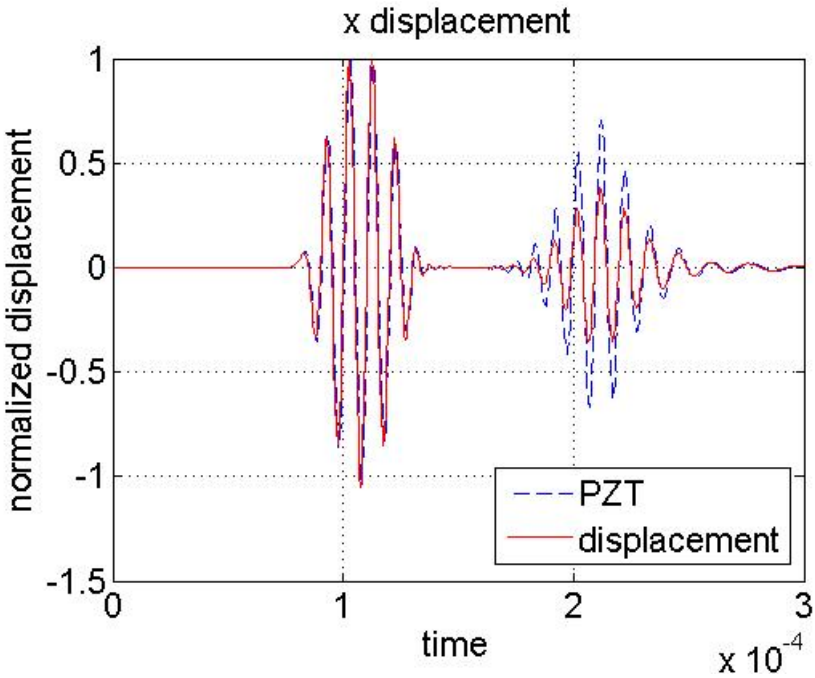

a

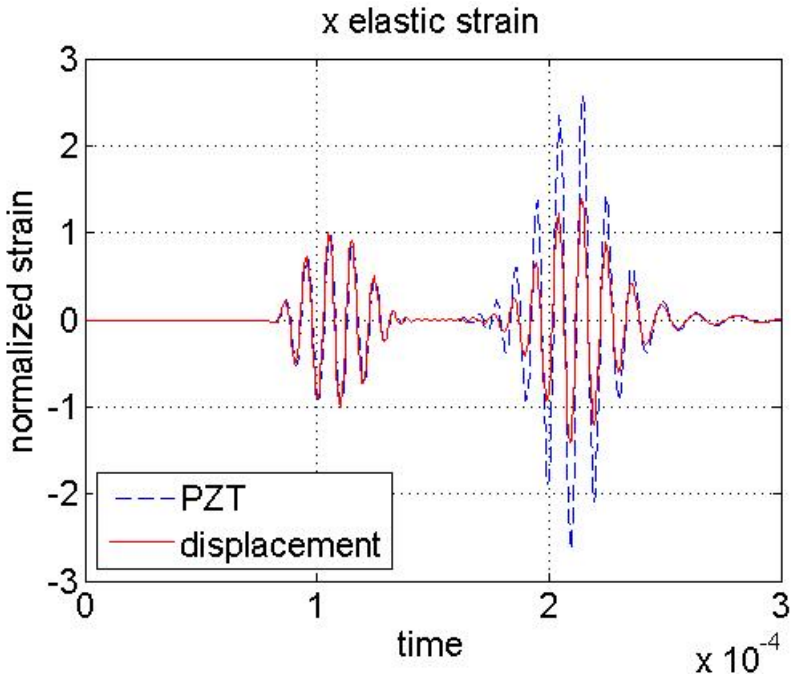

b

Figure 30. Comparison of the Horizontal Displacement (a) and Horizontal Elastic Strain (b) using two Different Methods of Lamb Wave Generation (Full Multiphysics Simulation and Two-node Simplification)

There is almost no difference in the S0 mode of Lamb waves, which is expected, but there is an amplitude difference in the A0 mode. Our study showed an increase of about 87% of the amplitude of the shear wave for the piezoelectric input. All the other parameters of the Lamb waves' modes, such as velocities and phases, are the same.

C. SUMMARY

Direct comparison of the results from the above static and dynamic simulations point to the conclusion that the method used for Lamb wave generation in finite element models is important. In fact, a two-node horizontal displacement method is a fair simplification and could be used only if the ratio of the amplitudes of the two waves is not very important. Otherwise, for structural health monitoring applications where the exact magnitude of the Lamb waves is vital, a full multiphysics simulation should be preferred.

V. EFFECTS OF PIEZOELECTRIC WAFER DEBONDING ON ACTUATOR AND SENSOR

For health monitoring applications, the accuracy of the sensor's output is vital. Fault alarms are some of the common characteristics of advanced systems, and they can increase the overall cost of use. For structures that use Lamb waves as a health monitoring tool, it is important to understand the effect of a possible debonding between the sensors and the structure that is, how a crack on the interface of the two materials can affect the Lamb waves and in general the whole health monitoring application. The problem can be divided into two parts. Initially, there is the debonding between the actuator and the structure, and the second part is the existence of a crack between the structure and the sensor. The first component of the problem can possibly affect the Lamb waves, whereas the second can affect the output signal of the sensor. In this study, the finite element model from Figure 9 was used to investigate both of these cases.

A. DEBONDING OF THE ACTUATOR

As already mentioned above, the starting point was the model described in Chapter III. A horizontal crack was introduced between the piezoelectric actuator and the aluminum plate as is shown in the following figure:

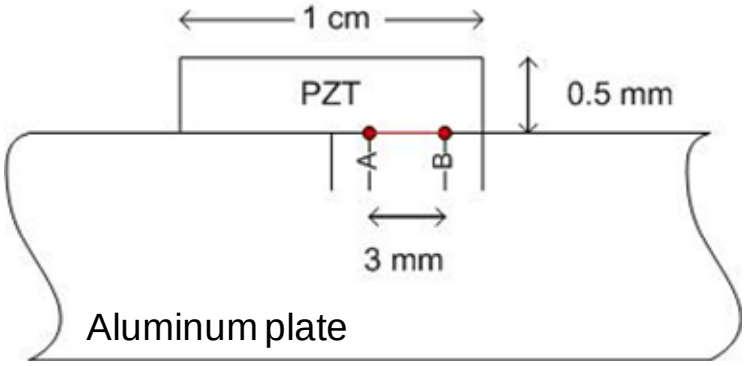

Figure 31. Graphical Representation of the Model with a Crack on the Interface between the Piezoelectric Material and the Aluminum.

It was a line crack 3 mm long. Contact elements were used at the top and bottom lines of the crack to prevent any overlapping of the two materials. Three models were compared: one with singular elements around the crack tips; one without singular elements; and, of course, one case without a crack. The case with the singular elements was chosen so as to investigate the effect of stress concentration around the crack tip on the Lamb waves. The quantities that were used for the comparison were the horizontal elastic strain at a point away from the actuator on the top surface of the aluminum plate. The distance was large enough so the two modes of Lamb waves were separated. This gave us the capability of seeing the effect of the debonding separately on the longitudinal and shear waves.

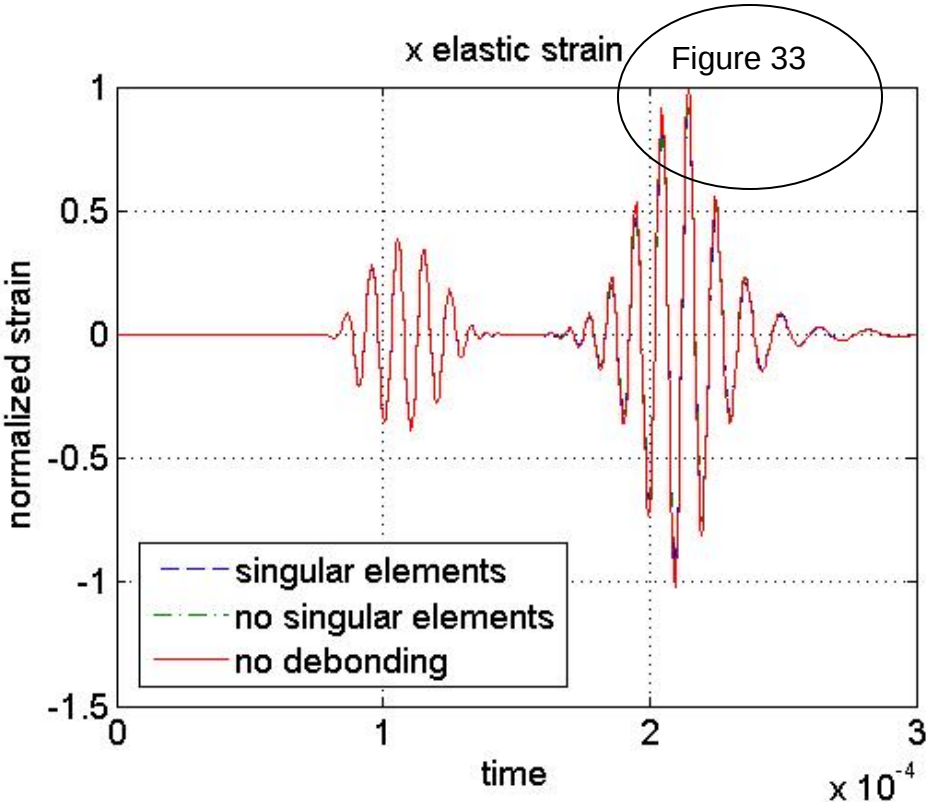

Figure 32. Small Difference in the Lamb Waves for a Debonding Actuator. The Difference is Obvious in the Amplitude of the Bending Wave. (Ellipse: A Magnification is Available in the next Figure)

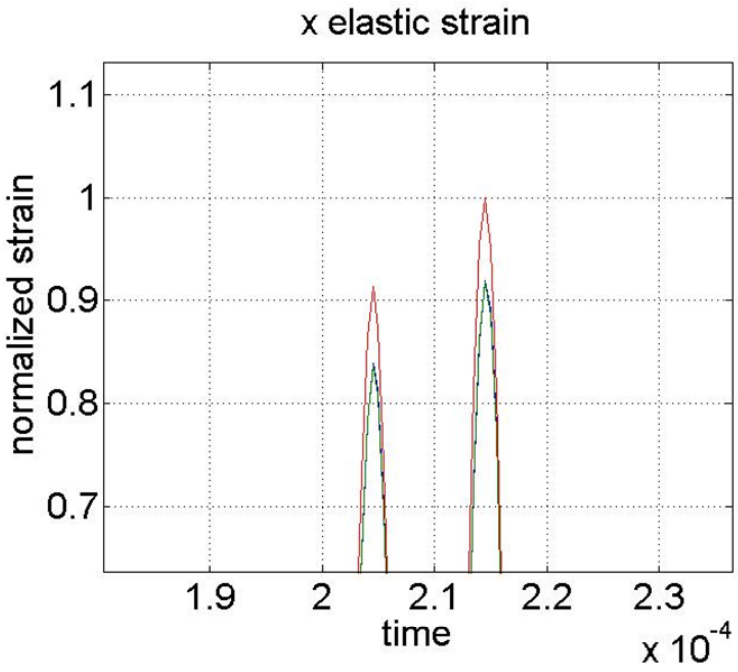

Figure 33. Nine Percent Difference in the Amplitude of the A0 Mode for the Debonding Actuator. No Difference Between using Singular Elements and not using Them.

The first figure shows that there is almost no difference between using singular elements and not using them. Both the S0 mode and the A0 mode are exactly the same. These similar responses indicate that higher fidelity modeling of actuator debonding is unnecessary in characterizing Lamb wave propagation.

A comparison of the cracked cases with the uncracked illustrates that this crack does not cause important change in the longitudinal wave. In fact, the first wave form was almost the same for the three cases. On the other hand, there was a difference in the amplitude of the shear wave. A closer look at the A0 mode, shown in the second figure, demonstrates a reduction of about 9% in the maximum amplitude of the wave.

Evaluating the above observation, an interesting comparison using the results from the previous chapter can be made. In Chapter IV, our study demonstrated that a two-node simplification decreases the amplitude of the

shear wave. Here, we have a small crack under the piezoelectric material, but if it were possible to increase the length of the crack by a lot, our model would look like the following:

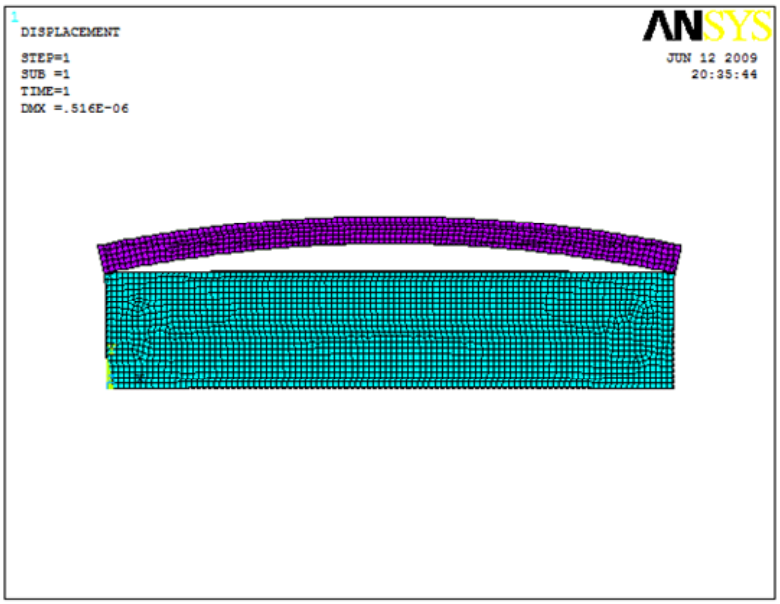

Figure 34. Theoretical Model of an Actuator With 100% Bebonding.

This model is closer to the two-node simplification that was analyzed in the previous chapter. Consequently, expanding the results from the debonding case produces results that match the results from the two-nodes excitation.

B. DEBONDING OF THE SENSOR

In modeling the debonding of the sensor, again a line crack was modeled between the piezoelectric material and the aluminum bar. The length was again 3 mm (30% of the sensor's length). For this case, contact elements were used around the crack; singular elements were introduced at the crack tips to model accurately the stress concentration. The generation of the Lamb waves was performed by the use of a piezoelectric actuator away from the sensor.

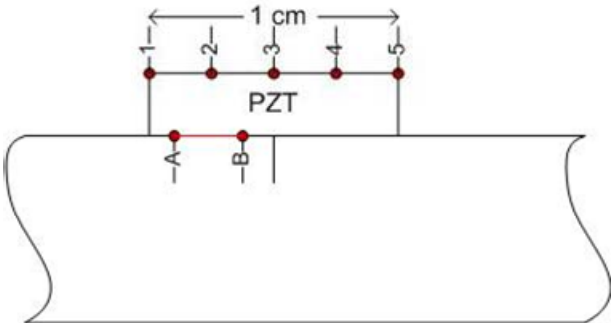

Figure 35. Graphical Representation of the Model with a Crack on the Interface Between the Sensing Material and the Aluminum. Voltage Output from Five Different Points was Compared.

To compare the cracked and the uncracked cases, the voltage output from the top of the sensor was the measured quantity. As there was a variation of the voltage from point to point along the top line of the sensor, five different points were chosen, as is shown in the above figure. The following set shows these outputs:

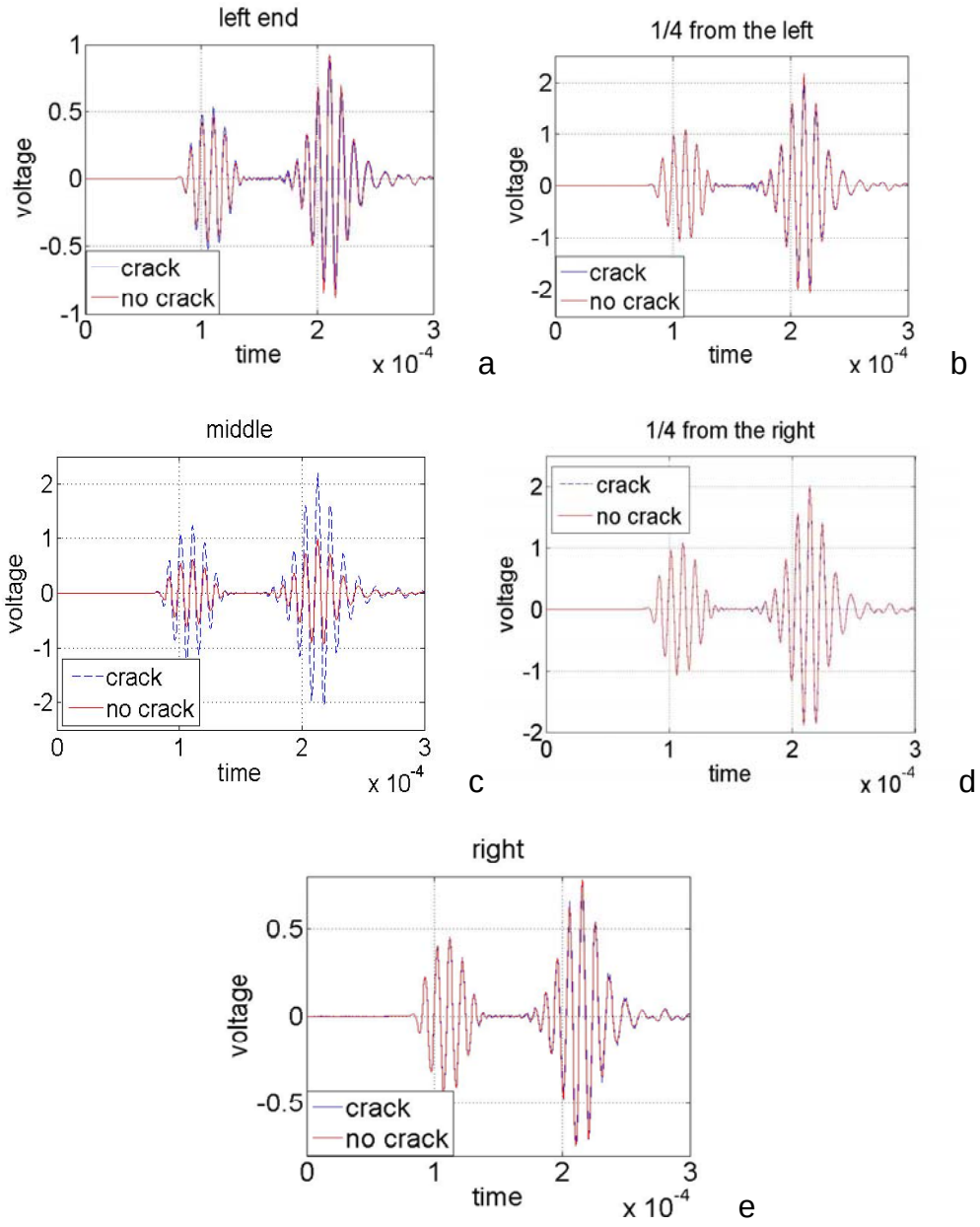

Figure 36. The Voltage Output at the Five Locations on top of the PZT Material as shown in Figure 32. Left End of the PZT (a), One-Quarter of the Length from the Left (b), Middle of the Sensor (c), Three-Quarters of the Length from the Left end (d), Right end (e).

The output from points two, four, and five of Figure 32 is almost the same whether or not we have a crack. By contrast, points one and five give different outputs. The next two figures focus on these points, and the third and fourth plots

give the voltage distribution on top of the PZT material between the uncracked and cracked cases for the S0 and A0 modes.

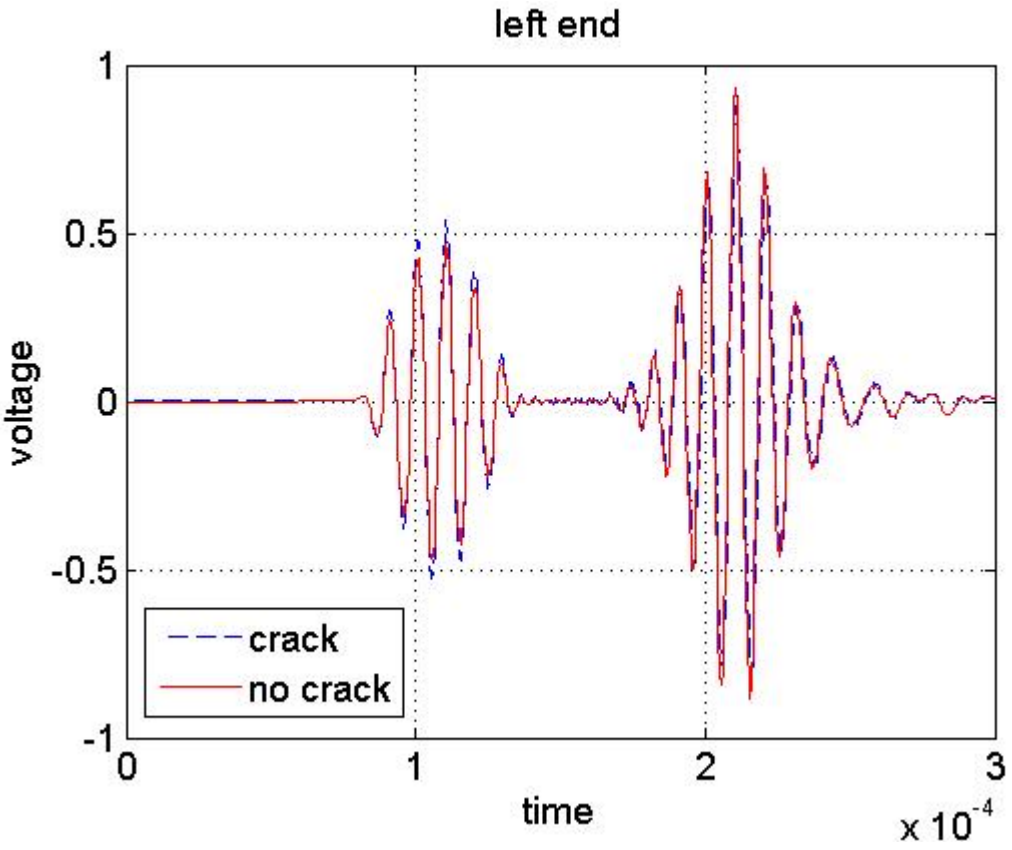

Figure 37. Voltage Output at Point 1 of Figure 32 for the Debonding and the No-crack Case.

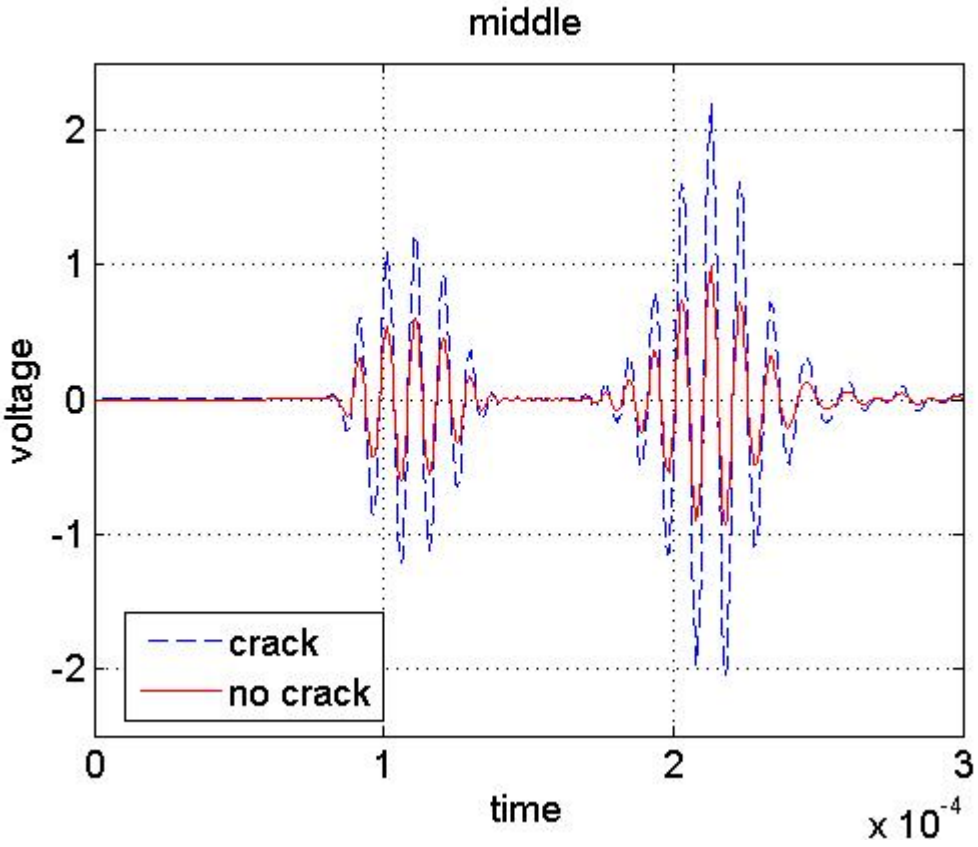

Figure 38. Voltage Output at Point 3 of Figure 32 for the Debonding and the No-crack Case

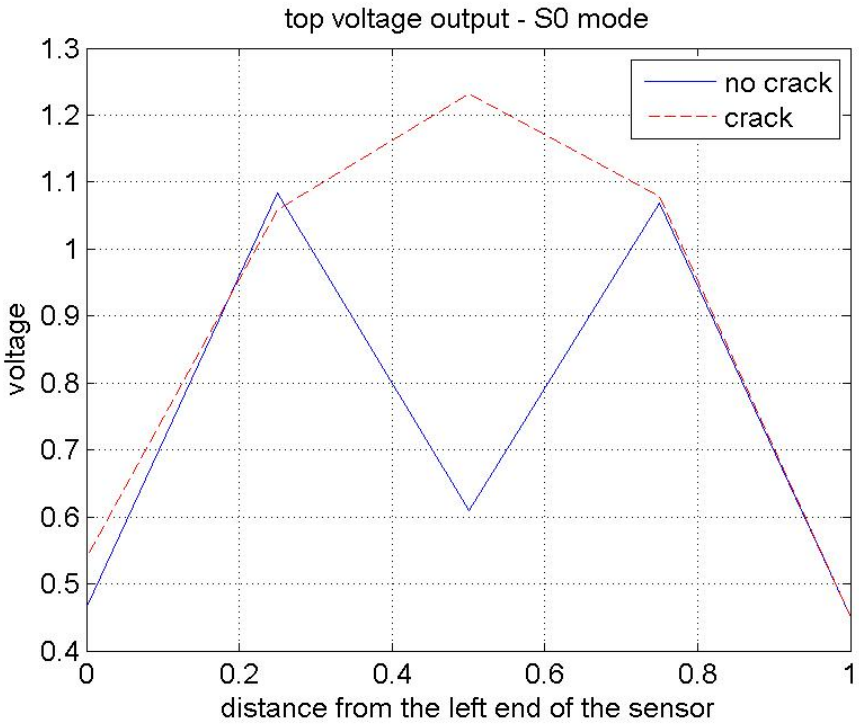

Figure 39. Max Voltage Output Throughout the Sensor With and Without Debonding-S0 Mode.

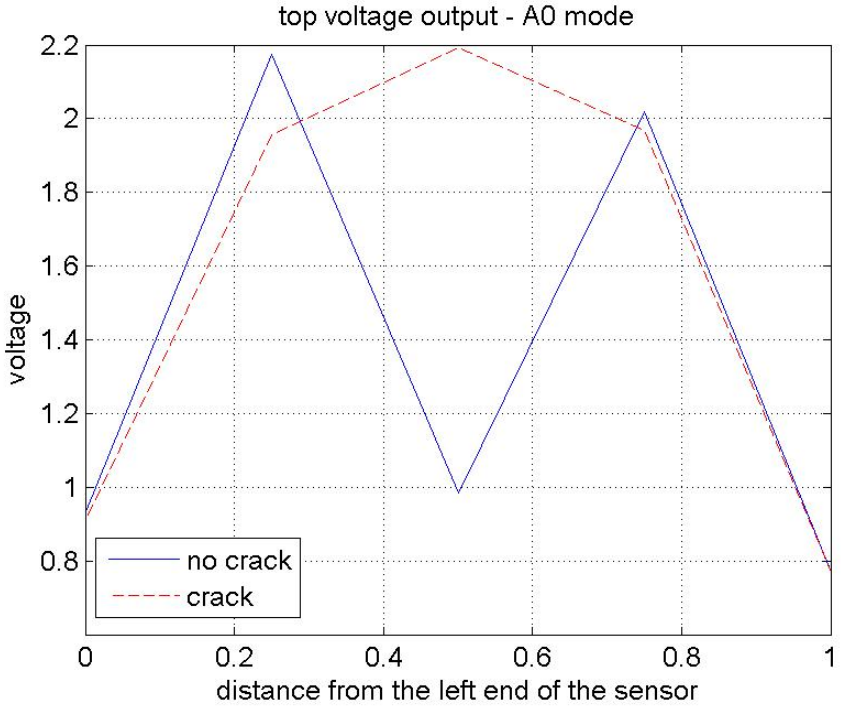

Figure 40. Max Voltage Output Throughout the Sensor With and Without Debonding-A0 Mode.

In the first figure there is an increase of the voltage output of about 15% for the cracked case. Furthermore, in the second figure the increase is almost 100%. This difference is caused from the localized increase of the stress–strain state around the crack tips. Point 1 is at the corner of the sensor, so the strain state did not change very much, but point 3 is close enough to the crack tip and has only one outer surface, so it was affected more. This localized increase of the voltage output would increase the overall output of the sensor for the debonding case.

The importance of these results drives us to investigate more the debonding of the sensor. For this reason, we included in the above model an adhesive layer between the aluminum and the piezoelectric material. Using [27] as a guideline, we used the properties of a common epoxy with the modulus of elasticity E=3 GPa, Poisson ratio of 0.37, and density of 1100 kg/m3. The thickness of the adhesive layer chosen was 0.05 mm, which is 1/10 of the sensor's thickness. The geometry was kept the same, but the finite element mesh was very dense. The crack was positioned between the adhesive layer and the piezoelectric material, and it was 30% of the length of the sensor. Again, we used contact elements around the crack tips and contact elements to avoid overlapping. The geometry of the new simulation is as follows:

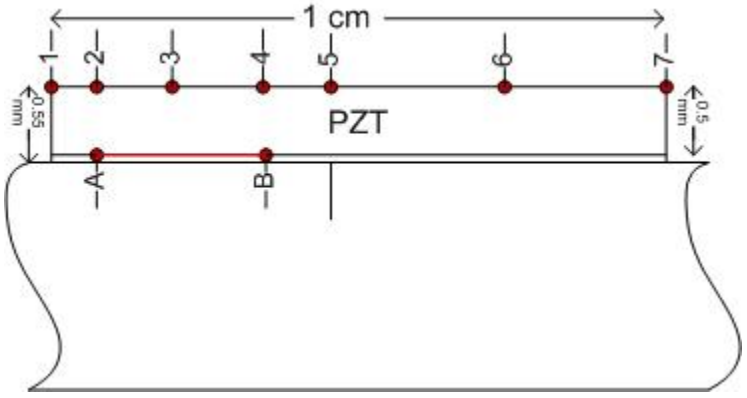

Figure 41. Geometry of the Piezoelectric Sensor with an Adhesive Layer. The Voltage Output was Measured at Seven Different Points.

As usual, we measured the voltage output at seven different locations as described in the above figure. Point 5 is at the middle of the piezoelectric material, points 3 and 6 are at a quarter of the distance from the ends, and points 2 and 4 are exactly above the crack tips. The crack simulation was run twice, first with contact elements and, second, without them. The following plots give the output:

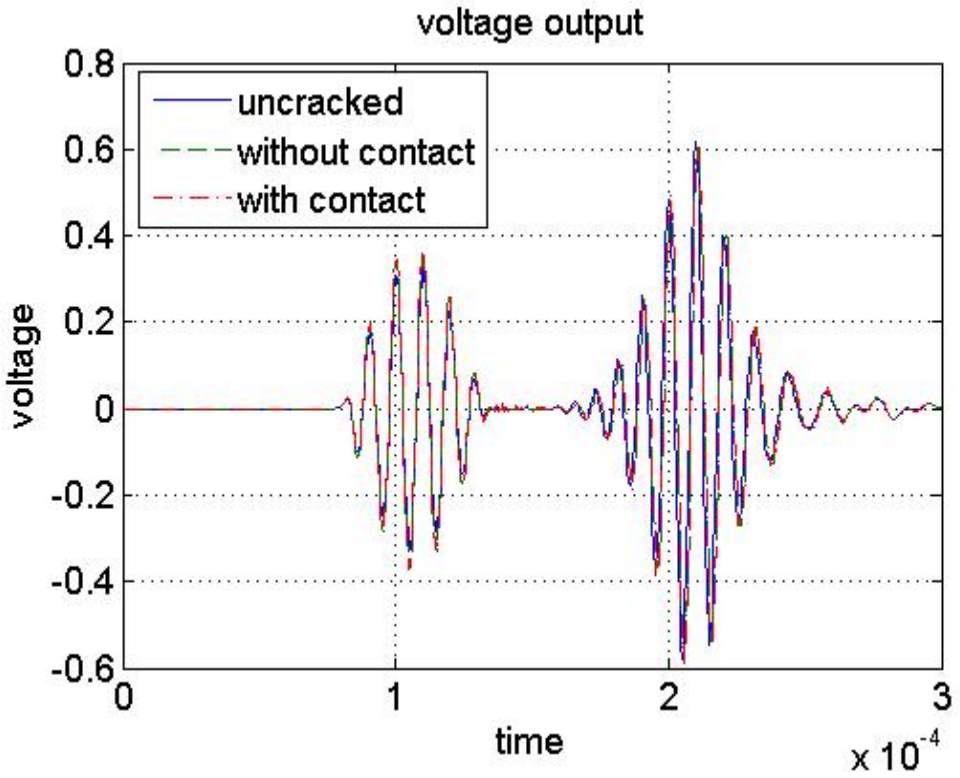

Figure 42. Voltage Output at Point 1 of Figure 36 of the Sensor With and without Debonding.

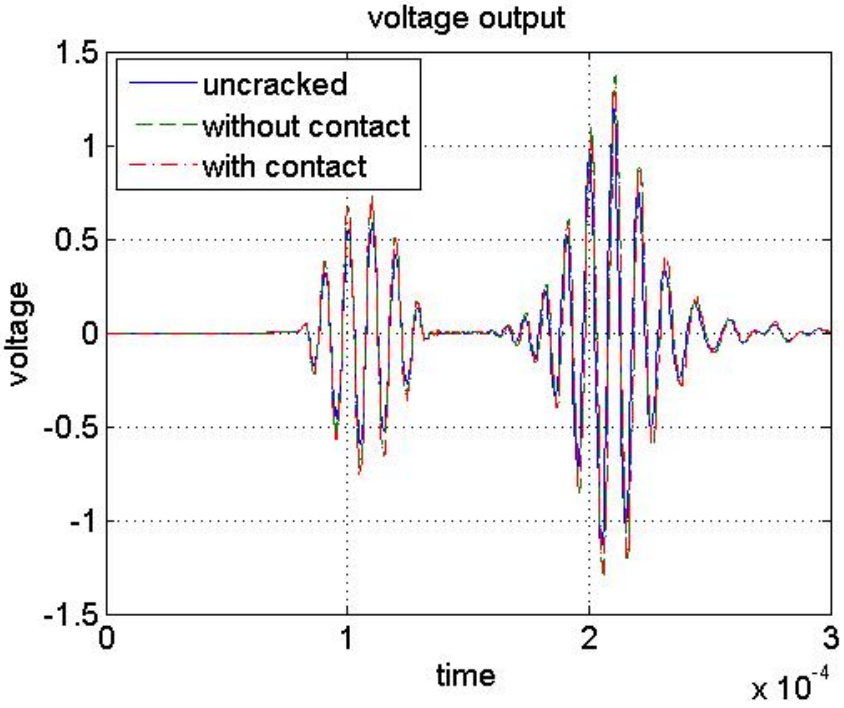

Figure 43. Voltage Output at Point 2 of Figure 36 of the Sensor With and Without Debonding.

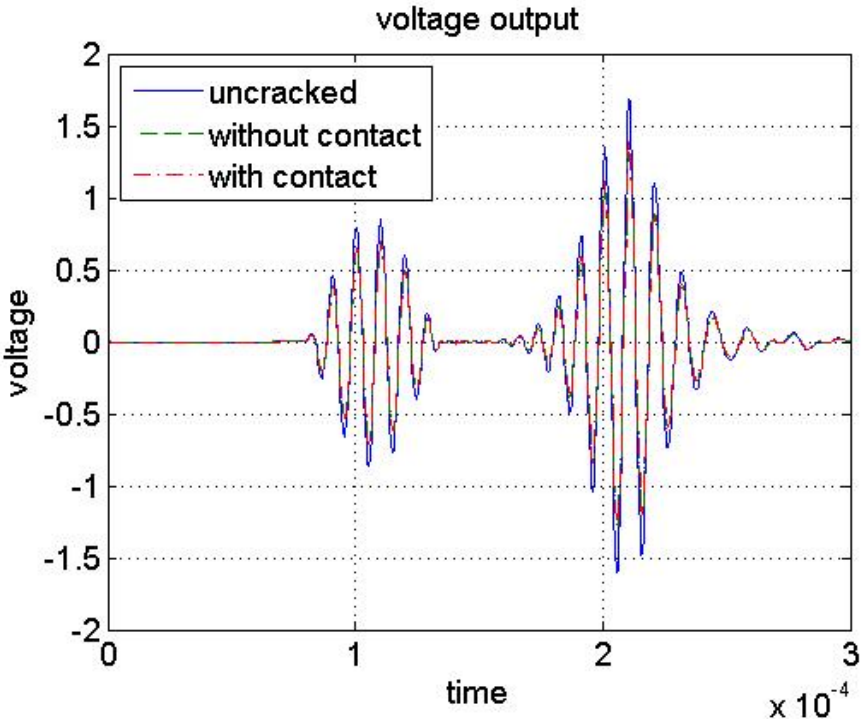

Figure 44. Voltage Output at Point 3 of Figure 36 of the Sensor With and Without Debonding.

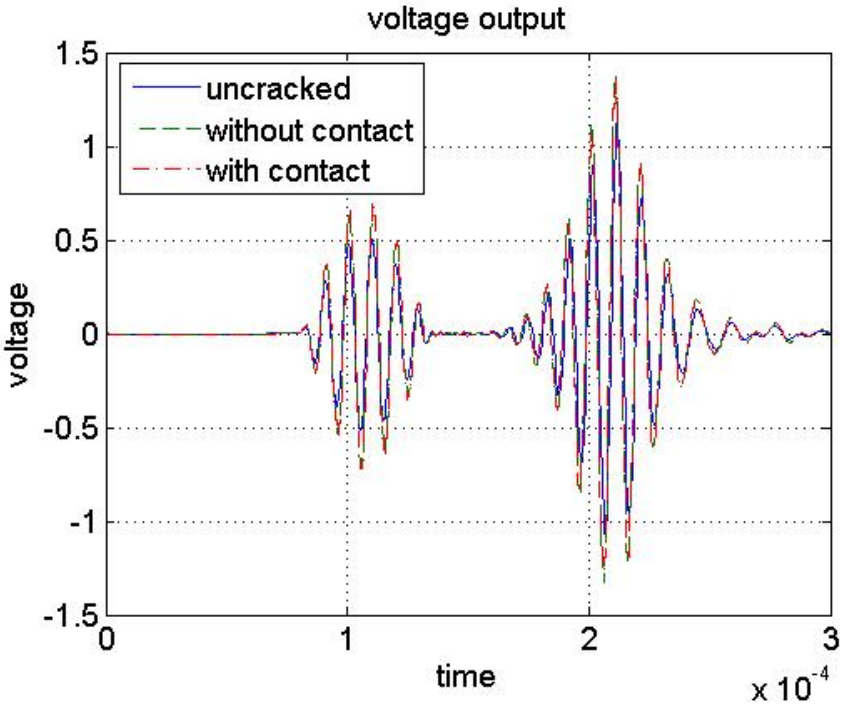

Figure 45. Voltage Output at Point 4 of Figure 36 of the Sensor With and Without Debonding

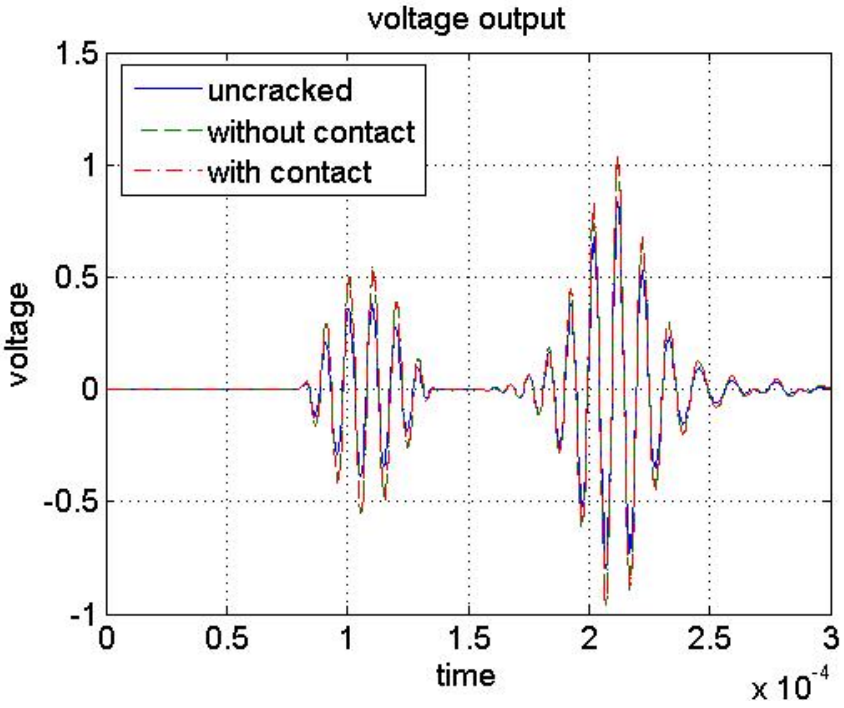

Figure 46 Voltage Output at Point 5 of Figure 36 of the Sensor With and Without Debonding.

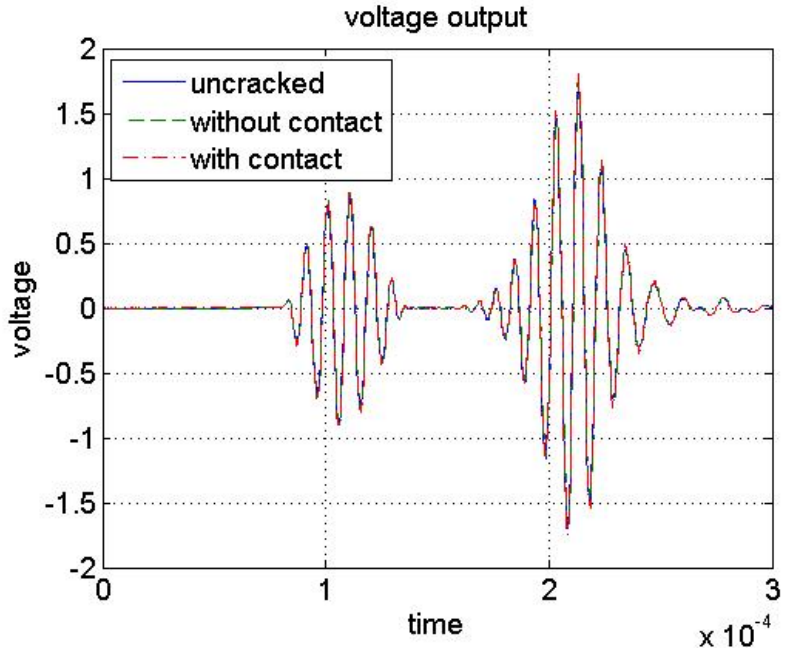

Figure 47. Voltage Output at Point 6 of Figure 36 of the Sensor With and Without Debonding.

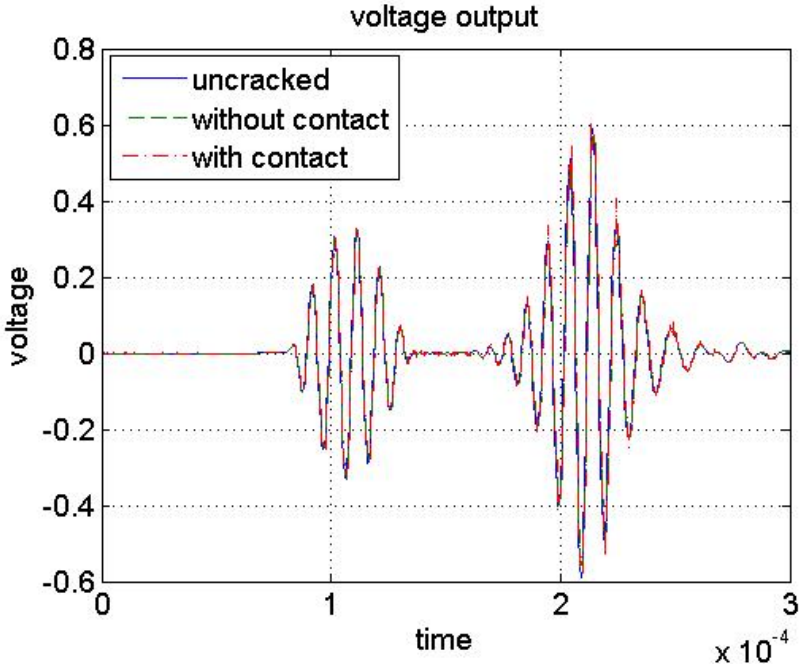

Figure 48. Voltage Output at Point 7 of Figure 36 of the Sensor With and Without Debonding.

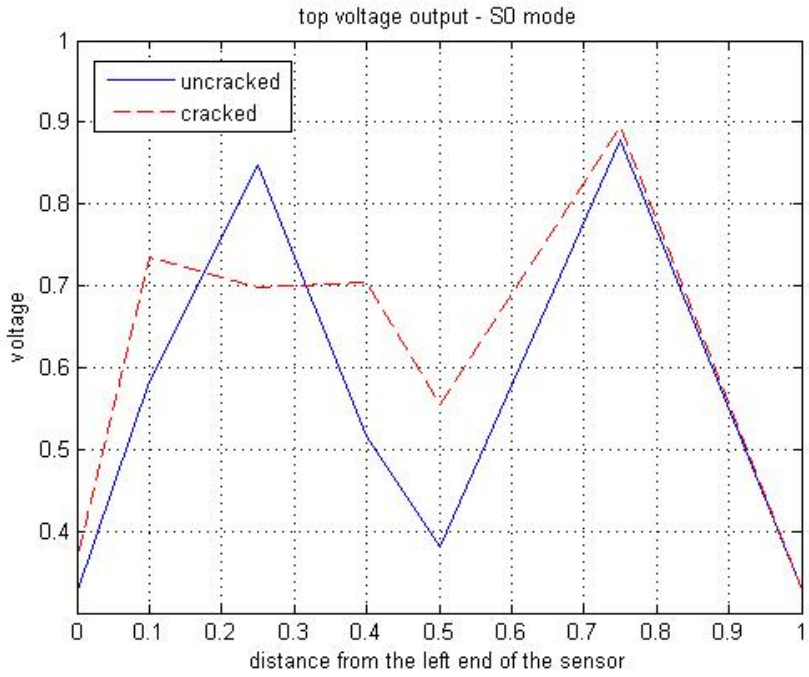

Figure 49. Max Voltage Output Throughout the Sensor With and Without Debonding-S0 Mode.

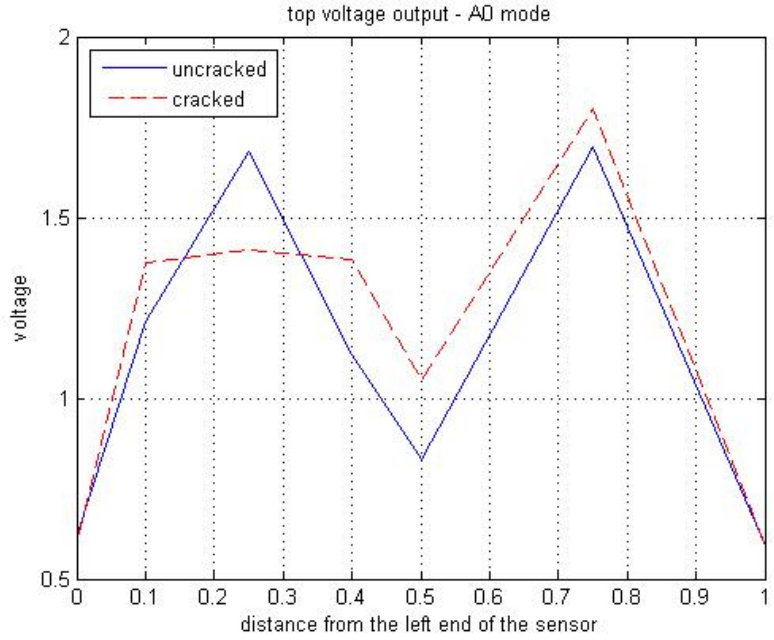

Figure 50. Max Voltage Output Throughout the Sensor With and Without Debonding-A0 mode.

Comparing the above set of figures with the output from the sensor with no adhesive layer, the following observations can be made. Initially, the existence of the adhesive layer decreases the voltage output of the sensor, an observation that is already mentioned in [28].

Secondly, the existence of the crack changes dramatically the stress field and the voltage output around it. In particular, the voltage increases close to the crack tips, whereas it decreases in the middle of the crack. Comparing the area below the curves of Figures 44 and 45, the overall voltage output of the sensor will increase because of the existence of a crack with these dimensions. The following graph gives a summary of the total voltage output for all the previously mentioned cases. The total voltage output of the sensor with the adhesive layer is lower than the output of the sensor without the layer. Moreover, the voltage difference between the no-crack and with-crack cases is not so large when adhesive layer is present. This difference is caused probably by the adhesive layer, although the mesh sizes were not the same, and any direct comparison must be performed carefully. Interesting future work could be done in this area with different crack sizes.

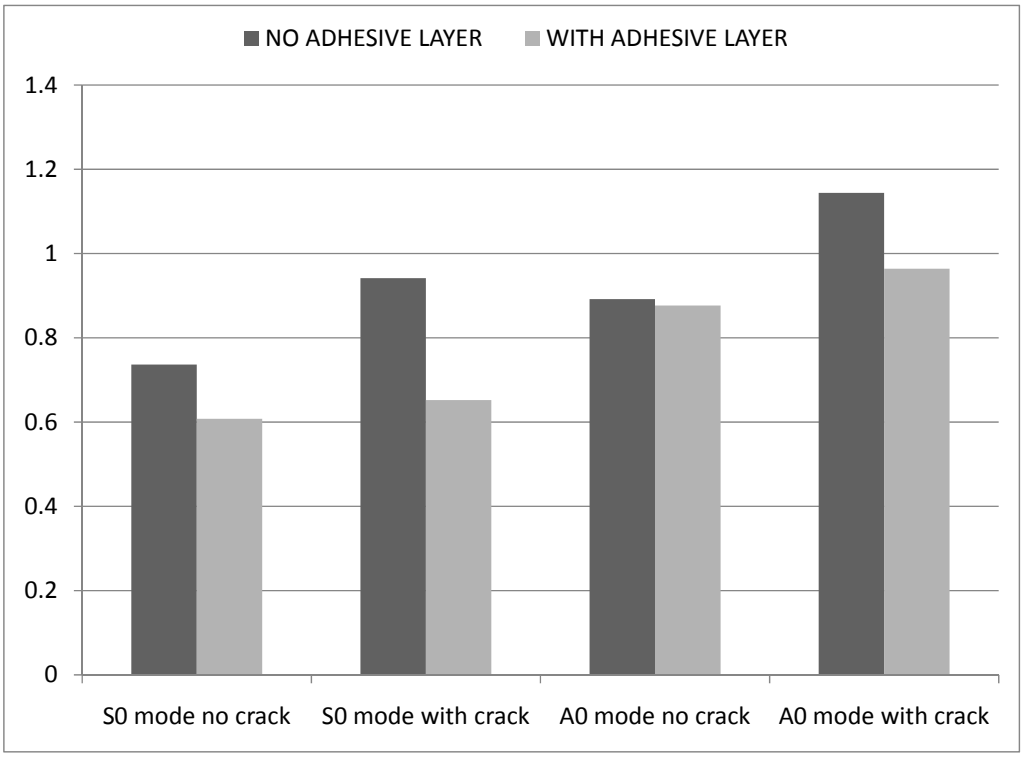

Figure 51. Total Voltage Output from the Sensor for Different Lamb Wave Modes With and Without Adhesive Layer.

Another interesting observation is the symmetrical voltage output throughout the top of the sensor for the uncracked case that has two picks at ¼ of the distance from the ends (Figure 49, 50). This phenomenon also exists in the previous simulation of this heading (Figure 33).

Despite the element size dissimilarity between the two models, the difference of the voltage output from the no-debonding/debonding sensor with the adhesive layer is more realistic. So, we believe that in detailed models such as the above, where the effect of debonding is questioned and accurate voltage distributions are the fair outcome, it is important to include all the details of the structure, such as adhesive layers. In other words, accurate and detailed output requires a model that includes not only major but also minor parameters.

C. SUMMARY

For structural health monitoring applications, the existence of cracks between piezoelectric materials and structures can be separated into two different sub-problems: debonding of the actuator and debonding of the sensor. For a crack length of 30% of the total length of the sensor, our study shows that the first problem decreases the amplitude of the shear wave. This phenomenon can be characterized conservatively for an SHM application. In fact, a decrease of the Lamb wave amplitude causes a decrease of the sensor's voltage output, and this gives an indication that there is potential damage in the structure or in the health monitoring system.

The second case of the problem (debonding of the sensor) is more crucial because it can mask potential damage of the structure. This is because the combination of increased voltage because of debonding, along with decreased voltage because of a potential damage in the structure, can give an uninfluenced overall signal output that is exactly the same as the one from a healthy structure. On the other side of the coin, this change of voltage output over the top area of the sensor can be used to identify the health of the sensor itself. Hopefully, as technology improves, more sophisticated sensors could be built, having the ability to measure, not the average voltage output, but the voltage distribution on top of them. This ability could be used to identify debonding or damaged sensors and, of course, to minimize the cost of checking the condition of sensors, especially on large structures monitored by SHM systems.

The above observations are, of course, based on a model having a specific crack length at the interface between the PZT and the aluminum. For future work in this field, someone could study the effect of the crack length and the crack position. For example, the crack could be on the other side of the adhesive layer or even in the middle of it as is shown in the next figure. It is also important to verify the finite element results with real experiments, although the generation of a crack between the sensor and the structure is not always easy.

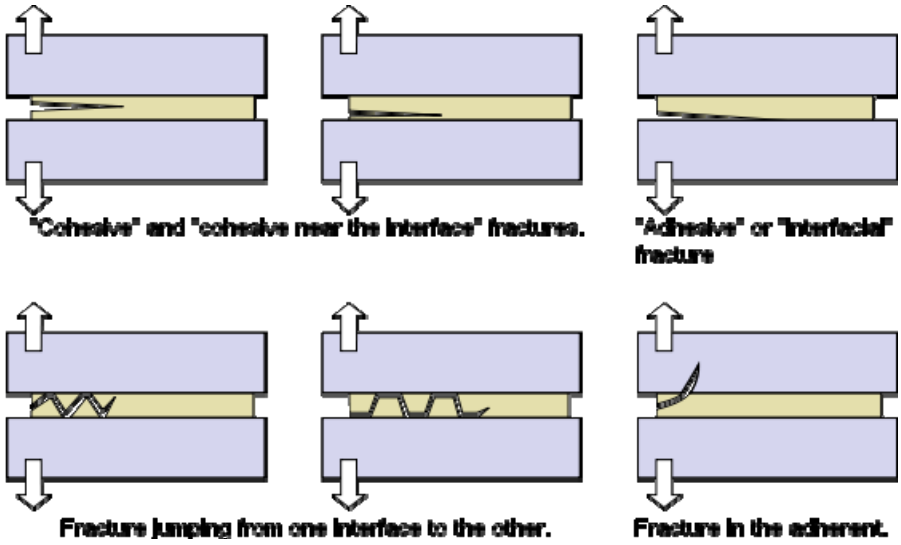

Figure 52. Different Types of Cracks in Adhesive Layers [From 29].

VI. CRACK MODELING AND IDENTIFICATION

In this chapter, Lamb waves were used to identify local damage inside the two-dimensional plate. As already mentioned in Chapter III, different types and dimensions of cracks were evaluated. In the first part of the chapter, the two commonly used techniques, “pulse-echo” and “pitch catch,” were used to identify the damage Giurgiutiu [14]. describes in great detail these two methods. Initially, the purpose was to validate our finite element model and verify that it is accurate enough to proceed to the third research question of this paper, which has to do with the effects of cracks on Lamb waves and the required fidelity of the crack. For all of the following simulations, a direct comparison was made between the results from the aluminum plate with and without a crack. The main quantities that are compared are the horizontal displacement and elastic strain of selected nodes caused by the same 5 circle, 100 kHz sinusoidal input of horizontal displacement or voltage used in all the previous chapters. The displacement was chosen because it is one of the most accurate nodal properties, and, of course, it is a quantity that can be understood and compared easily. The elastic strain was chosen because it is a number that can be easily measured in real experiments using strain gauges or piezoelectric sensors.

It is important to mention one more time that the simulations of Sections A and B of this chapter were parts of our initial study and model development, so they are presented here as background knowledge for work. Although these parts do not answer any of the research questions, they give some interesting information that can be used for the evaluation of the final model described in Section C, which has a piezoelectric actuator, a piezoelectric sensor, and a line crack with singular and contact elements.

A. VERTICAL CRACKS

1. Dimensions 1 mm x 50 μm

For the first simulation, a vertical crack with dimensions 1 mm x 50 μm was used. It was placed on the center line of the aluminum plate, which had a relatively small length of 0.6 m. Lamb waves were created using the “two-node approximation” that was discussed in Chapter IV. The geometry of the model can be shown in the next figure:

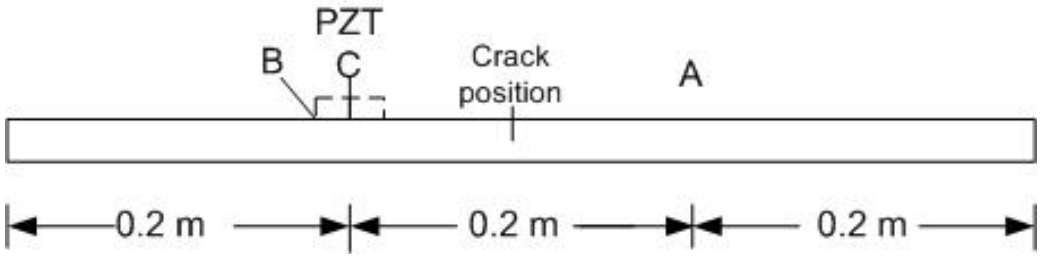

Figure 53. Model With a Vertical Crack of 1 mm x 50 μm.

Results from point (A) 0.4 from the left, point (B) 0.0195 from the left, and point (C) 0.2 from the left will be compared. Point (B) is the node where the displacement was applied, and point (C) is exactly at the middle between the two moving nodes. In the real experiment, it is difficult to measure the displacement at point (C) because of the existence of the piezoelectric material. But this point will hopefully give us a clear look because the x displacement is zero during the time period of the applied displacement.

For this first attempt to identify a crack, an important concern was to avoid overlapping of the nodes that form the area of the crack. So, the same simulation was run two times, first without contact elements and, second, with contact elements. The figures that follow give the x displacement and x elastic strain for all the above points and for the three cases (no crack, with crack/no contact, with crack/with contact).

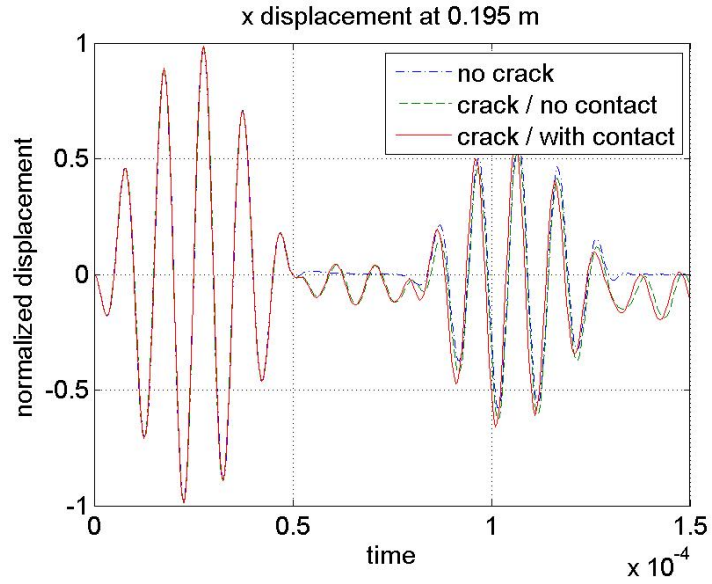

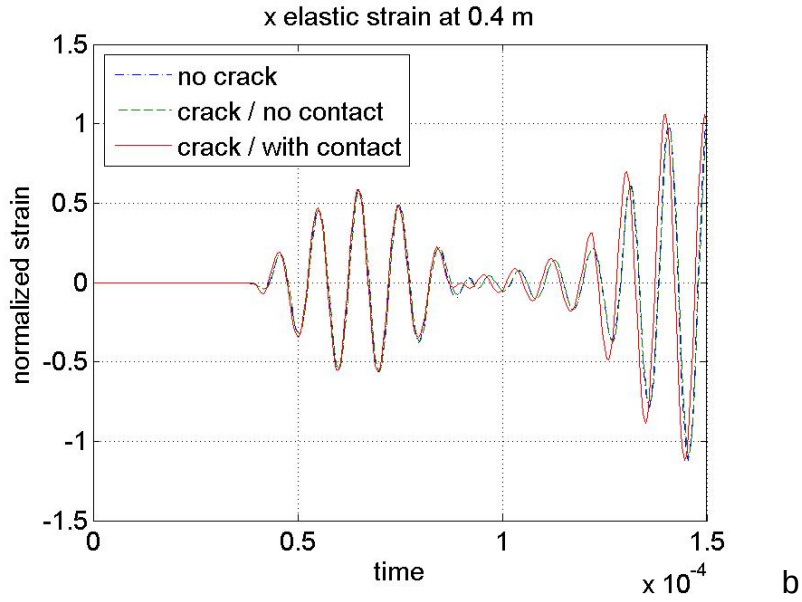

Figure 54. Horizontal Displacement (a) & Elastic Strain (b) at Point A, 0.4 m from the Left.

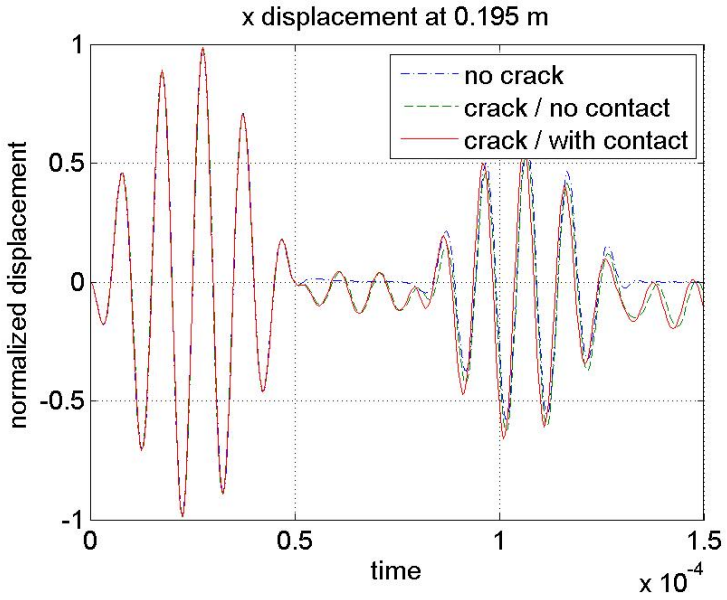

a

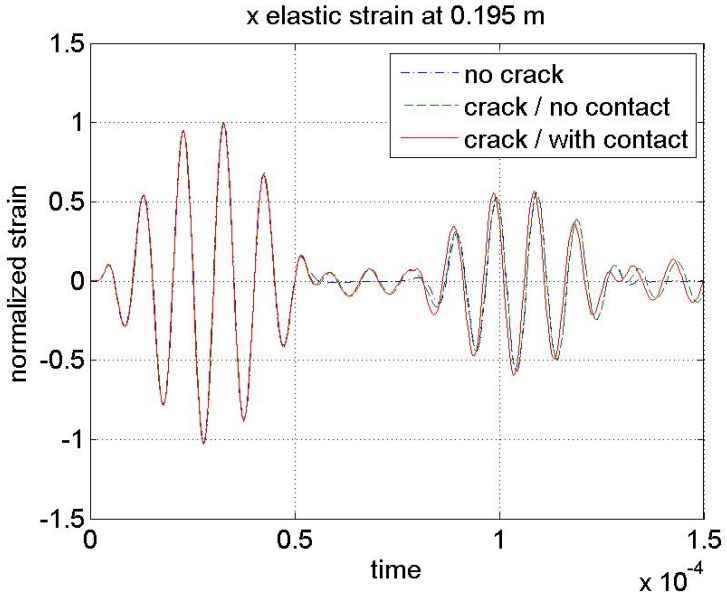

b

Figure 55. Horizontal Displacement (a) & Elastic Strain (b) at Point B, 0.195 m from the Left.

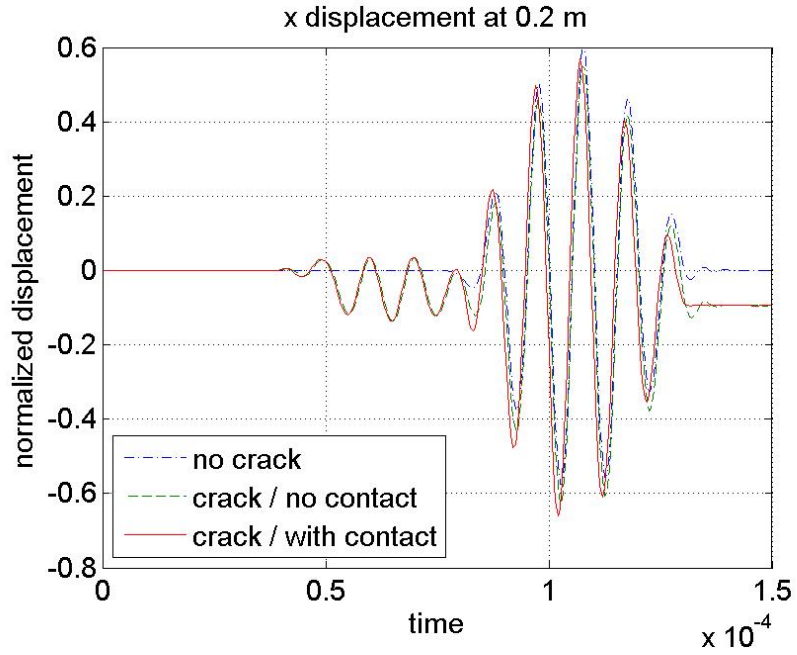

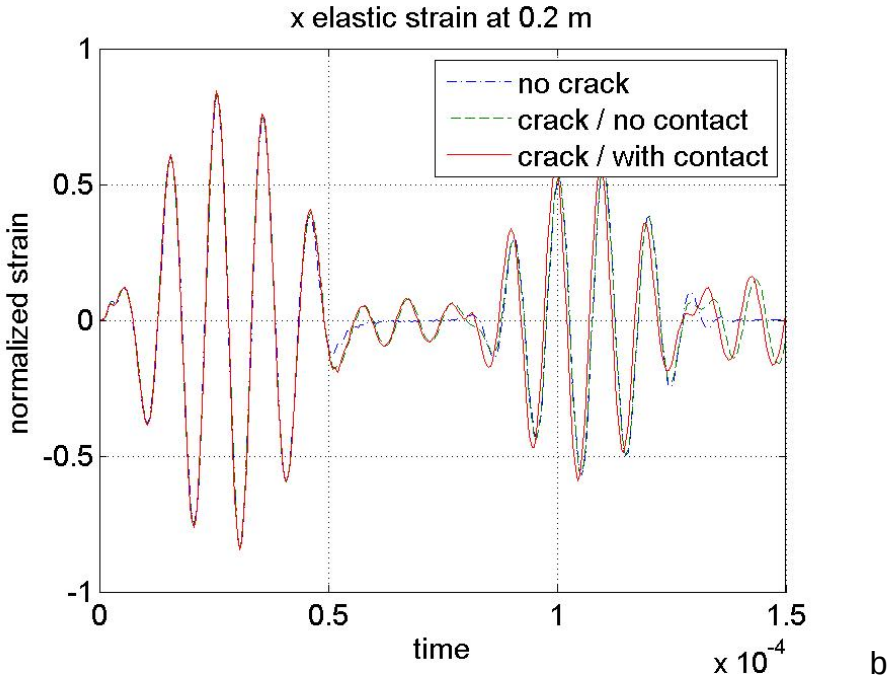

Figure 56. Horizontal Displacement (a) & Elastic Strain (b) at Point C, 0.2 m from the Left.

Comparing the above figures, the response with and without contact elements is exactly the same at every point. This means either that for these cracks' dimensions there is no overlapping of the nodes that form the crack, or

that a possible small overlapping does not affect the solution. The displacement of some of the nodes that form the crack was checked, and it was smaller than the opening of the crack. So, this crack did not close during this simulation.

Another interesting point is the existence of an almost constant negative value of horizontal displacement for the case of the cracked beam (Figure 53). This constant term is not present in the figure of the elastic strain.

In Figure 55, we can see the existence of a second wave with smaller amplitude between the waves that are present in the uncracked beam. This wave can be used to identify the position of the crack using the pulse-echo technique. But the exact starting point of this wave is only present in Figure 56, which is the node between the two moving ones. Multiplying the velocity of the longitudinal wave with the time, we can find the exact point of the crack. From all the other graphs, we have a clear indication that the structure is damaged, but it is difficult to see exactly the starting point of the reflected wave. This model has the disadvantage of a relatively small length of aluminum plate, which does not allow the waves to be separated.

The next step was to compare the Fast Fourier Transform (FFT) of the received wave at point A, point B, and point C. As we can see further down, the spectrum of the beam with the crack includes higher frequencies than the other. This is an indication of damage in the plate.

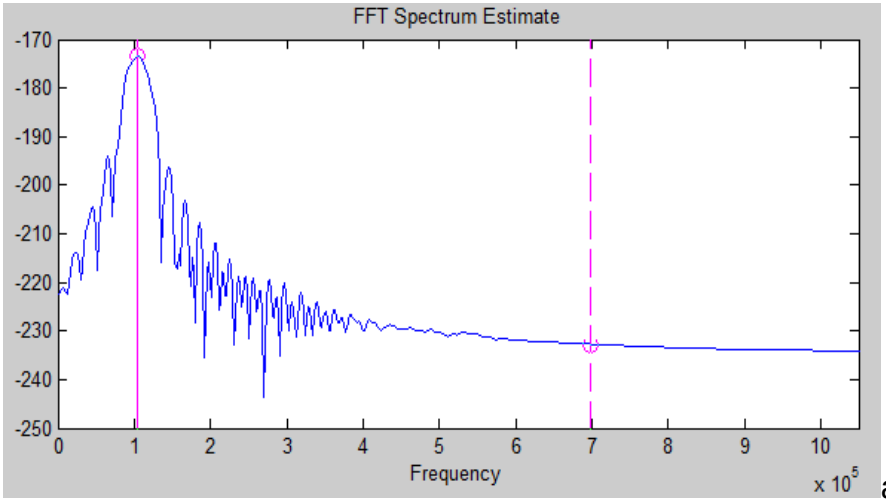

a

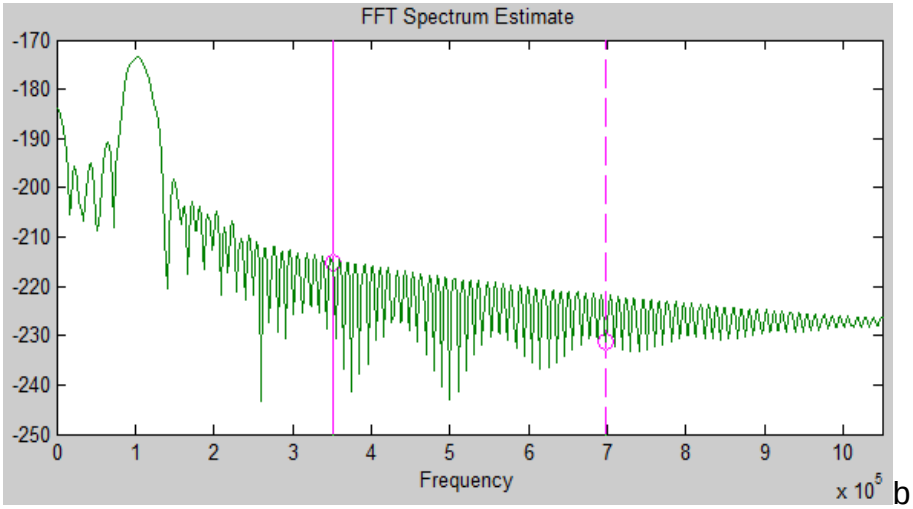

b

Figure 57. FFT of Horizontal Displacement from Point A at 0.4 m: Uncracked Case (a), Cracked/No Contact Case (b).

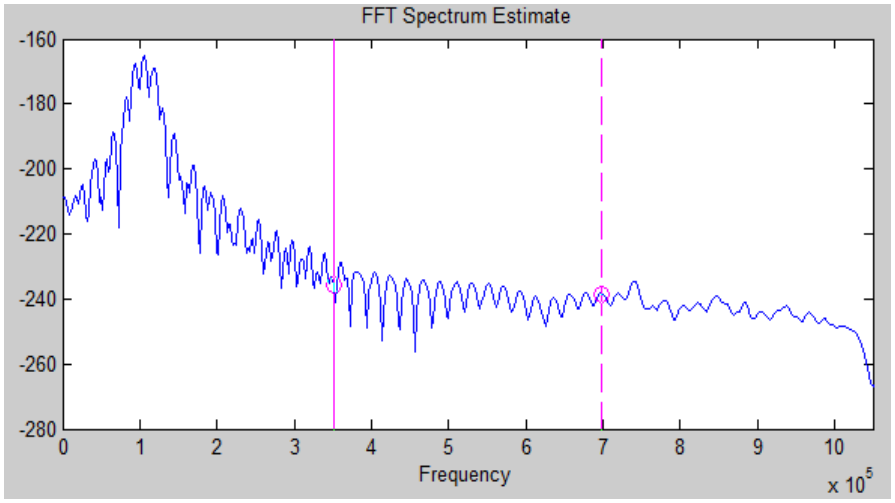

a

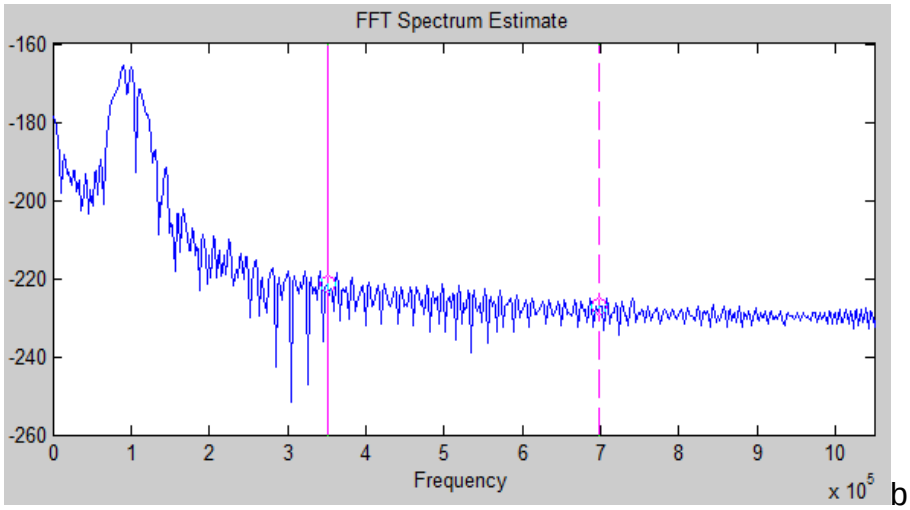

b

Figure 58. FFT of Horizontal Displacement at Point B, 0.195 m from the Left End of the Plate. No Crack Case (a), With Crack/No Contact Elements (b).

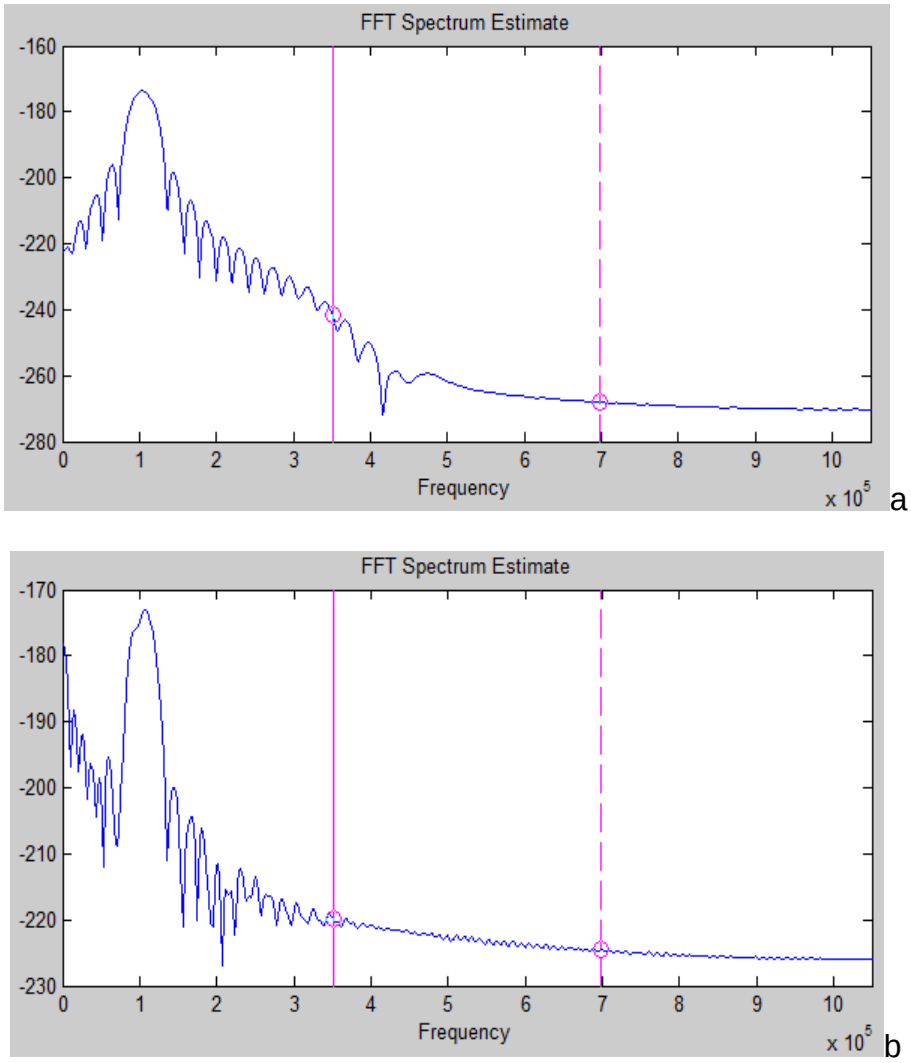

Figure 59. FFT of Horizontal Displacement at Point C, 0.2 m from the Left End of the Plate. No Crack (a), With Crack/No Contact Elements(b).

It seems that the frequency spectrum depends on the point where we measure the signal. There is a central frequency that matches the excitation frequency (100 kHz), but the rest of the frequency spectrum depends on the point of measurement. A possible answer is because of the dispersion properties of the antisymmetric type of waves. At every point, the longitudinal wave is almost the same, but this is not the case for the bending wave. Moreover, on the left of the crack, three waves are present: the S0 and A0 from the source and the reflection from the crack. But on the right of the crack there are only two: the S0

and A0 that are, of course, influenced by the crack. The next comparison was between the FFTs of the elastic strain at different locations. Again, we compared the FFT at three points (A, B, C) at distances of 0.4, 0.195, 0.2 meters from the left end of the plate, respectively.

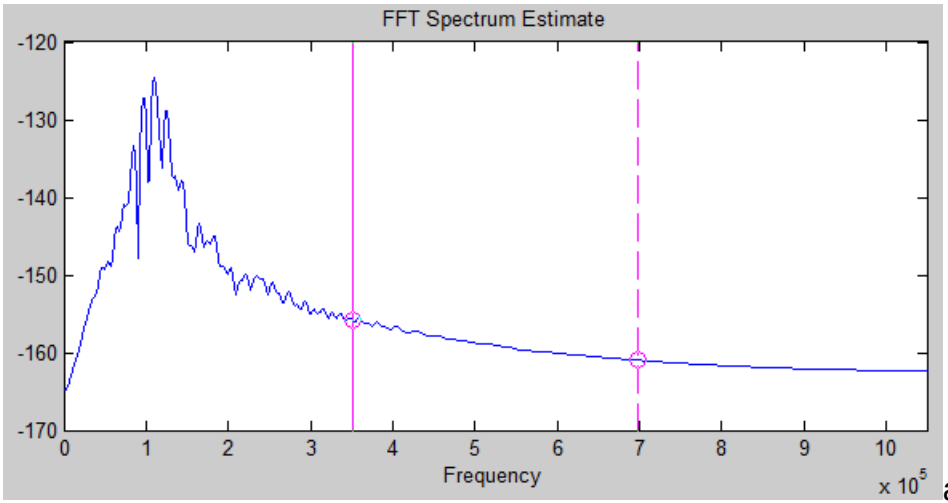

a

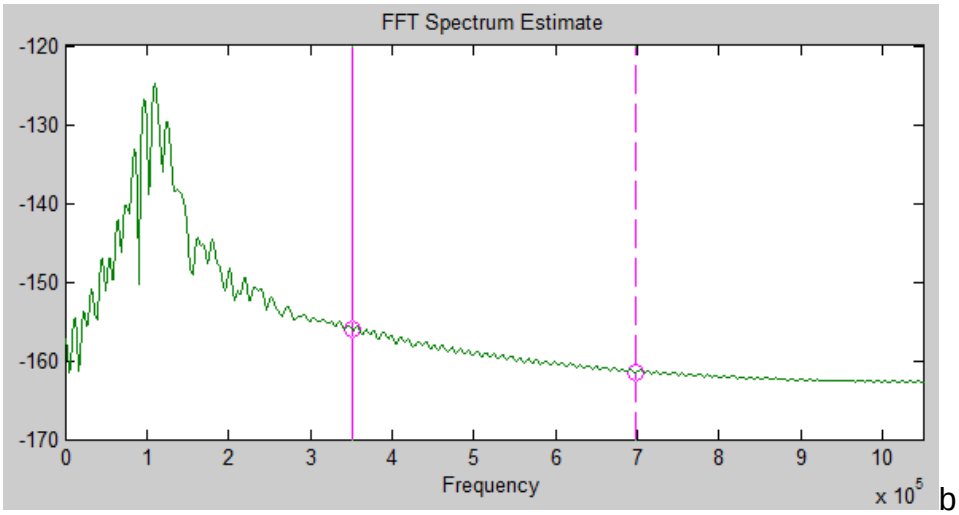

b

Figure 60. FFT of Horizontal Strain at Point A, 0.4 m from the Left End of the Plate. No Crack(a), With Crack/No Contact Elements(b).

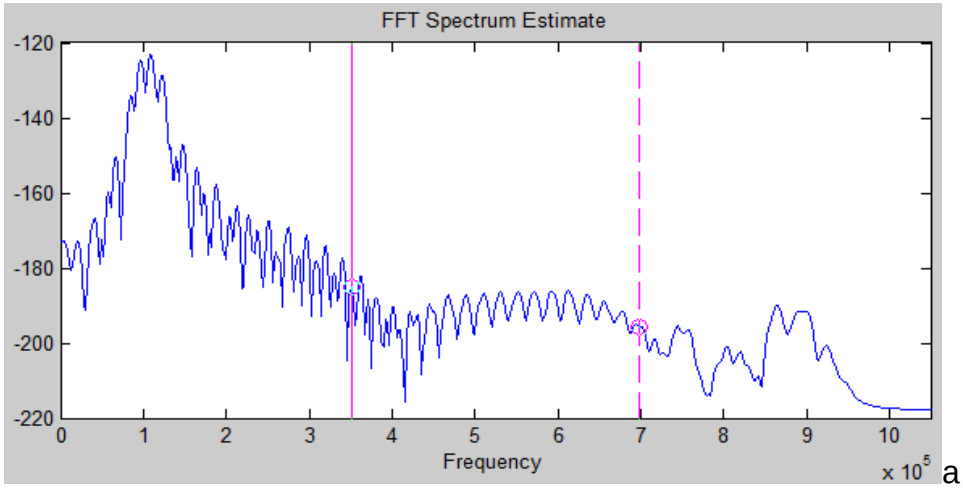

a

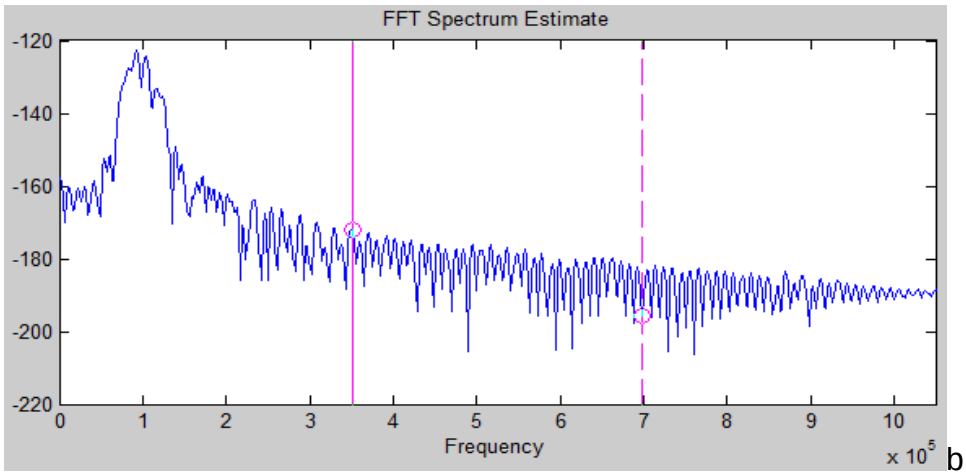

b

Figure 61. FFT of Horizontal Strain at Point B, 0.195 m from the Left End of the Plate. No Crack(a), With Crack/No Contact Elements(b).

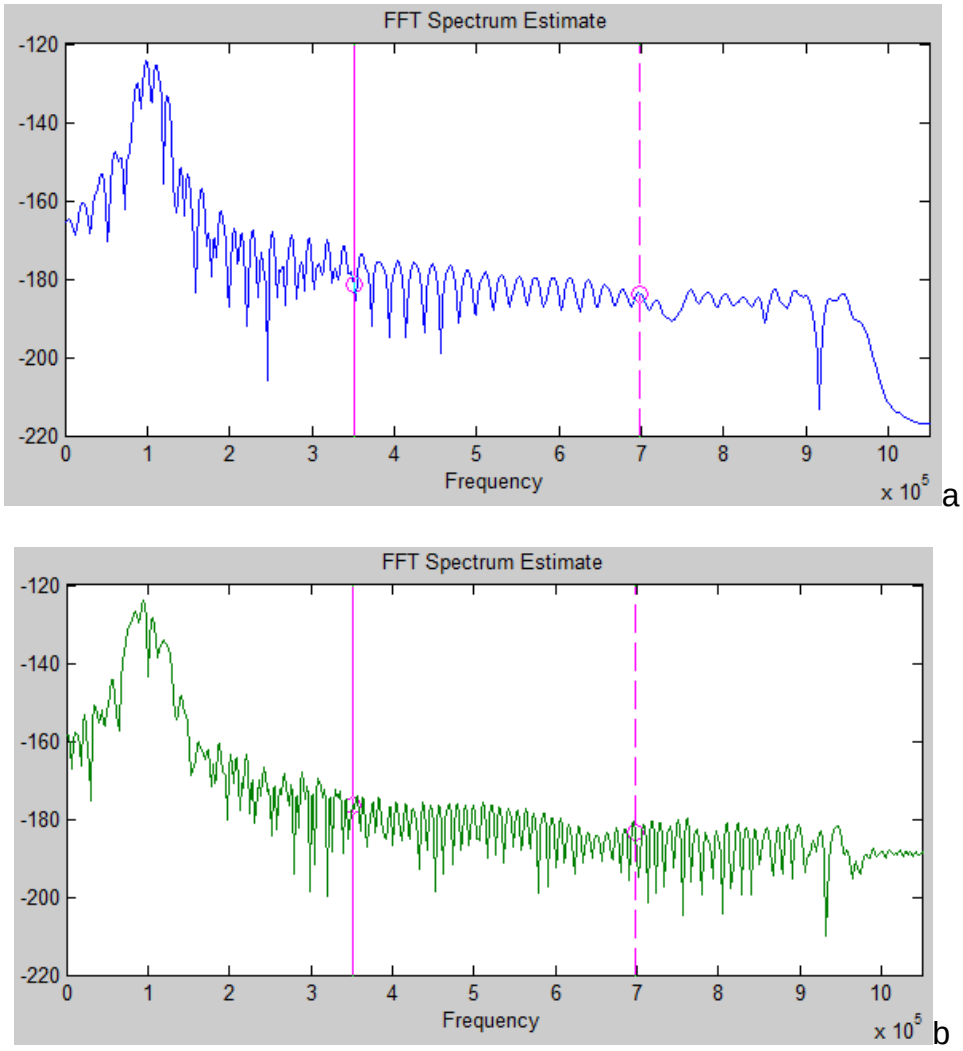

Figure 62. FFT of Horizontal Strain at Point A, 0.2 m from the Left End of the Plate. No Crack(a), With Crack/No Contact Elements(b).

From the above figures, it is clear that the damaged plate includes more and higher frequencies than the healthy plate. Again, the FFTs are not the same among the different points. So, the use and processing of the measured signal in a real structure must be handled with great care. The signals must be collected at exactly the same points. Another technique would be probably to filter the input so as to collect only the S0 type of wave (longitudinal), which does not change very much.

2. Dimensions 0.6 mm x 50 μm

The second model was exactly like the above but it had a vertical crack with dimensions 0.6 mm x 50 μm in the middle of the plate. Once again, we checked the response at the same three points A, B, C. In this part, only the horizontal displacement is presented.

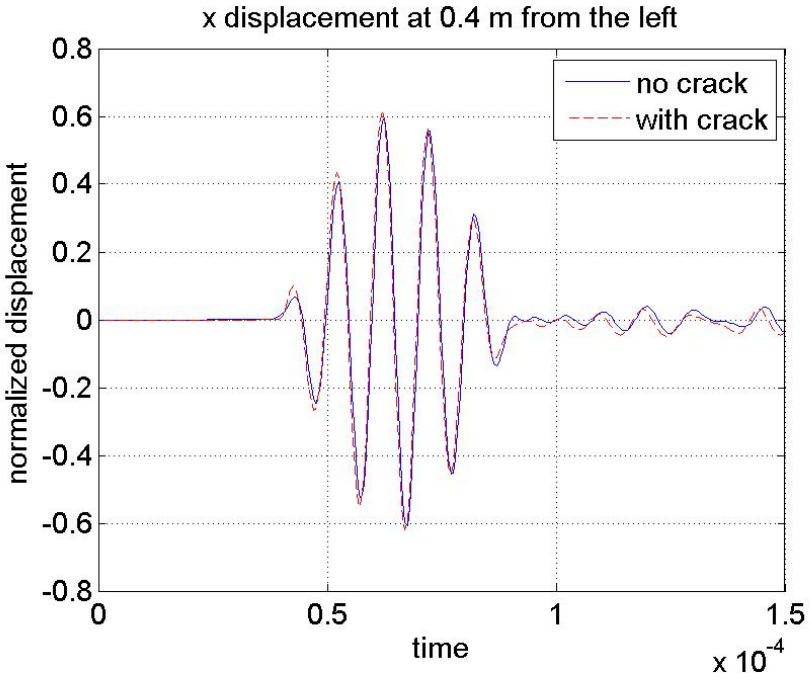

Figure 63. Horizontal Displacement at Point A, 0.4 m from the Left.

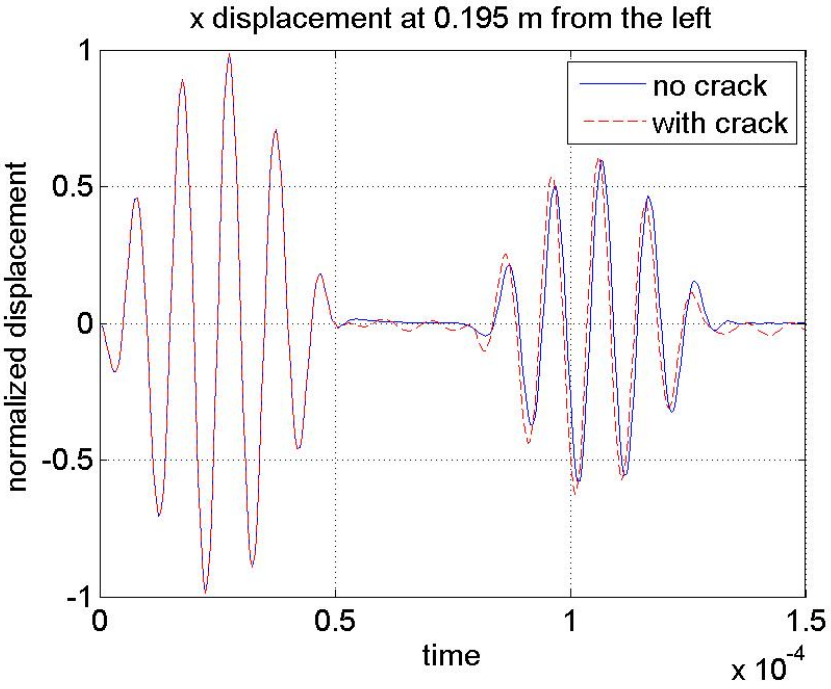

Figure 64. Horizontal Displacement at Point B, 0.195 m from the Left.

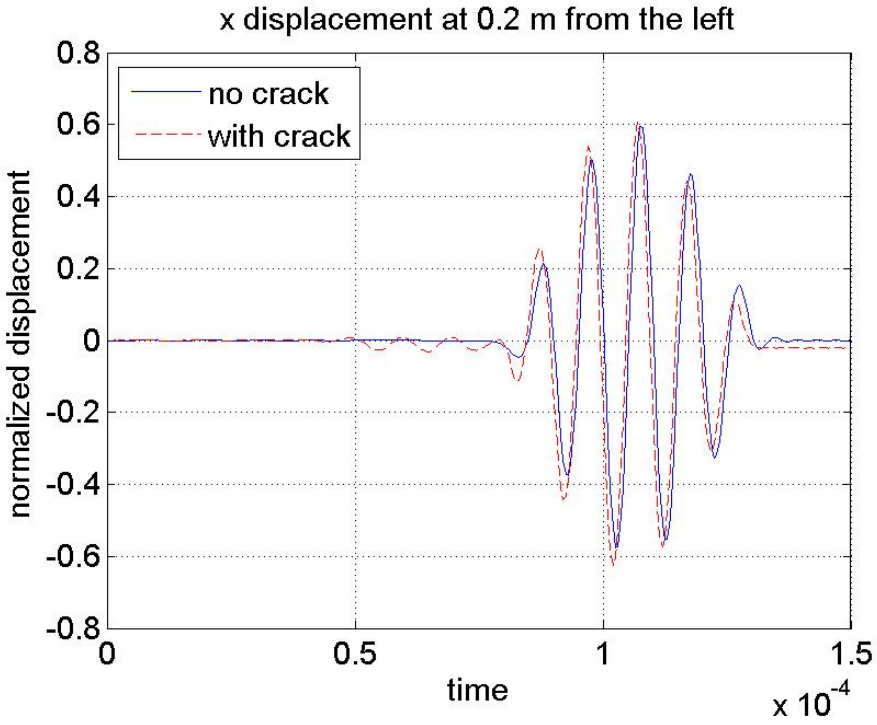

Figure 65. Horizontal Displacement of the Plate With and Without Crack, Distance 0.2 m from the Left

Like the previous simulation, there is an obvious difference on every line of the above figures between the displacement of the cracked plate and the displacement of the uncracked one. The difference is less obvious compared to the previous simulation because the length of the crack is shorter. The Fourier transforms of the above signals are the following:

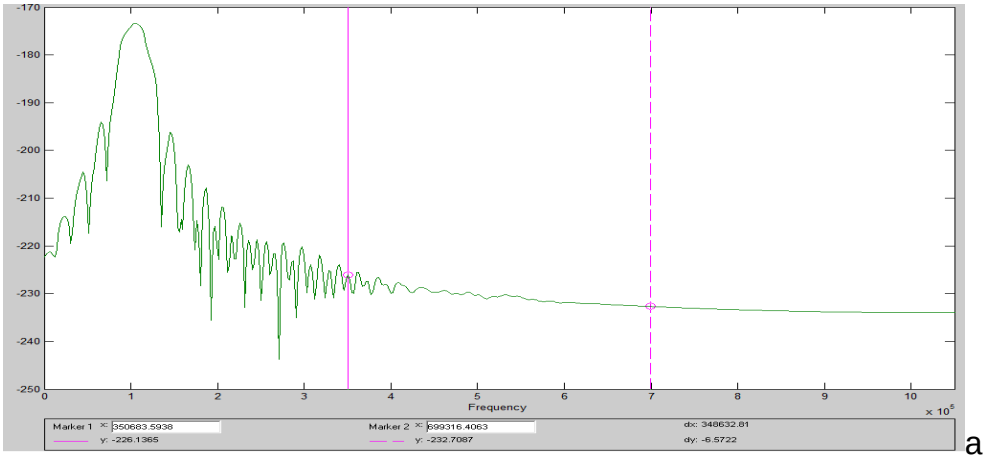

a

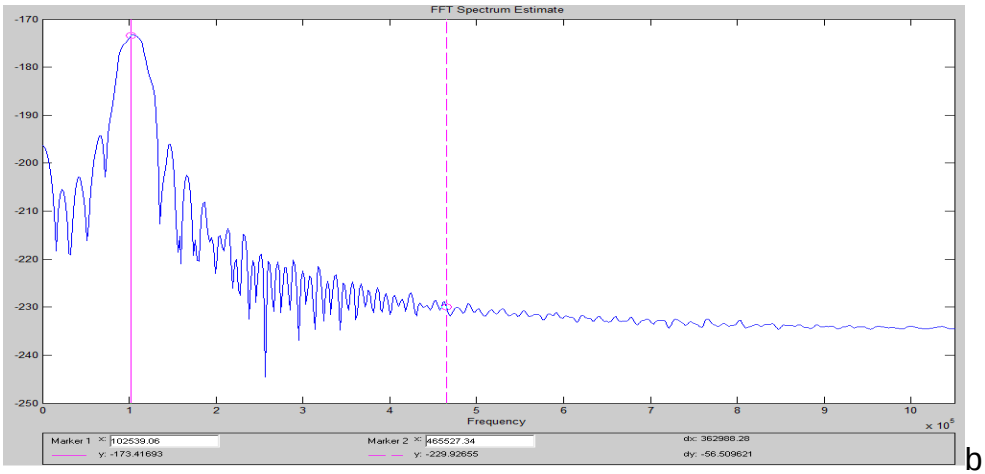

b

Figure 66. FFT of Horizontal Displacement at 0.4 m from the Left. Without Crack (a), With Crack (b).

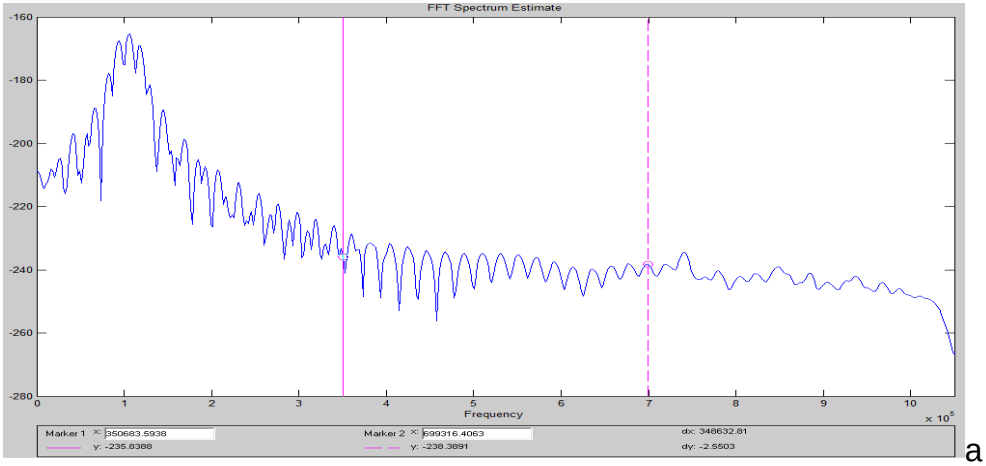

a

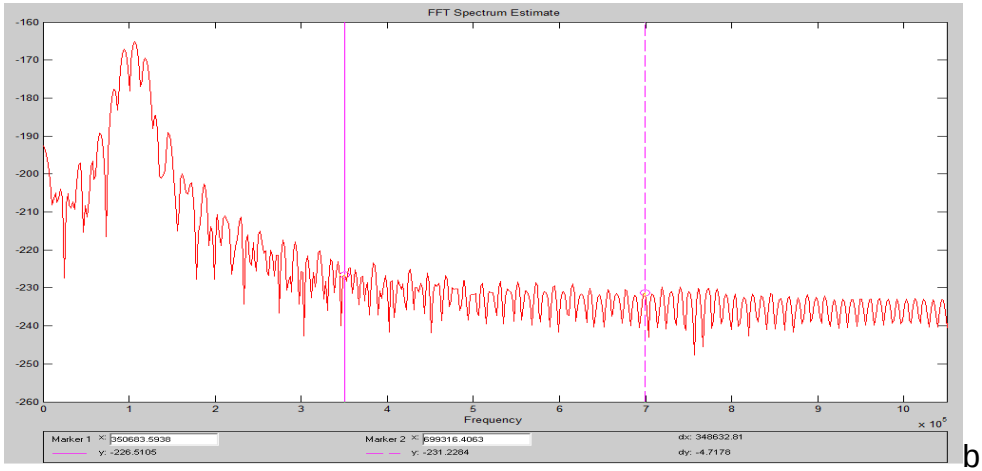

b

Figure 67. FFT of Horizontal Displacement from 0.195 m. No Crack (a), With Crack (b).

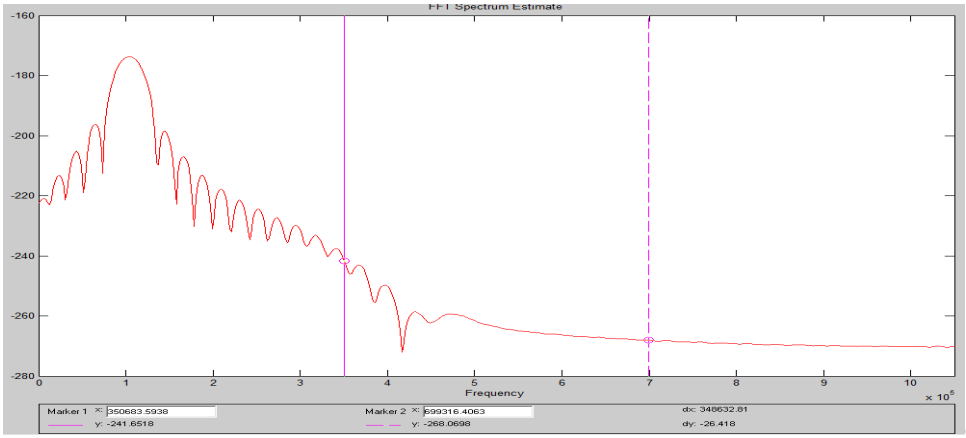

a

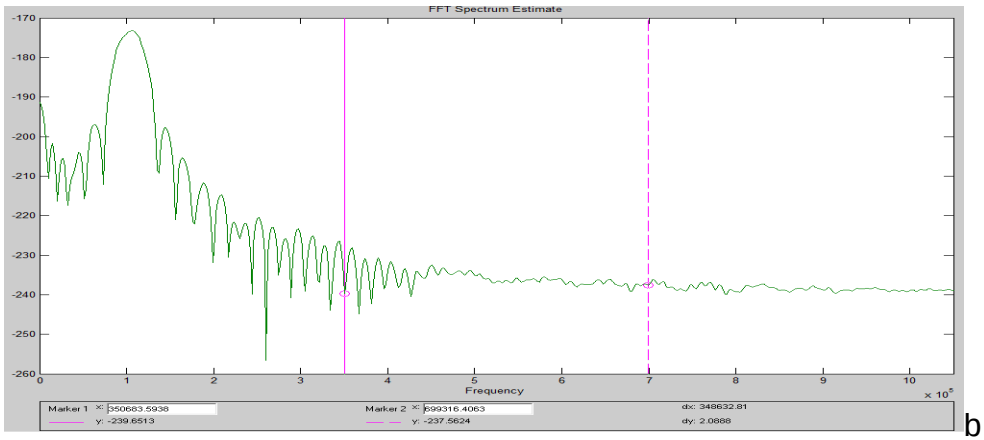

b

Figure 68. FFT of Horizontal Displacement from 0.2 m. No Crack (a), With Crack (b).

It is obvious one more time that the damaged plate contains higher frequencies but the difference is less compared to the previous simulation.

3. Dimensions 0.5 mm x 5 μm

Continuing the investigation of the crack influence on the Lamb waves, the crack dimensions were reduced to 0.5 mm x 5 μm, again in the vertical direction. The horizontal displacement from the points A and C are the following:

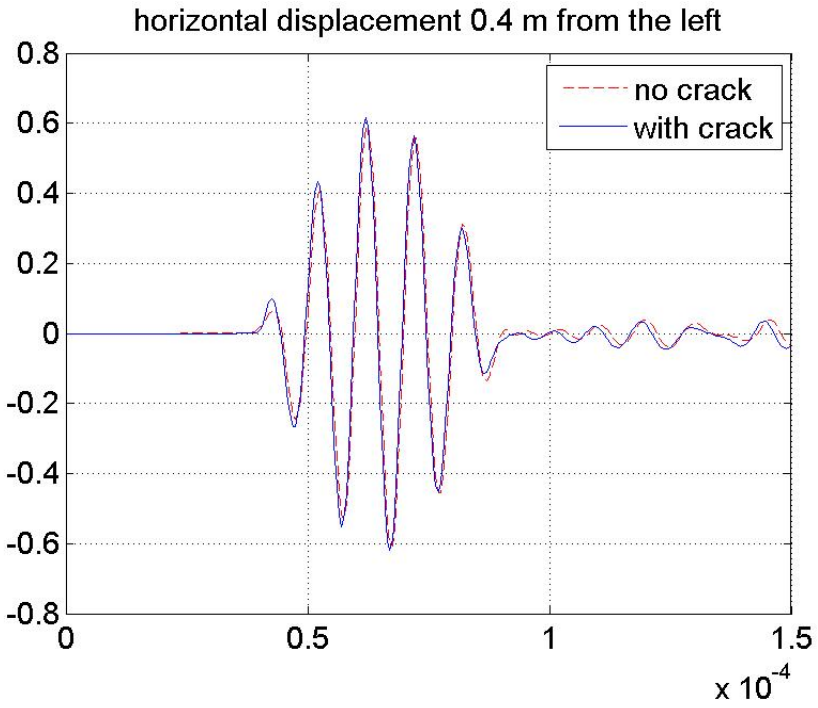

Figure 69. Horizontal Displacement at 0.4 m.

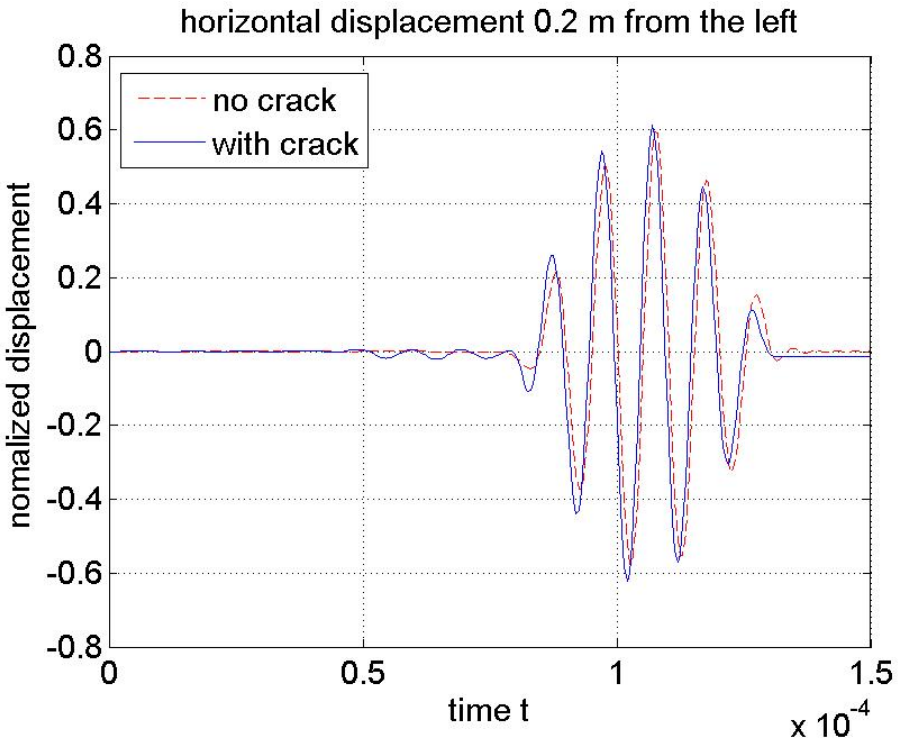

Figure 70. Horizontal Displacement at 0.2 m.

The difference between the cracked and uncracked cases is less obvious. The FFT at the above points follows:

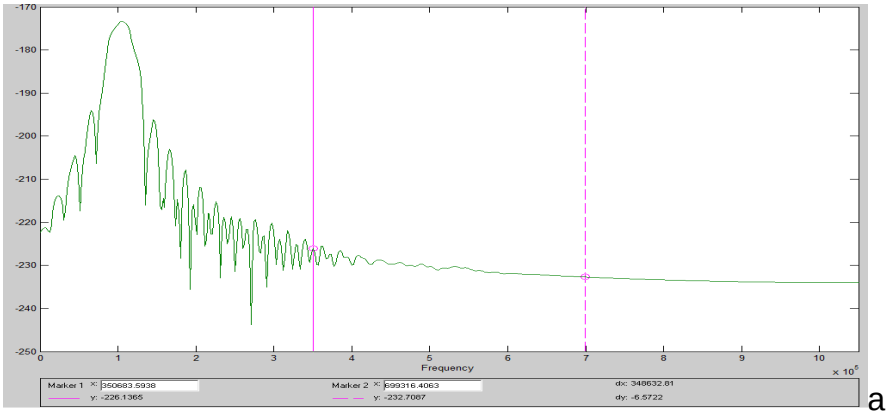

a

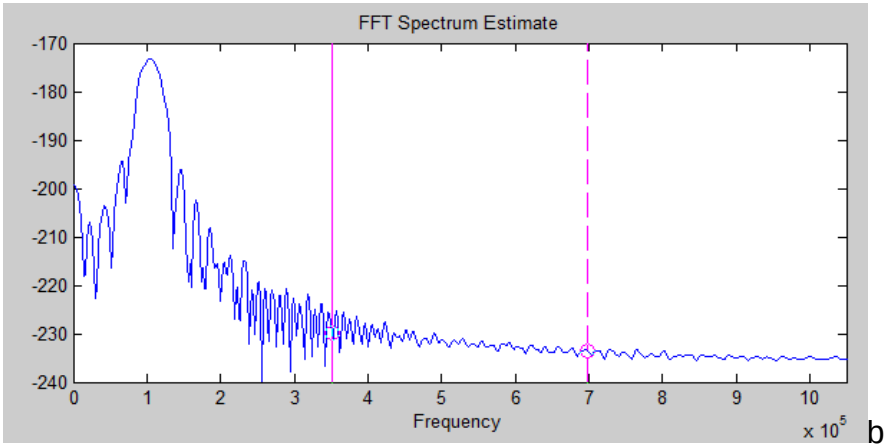

b

Figure 71. FFT of the Horizontal Displacement from 0.4 m. No Crack (a), With Crack (b).

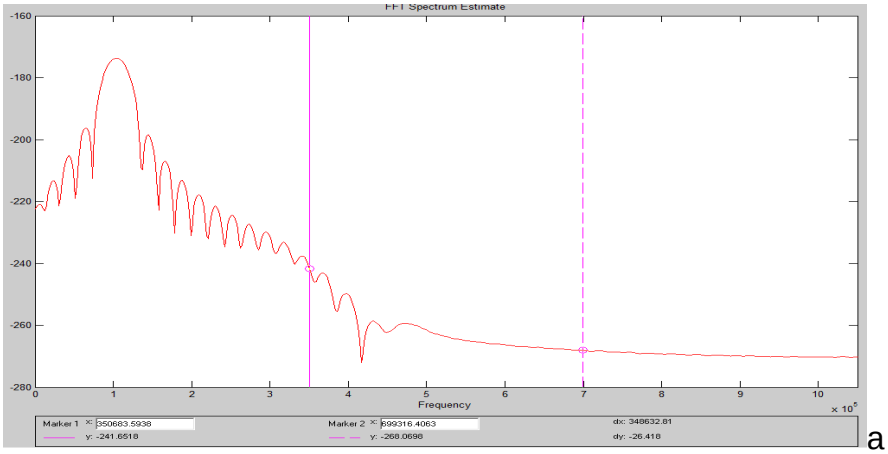

a

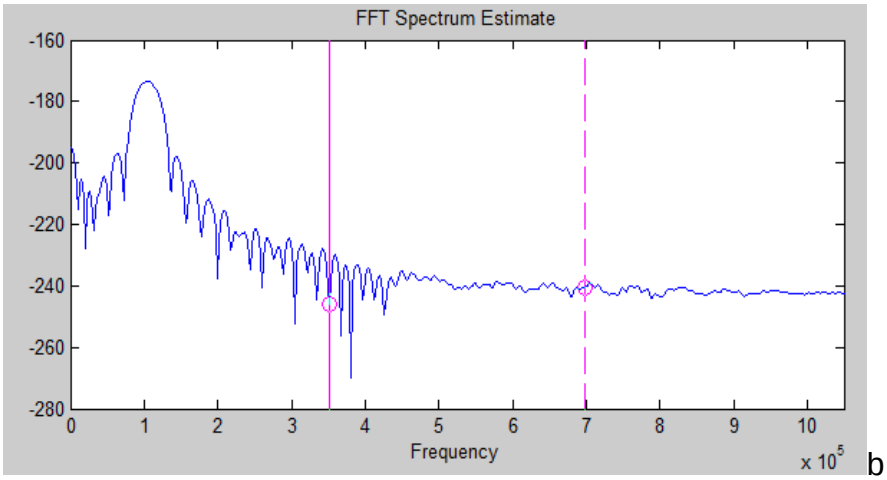

b

Figure 72. FFT of Horizontal Displacement from 0.2 m. No Crack (a), With Crack (b).

Both FFTs are different compared to the homogeneous plate.

B. HORIZONTAL CRACK.

1. Dimension 1 mm x 0.5 µm

The second part of this chapter deals with a horizontal crack. Using the model from Figure 50, one small horizontal crack was inserted in the aluminum plate with dimensions 1 mm x 0.5 µm. The crack was placed in the center line of the plate. Although this type of crack is not so common in metallic materials, it

was interesting to model it, as this can lead us to the modeling of delaminations in composite materials. One more time, the Lamb waves were modeled using the two-node simplification.

The following figures give the horizontal displacement and the fast Fourier transform of this signal for a point on the top surface of the plate.

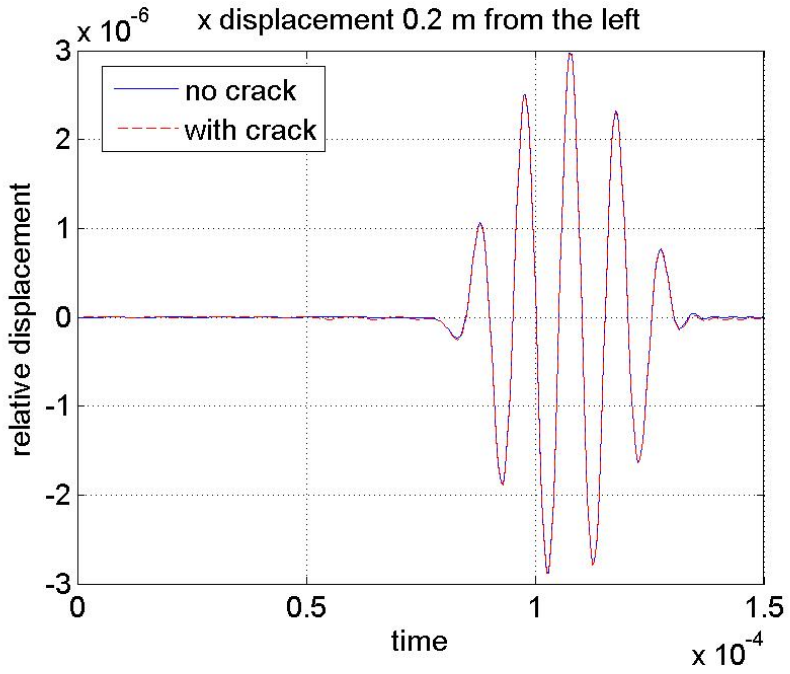

Figure 73. Horizontal Displacement from 0.4 m.

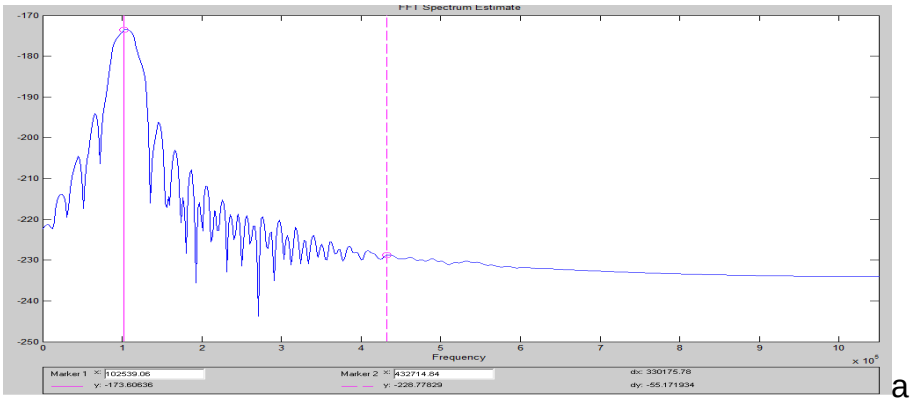

a

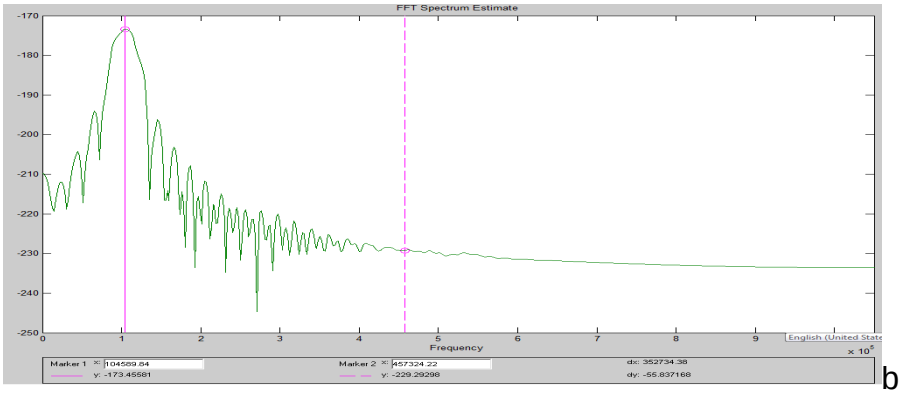

b

Figure 74. FFT of Horizontal Displacement from 0.4 m.

There is almost no difference between the horizontal displacements of the cracked and the uncracked ones and their Fourier transforms. This is reasonable, as this crack is too small to be detected.

2. Summary

From the preliminary simulations described in the previous headings, the following conclusions can be made: The finite element model is capable of capturing both the pulse-echo and pitch-catch techniques. The first can be used to identify the exact position of the crack, but it requires a large distance between the signal generation and the crack. The reflected signal from the crack must be collected at a “quiet” position so as to be identified easily. For these simulations, where the horizontal displacement was compared, the best point was the middle node on the center between the nodes that generate the Lamb waves. In real applications, this cannot be done easily.

The second technique (pitch-catch), with the help of FFT, is capable of identifying damage in the material, but it does not give the position of the crack. This technique does not have limitations regarding the distance between the crack and the Lamb wave generator, but it is important to compare the FFT of signals collected from the same point. This is because the study shows that the FFT of the displacement output is not the same at every point of the material.

C. CRACK MODELING FIDELITY - USE OF CONTACT ELEMENTS VERSUS NO CONTACT ELEMENTS

Crack modeling is one of the most important issues in finite element simulations as they adapt characteristics that are difficult to simulate. Some of them are the increase of stress around the crack tip and the extremely small thickness or initial opening distance. In this thesis, one of our research questions was the crack modeling fidelity. For this, the importance of the contact elements needs to be evaluated. The purpose of these non-linear elements is to avoid overlapping of the two sides of the crack as a result of the motion of the nodes that form the crack.

To evaluate the importance of contact elements, the following model was developed. It consists of an aluminum plate with a 2.5-m length and a 2-mm thickness. It has three piezoelectric patches with dimensions of 2 cm x 0.5 mm as shown in the following figure:

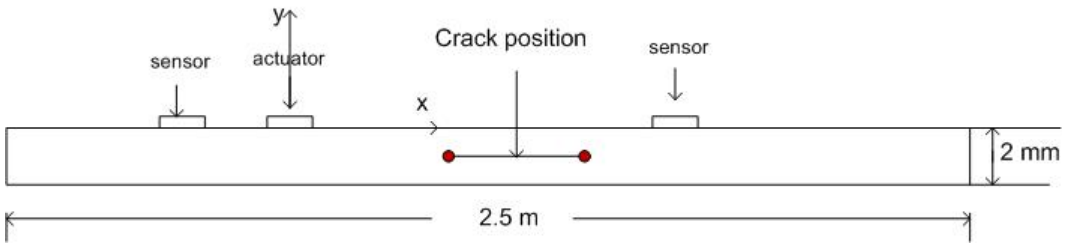

Figure 75. The Model with the Horizontal Line Crack.

Two different piezoelectric materials were used. The actuator and sensor to the right of the crack were modeled from PZT-4. The sensor to the left of the crack was from PVDF. In the center line of the aluminum one horizontal crack was inserted with a length of 10 cm. The crack was a line crack with zero thickness. Singular elements were used around the crack tips, and contact elements were inserted to avoid overlapping of the two sides of the crack. The Lamb waves were generated by applying voltage difference on the top and bottom lines of the PZT-4 actuator. The simulation was run two times: one with contact elements and one without contact elements. All the other parameters

were kept constant (element size, time step, singular elements, and boundary conditions).

First, the voltage output of the piezoelectric actuator is presented in the following figure:

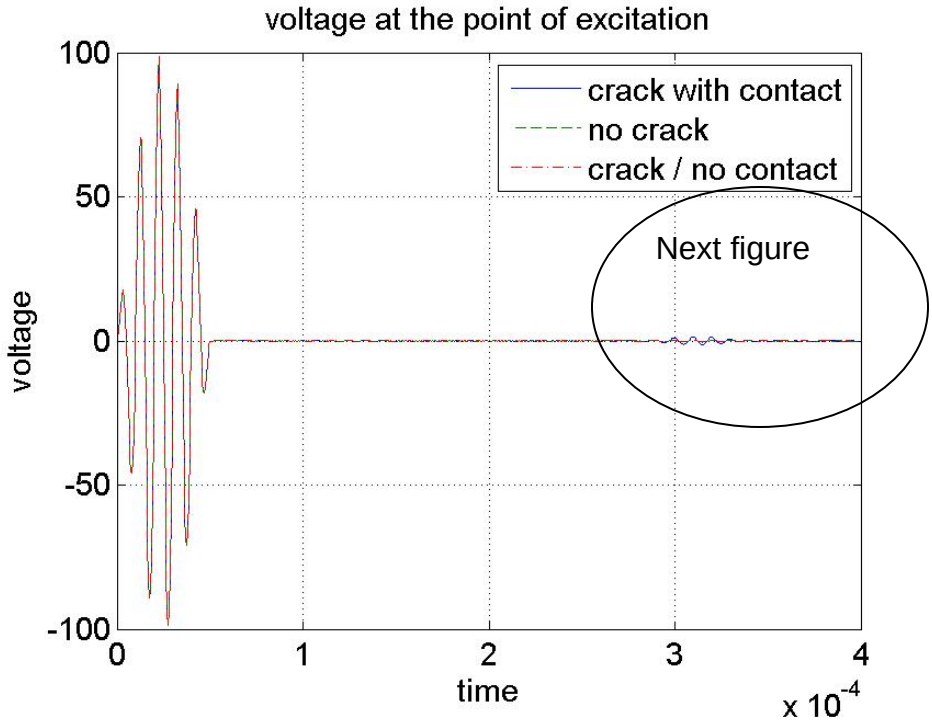

Figure 76. Voltage Output from the Actuator of Figure 72. A Reflected Wave from the Crack is Present Inside the Ellipse.

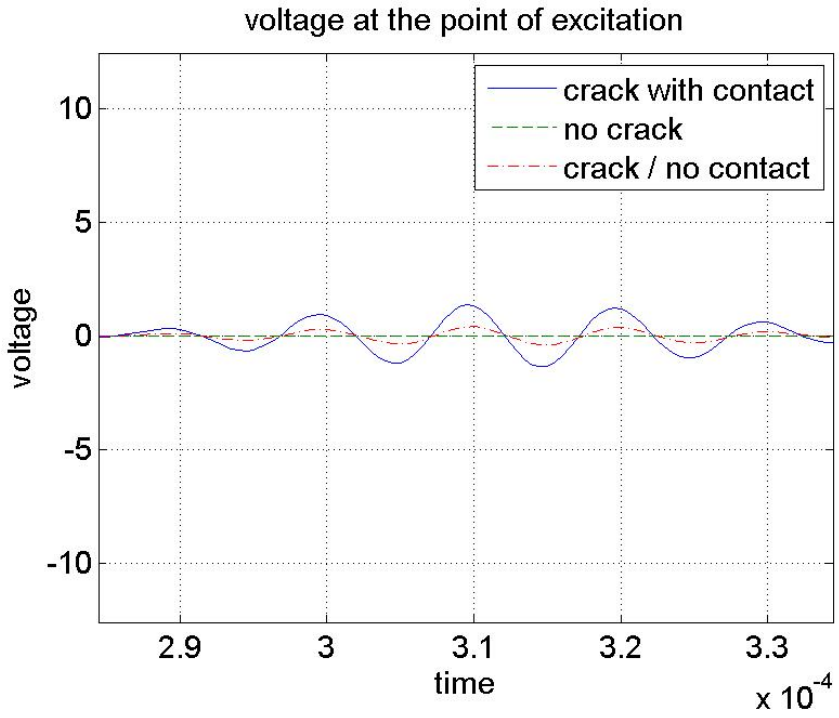

Figure 77. Closer Look inside the Ellipse of Figure 73.

From time zero until 50 μsec, the input voltage is shown. At time 290 μsec, the reflection from the crack is present. The pulse-echo technique gave the reflection wave from the crack. This signal can be used to locate the exact position of the crack.

On the one hand, the reflected wave differs a lot between using and not using contact elements. The longitudinal wave reflects more for the case with the contact elements. In fact, the simulation proves an increase of about 200% in the amplitude of the reflected wave. This difference can prove that the use of contact elements is important for an accurate simulation when there is overlapping of the two sides of the crack as in this case.

On the other hand, a simulation without contact elements is much faster as it is a linear analysis. Moreover, the results are conservative. The output of the simulation with contact elements, which is closer to reality, is larger than the no-contact case. So, in designing problems, the engineer could use the output from the linear simulation as the lower limit of the real voltage output.

The next important output of the simulation is the voltage from the sensor to the right of the crack, which is presented in the next figure. The first wave form is the voltage output because of the longitudinal wave and the second because of the bending mode. There is an interesting difference at the A0 mode. Both the contact case and the no-contact case are not very far apart, even though they are both different from the no-crack one.

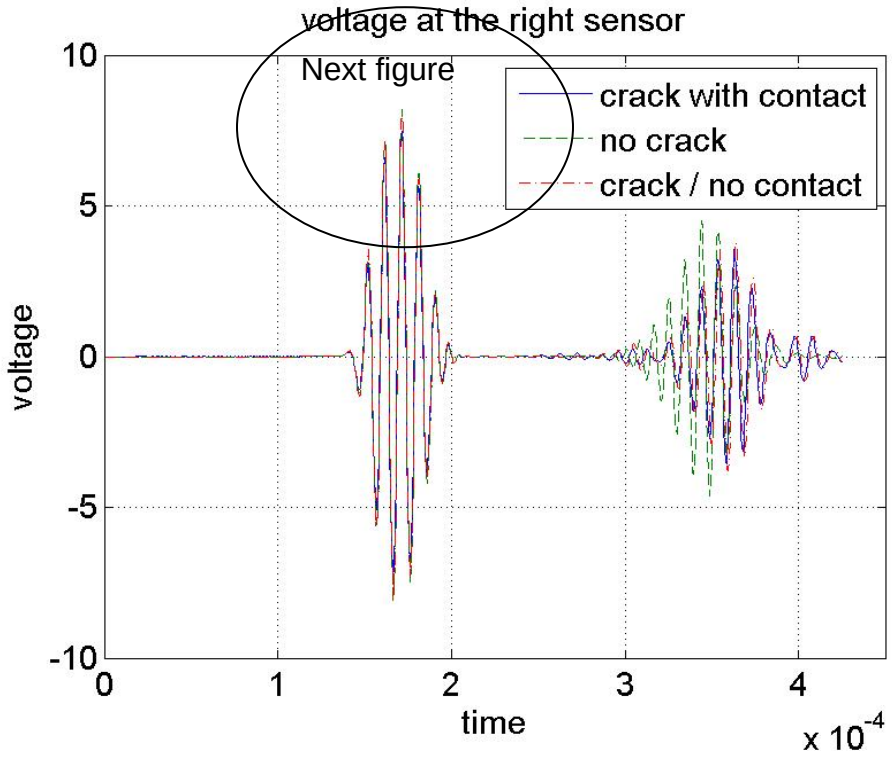

Figure 78. Voltage Output from the Sensor on the Right Side of the Model in Figure 72. It Demonstrates the Difference when using Contact Elements.

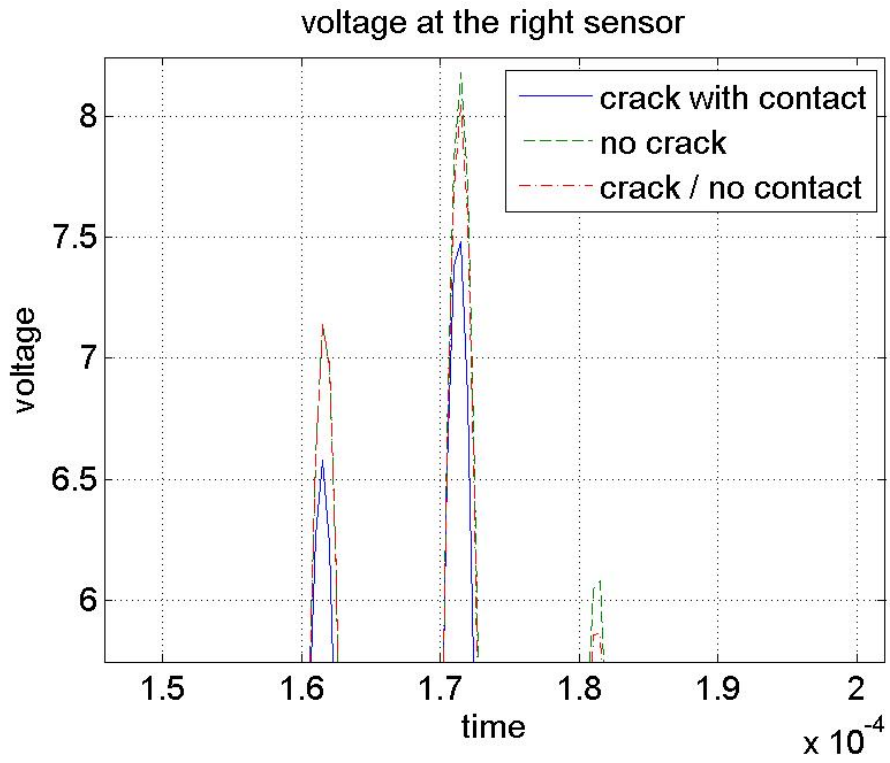

Figure 79. Closer Look inside the Ellipse of Figure 75.

Moreover, a closer look at the first S0 mode demonstrates a reduction of the voltage amplitude for the two cracked cases. In fact, this reduction is more obvious with the use of contact elements. This observation follows the principle of conservation of energy. In the previous paragraph we showed an increase of the reflected wave for the case in which contact elements were used.

The final step of the comparison is the Fourier transform of the signal from this sensor. The next two figures give the FFTs.

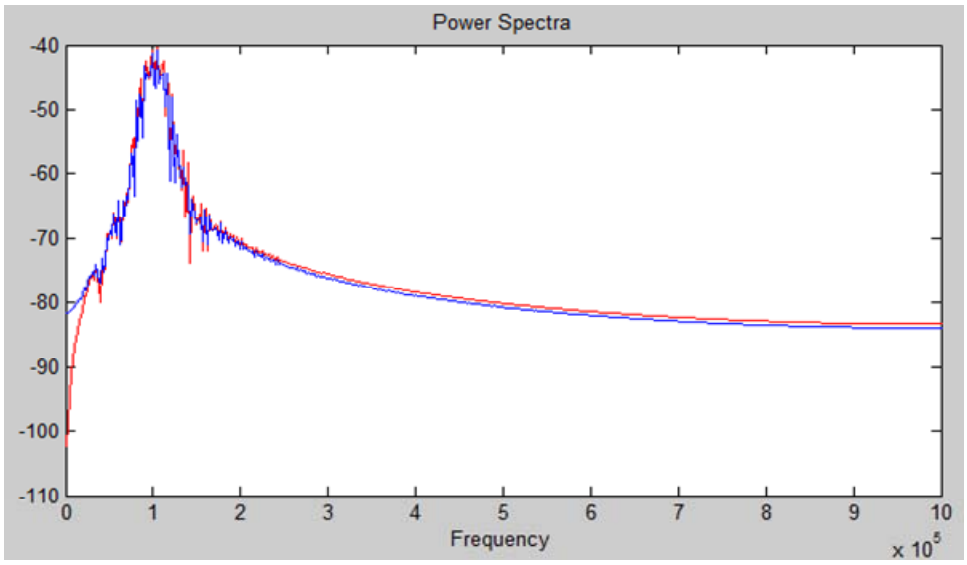

Figure 80. FFT of the Voltage Output from the Actuator of Figure 72. No Crack: Red; with Crack: Blue.

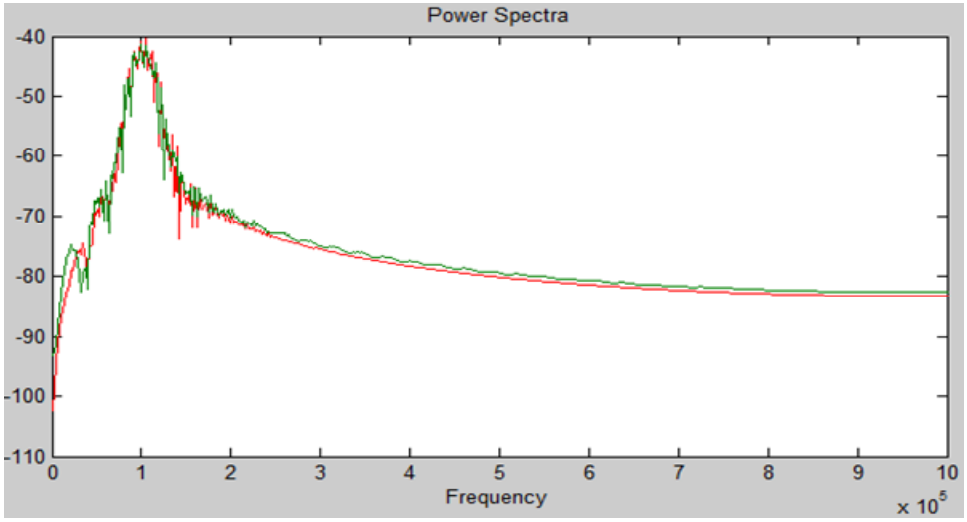

Figure 81. FFT of the Voltage Output from the Right Sensor of Figure 72. No Crack: Red; with Crack: Blue.

There are definitely differences between the cracked and no-cracked cases. This can indicate a damaged structure. As a drawback, the existence of higher frequencies is not as obvious as in the initial simulations of this chapter.

VII. CONCLUSIONS AND RECOMMENDATIONS

A. CONCLUSIONS

This thesis verified the use of Lamb waves for crack identification. In Chapter III, the two wave forms were identified and some basic characteristics, such as the frequency dependent, were evaluated. As already mentioned, structural health monitoring techniques based on Lamb waves could use the advantages of both modes of Lamb waves for a more accurate result. Crack identification using the pulse–echo technique is probably better for using the advantage of the S0's constant shape and higher velocity whereas when using the pitch-catch technique, the SHM system can easily identify damage initially from a reduction in the amplitude of the longitudinal wave and, secondly, from the change in the easily affected shear wave because of the crack's existence, which changes the local properties of the rod.

Different Lamb wave generation techniques were evaluated in Chapter IV. The research showed that the application of horizontal force or displacement as a simplification of the actual piezoelectric actuator generates two Lamb wave modes. On the other hand, the above two-node simplification changes the amplitude ratio of the S0 and A0 Lamb waves mode compared with a simulation that includes a piezoelectric actuator. In particular, a 45% difference was observed in the shear wave for the same amplitude as the longitudinal wave. No other effect on the two wave forms was observed (frequency, period, velocity).

The existence of a crack between the piezoelectric material and the structure was analyzed in Chapter V. An actuator having a debonding length 30% of its entire length was evaluated. The simulation showed no difference in the S0 mode, but the amplitude of the A0 mode was decreased around 9%. This phenomenon can be expanded to mach with the results described in the previous paragraph. For structural health monitoring applications, this amplitude decrease

can be characterized conservatively as it indicates a potential damage of the structure or a problem on the health monitoring system.

The existence of a crack between the piezoelectric sensor and the structure was also analyzed. For the same debonding length (30% of the sensor's total length), the research showed an increase in the voltage output close to the crack's tips. The effect was reduced when an adhesive layer was inserted between the structure and the sensor. This local phenomenon can increase the overall voltage output of the piezoelectric sensor and mask some potential voltage reduction caused by damage in the structure. In other words, if both damage in the structure and debonding of the sensor are present at the same time, it is possible to have no change in the output of the sensor.

Both pulse-echo and pitch-catch techniques were demonstrated and gave good results for horizontal and vertical cracks in Chapter VI. The first part of this chapter shows that the vertical cracks are easier to identify because they reflect more and the FFT of the collected signal after the crack differs a lot from the uncracked case. The importance of using contact elements for crack modeling was also investigated. The model showed that a crack without contact elements is capable of capturing the physics of the interaction with the Lamb waves; however, for a horizontal crack with a 10-cm length, the reflection from the crack was 200% more using contact elements. This proves that for accurate finite element simulations the model should include contact elements.

B. RECOMMENDATIONS AND FUTURE WORK

The above conclusions were based on finite element simulation using the commercial software ANSYS. It would be interesting to verify experimentally some of the results, although some of them are difficult to achieve. For example, the generation of a crack between the piezoelectric material and the structure is challenging. The paper models a simple parallelogram, homogeneous aluminum plate. The next step would be the application of the knowledge from this paper to non-homogeneous materials such as composites. It would be attractive to

expand the simulation limits and try to locate delamination in composite materials. Moreover, no damping was used in all of the above simulations. In future work, someone could evaluate the influence of damping on the longitudinal and shear wave. The creation and evaluation of a three-dimensional model is also fascinating. Finally, the modeling of different crack sizes inside the adhesive layer between the piezoelectric material and the structure could investigate more their effect on the total voltage output of the sensor.

THIS PAGE INTENTIONALLY LEFT BLANK

LIST OF REFERENCES

[1] H. Speckmann, H. Roesner, “Structural Health Monitoring: A Contribution to the Intelligent Aircraft Structure,” *Proceeding of ECNDT 2006*, 9th European Conference on NDT, Berlin, Germany, September 2006.

[2] European Aeronautic Defence ans Space Company (2009, Sept, 14). Structural Health Monitoring . *European Aeronautic Defence ans Space Company*. [Online] Available FTP: http://www.eads.net/1024/fr/madebyeads/endurance/shm.html.

[3] I. A. Viktorov, *Rayleigh and Lamb waves: physical theory and applications*. Plenum Press, New York, 1967.

[4] A.B. Coppens and O.B. Wilson, “Elements of sound transmission in beams,” Naval Postgraduate School, Monterey, CA, final report, 14 Apr.–30 Sep., 1978.

[5] Scandrett Clyde, “The propagation of time harmonic Rayleigh-Lamb waves in a biomaterial plate,” Naval Postgraduate School, Monterey, CA, Technical Report, ADA216834, Oct. 1988–Sep. 1989.

[6] Se Jim Han, “Finite element analysis of lamb waves acting within a thin aluminum plate.” Master’s thesis, Air force Institute of Technology, Dayton, OH, 2007.

[7] Steven E. Olson, Mark M Derriso, Martin P. DeSimio, “Analytical modeling of lamb waves for structural health monitoring,” Conference paper, Third European Workshop on Structural Health Monitoring, Granada, Spain, July 5–7, 2006.

[8] N.B. Spedding, “The effect of sensor geometry on the use of polyvinylidene fluoride (PVDF) as an acoustic emission sensor,” *Insight*, vol. 38, pp. 37–40, 1996.

[9] B. C. Lee and W. J. Staszewski, “Modeling of lamb waves for damage detection in metallic structures: Part I Wave Propagation; Part II Wave interactions with Damage,” *Smart Materials and Structures*, vol. 12, pp. 804–824, 2003.

[10] B. C. Lee and W. J. Staszewski, “Lamb wave Propagation modeling for damage detection: Part I Two Dimensional Analysis; Part II Damage Monitoring Strategy,” *Smart Materials and Structures*, vol. 16, pp. 249–274, 2007.

[11] Jeong-Beom Ihn and Fu-Kuo Chang, “Detection and monitoring of hidden fatigue crack growth using a build in piezoelectric sensor / actuator network: Part I. Diagnostics,” *Smart Materials and Structures*, vol. 13, pp. 609–620, 2004.

[12] Jeong-Beom Ihn and Fu-Kuo Chang, “Detection and monitoring of hidden fatigue crack growth using a built in piezoelectric sensor /actuator network: Part II: Validation using riveted joints and repair patches,” *Smart Materials and Structures*, vol. 13, pp. 621–630, 2004.

[13] Seth S Kessler, S. Mark Spearing, and Constantinos Soutis, “Damage detection in composite materials using Lamb Wave methods,” *Smart Materials and Structures*, vol. 11 pp. 269–278, 2002.

[14] Victor Giurgiutiu, “*Structural Health Monitoring with Piezoelectric Wafer Active Sensors*,” AP, 2008.

[15] Young W Kwon and Hyochoong Bang, “*The Finite Element Method Using Matlab*’, 2d ed., CRC Press, 2000.

[16] P. Delsanto, T. Whitcombe, H. Chaskelis, R.B. Mignogna, “Connection machine simulation of ultrasonic wave propagation materials I: the one dimensional case,” *Wave Motion*, vol. 16, pp. 65–80, 1992.

[17] P. Delsanto, T. R. S. Schecher, H. Chaskelis, R. B. Mignogna and R.B.Kline, ”Connection machine simulation of ultrasonic wave propagation in materials. II: The 2 dimensional case,” *Wave Motion*, vol. 20, pp. 295–314, 1992.

[18] P. Delsanto, T. R. S. Schecher, H. Chaskelis, R. B. Mignogna, and R.B, Kline, “Connection machine simulation of ultrasonic wave propagation in materials. II: The 2 dimensional case,” *Wave Motion*, vol. 26, pp. 329–339, 1997.

[19] J. Marckerle, “Finite-element modeling of non-destructive material evaluation, an addendum: A bibliography (1997–2003),” *Modeling and Simulation in Material Science and Engineering*, vol. 12, pp. 799–834, 2004.

[20] Z. Su, “Fundamental Lamb Mode-based Delamination Detection for CF/EP Composite Laminates Using Distributed Piezoelectrics,” *Structural Health Monitoring*, vol. 3, pp. 43–68, 2004.

[21] D. N. Alleyne and P. Cawley, “The interaction of Lamb Waves with Defects,” *IEEE Transactions on Ultrasonics, ferroelectrics and Frequency Control*, vol. 39, pp. 381–397, 1992.

[22] E. Moulin, J. Assaad, C. Delebarre, H. Kaczmarek, and D. Balageas, “Piezoelectric transducer embedded in composite plate: application to Lamb wave generation,” *Journal of Applied Physics*, vol. 82, pp. 2049–2055, 1997.

[23] Lawrence W. Braile. (2009, 09, 14). Seismic Waves and the Slinky: A Guide for Teachers, Purdue University. Available: http://web.ics.purdue.edu/~braile/edumod/slinky/slinky.htm.

[24] LIU Zhenqing, “Lamb Wave Analysis of Acousto-Ultrasonic Signals in Plate,” presented at the 15th World Conference on Nondestructive Testing, Roma, Italy, 15-21 October 2000.

[25] APC International Ltd, “*Piezoelectric Ceramics: Principles and Applications,*” 2002.

[26] Standards Committee of the IEEE Ultrasonics, Ferroelectrics, and Frequency Control Society, USA, “*IEEE standard on piezoelectricity,*” 1988.

[27] Robert D. Adams, J Comyn, W.Charles Wake,” *Structural adhesive joints in engineering,*” 2d ed. Chapman and Hall, 1997.

[28] Sungwon Ha, “Modeling Lamb Wave Propagation Induced by Adhesive Bonded PZTS on Thin Plates,” Ph.D. dissertation, Stanford University, Palo Alto, CA, 2009

[29] Wikipedia. (2009, 09, 14). Adhesive. *Wikipedia* [Online]. Available: http://en.wikipedia.org/wiki/Adhesive.

INITIAL DISTRIBUTION LIST

1. Dudley Knox Library
   Naval Postgraduate School
   Monterey, California

2. Defense Technical Information Center
   Ft. Belvoir, Virginia

3. Professor Young W. Kwon
   Naval Postgraduate School
   Monterey, California